AXIALLY-LOADED CENTRIFUGE PILE TESTS

John E. Christenson

and

Ronald F. Scott

Final Report Through October 31, 1980

for

American Petroleum Institute
OSAPR Project 13

March 1, 1982

Soil Mechanics Laboratory
Division of Engineering and Applied Science
California Institute of Technology
Pasadena, California 91125

TABLE OF CONTENTS

PREFACE

R. F. Scott

A previous report to API (1980) discussed an attempt at driving model piles in the centrifuge during flight by means of a model pile-driver. Both electrical solenoid and air-operated systems were tested, and some of the results were presented in that report. A further modification of the pneumatic pile-driver was subsequently tried out; it was not successful.

While pile-driving apparatus was being worked on experiments on axially loaded piles continued. A typical pile was located in the centrifuge container with its tip embedded in a layer of soil at the bottom of the container at one g. Soil was subsequently placed and compacted by hand around the pile, still at one g. After the installation of the usual instrumentation, the centrifuge was activated to bring the pile, soil, and container up to the selected g-level, for axial load tests. In this report, the pile-loading experiments are described.

A number of the tests were designed to be the model equivalent of some full-scale pile tests, so that quantitative comparisons of behavior could be made. It was intended that the analyses of the performance of the model piles would be followed by a detailed discussion of the pile-soil shear stress-displacement functions ("t-z" curves) in relation to soil properties, with a view to constructive guidelines for t-z curve development. However, it is apparent in the material which follows that the axial top load-displacement behavior of the model piles is so much softer than that of the prototype piles that there is a real question as to the identification of these model tests with prototype performance. It was therefore decided that, although t-z curves had been developed for each model test, it was not appropriate to try to relate them to idealized soil models for the construction of template functions. In the description of the work which follows this last step, therefore, does not appear.

The bulk of this report is taken up with a Civil Engineer's thesis devoted to the pile tests, and written by John E. Christenson, under the guidance of Ronald F. Scott. In the thesis, the opinions expressed in many instances are Christenson's alone, although here and there they are modified by interaction between Christenson and Scott. In particular, with reference to the lack of an apodictic correspondence between the model and prototype compliances, Christenson ascribes the difference

principally to the variation of acceleration along the model pile, and to interaction between model pile and the container wall. He considers the effect of driving the model pile in flight to be of secondary importance. The interaction between pile and wall is considered by Christenson to have an effect through wall friction; that is to say, as the centrifuge is brought up to speed, the tendency of the soil to compress is resisted by pile and container wall friction, and thus lateral pressure on the pile does not fully develop. This contention could most easily be evaluated by performing tests on the same pile in the same soil in a larger container. Such a vessel is not available for the Caltech centrifuge. The writer (Scott) assigns a greater importance to the model pile-driving requirement from two points of view. First, if the soil could be centrifuged without the pile, then the lateral pressures might be more realistic even in the limited size of the existing container. Second, subsequent driving of the pile, at scale g, into the soil would tend to break down any arching action that did develop, as well as, and more importantly, to develop the proper pressure distribution in the immediate pile vicinity, and lateral pressure on the pile. Soil volume changes next to the pile which presumably play a significant part in the pile's subsequent response would be generated by the driving. For the present, this must remain an open question. There remains, of course, the usual soil mechanics problem, that the prototype soil, although essentially of the same type and at the same unit weight or void ratio as the model material, may have entirely different deformational properties, because of its different structure, or through the development of interparticle bonds or cementation in time. If this accounts for the differences in the present study, then the centrifuge pile tests do have validity, and the t-z curves produced would be worth examination. The only way to come to a conclusion on this matter would seem to lie in either carrying out model pile-driving studies, to see if driving changes the pile behavior significantly, or in performing both full-scale and centrifuge pile studies concomitantly, so that close control could be exercised over the soil characterization tests. It should be noted that one series of tests, Test 2, has been omitted from this report.

ACKNOWLEDGMENT

Some of the tests described in this report were performed by J. Christenson and John Lee, a few by J. Lee and R. F. Scott. The instrumentation for all the tests was devised and assembled by J. Lee, who also supervised the recording equipment, and centrifuge operations in general.

REFERENCE

Scott, R.F., *Analysis of Centrifuge Pile Tests; Simulation of Pile-Driving*, Report through Sept. 30, 1979 for American Petroleum Institute OSAPR Project 13, California Institute of Technology, Pasadena, CA, 91125, June 20, 1980.

CHAPTER 1

INTRODUCTION

This report concerns investigations of the behavior of piles under axial loading using centrifugal modeling and t-z analysis. The results of five centrifuge model pile tests on instrumented piles are presented. The present chapter puts this work into perspective, both with relation to current practical concerns with pile performance and existing analytical techniques.

1.1. Piles and the History of Their Use

The pile is a foundation element having the geometric shape of a bar or beam which is emplaced in the ground with its axis at or near the vertical for the purpose of contributing support to other foundation subassemblies and a superstructure. A pile operates by transferring the burden presented by the structure above it to the soil all along its length and at its base, with the distribution of load transfer dependent on properties of both the pile and the soil. Some examples of structures drawing on piles for support are pictured in Figures 1.1 and 1.2 below. In Figure 1.1 are shown (a) the concrete pile cap and base for a steel tower, (b) a continuous footing, (c) a guy wire, (d) the cap or grid of beams forming the base of a massive building, (e) a bridge abutment, (f) a relieving platform wall, (g) a wharf, and (h) a light station, and in Figure 1.2, the templet or substructure for an ocean drilling platform.

A simple, versatile structure which enables construction on ground where it would otherwise be impossible, the pile entered the service of man early in his cultural-technological development. In Switzerland and neighboring areas of Germany, Italy, and France, beginning in the Stone Age during the fourth millenium B.C. and continuing into the Bronze and Iron Ages, agropastoral men drove timber piles to support dwellings and livestock barns on marshy lakeshore soils. The Romans utilized driven wooden piles in bridge construction. In the modern era, piles made of wood and emplaced by driving were predominant until the nineteenth century. With the coming of the Industrial Revolution, piles were called upon to support ever larger and more complex superstructures in increasingly difficult

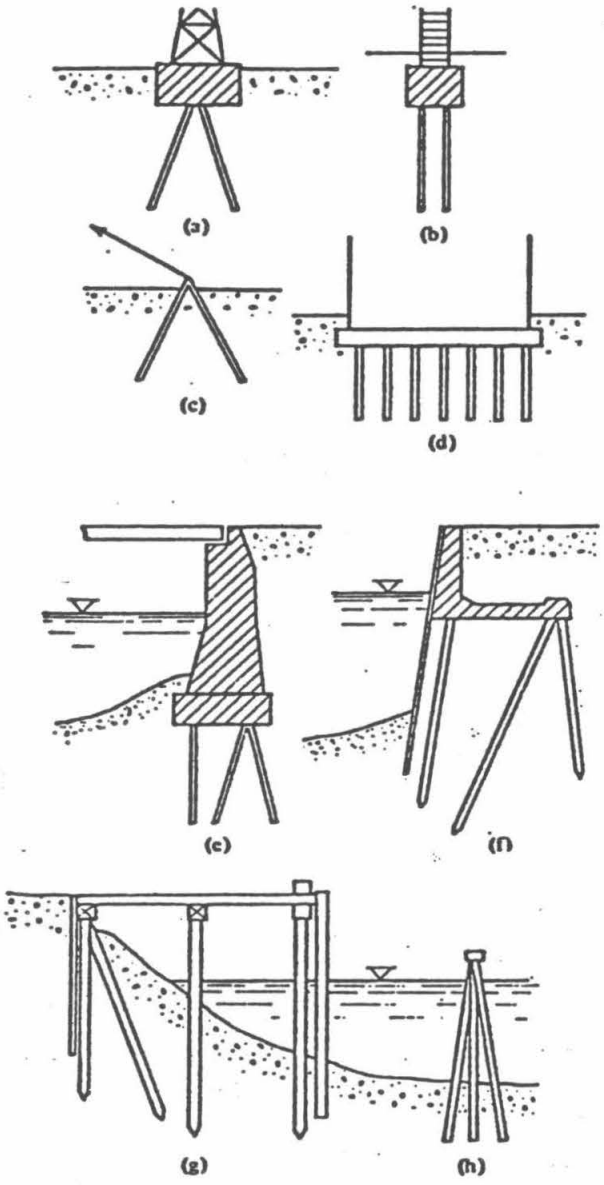

Figure 1.1 Examples of pile use (from ref. 24)

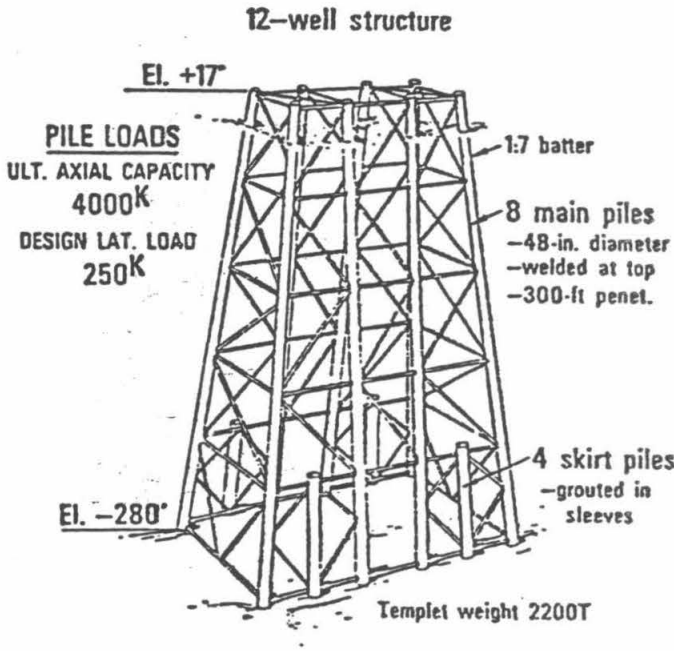

Figure 1.2 Ocean platform substructure (from ref. 28)

ground. Pile materials and installation procedures soon proliferated to the varieties in use today. Concrete and steel joined wood as common materials and drill-and-grout installation developed as an alternative to driving [18,24,51].

1.2 Fundamental Aspects of the Analysis of Piles

Foundation systems in which the pile plays a part will often demand the use of many piles, as well as other foundation elements, such as continuous footings and mats. Important foundation design problems related to pile performance include the effects of closely spaced piles on one another and the behavior of the foundation system as a whole, the interaction of the superstructure with the various foundation elements. However, the fundamental question in the design of pile foundations concerns the load-displacement behavior of a single pile. This is the starting point for calculations of the type, number, and dimensions of piles required to support a particular structure.

Of principal concern are loads applied to the pile having two orientations, along and perpendicular to the pile axis. As illustrated in Figure 1.3, below, the force F delivered to the top of the pile by the superstructure may be separated into axial and lateral components F_a and F_b, which are taken as producing pile top displacements δ_a and δ_b, respectively. The general problem of a pile in lateral loading consists in determining the relationship between the lateral forces and displacements F_b and δ_b, and the axial loading problem, the relationship between F_a and δ_a, or $\delta_a(F_a)$. It is the latter problem which is the subject of this thesis.

The axial force which a superstructure presents to the top of the pile will, in general, vary as a function of time. However, except in cases of seismic loading, which this thesis does not treat, these variations in load will take place slowly enough so that dynamic effects on pile behavior are negligible. Thus, analysis may be quasi-static, *i.e.*, it may assume that the pile is in static equilibrium at all times. It is useful to speak of a sequence of applied loads and the associated equilibrium states of the pile as a loading path, and to refer to pile conditions at specific points in the loading sequence in terms of a parameter τ which increases with time. The functional notation $\delta_a[F_a(\tau)]$ indicates the dependence of pile top behavior on the loading sequence parameter.

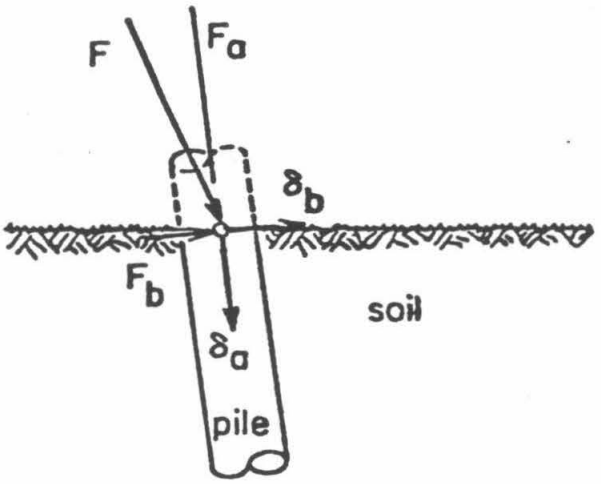

Figure 1.3 Axial and lateral loads and displacements

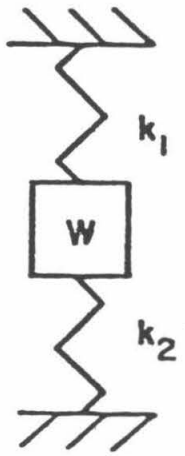

Figure 1.4 System composed of two springs bearing a weight W, in static equilibrium

The axial pile displacement δ_a associated with an applied load F_a depends on the deformational characteristics of both the pile and the soil mass in which it is embedded. The pile is composed of linearly-elastic materials and, since it is designed to withstand the very high stresses associated with driving, does not yield under static loads. The pile can be satisfactorily idealized as the one-dimensional elastic bar of classical mechanics. It is much more difficult to adequately characterize the behavior of the soil mass surrounding the pile. A fundamental reason for this is the complexity of soil material behavior. In the range of stresses to which they are exposed in the soil-pile system, soils exhibit yielding as well as reversible deformations. Their stress-strain behavior is nonlinear, the strain response to an increment of stress dependent on the current stress state. Soil behavior is also strongly dependent on stress-history, the loading path by which a certain stress state has been reached.

The extensive loading history of the soil mass in the vicinity of the pile presents another important obstacle to formulating a satisfactory description of the mechanical behavior of the soil mass. Soil investigations are carried out at any site of construction or pile load testing to determine the profile of soil types and their mechanical properties, but even when a clear picture is gained of original soil properties and *in-situ* stress states by means of laboratory and field soil testing, there is still great uncertainty concerning the stress states and mechanical properties of soil in the neighborhood of the pile following its installation, because of the intense loading of this material during that process. The matter may be viewed in terms of stress-induced inhomogeneity in the soil adjacent to the pile. If the axially-loaded pile's axis is vertical, conditions in the soil mass will have rotational symmetry about the pile axis, but the soil properties will exhibit radial inhomogeneity due to both installation and subsequent foundation loading. A specific associated phenomenon is radial soil consolidation; especially significant consolidation effects are observed in clays subjected to installation loading. Loading can also produce variation with depth in the properties of the soil near the pile. Vertical inhomogeneity may be induced in the soil mass as the result of the non-uniform distribution with depth of axial pile movements. These effects may become especially significant under conditions of repeated or cyclic loading.

There are two chief sources of difficulty in analyzing the behavior of piles in axial loading. One is the characterization of the soil mass, as discussed above. The other is soil-structure interaction. The soil-pile system exhibits a high degree of soil-structure interaction, which is to say that the deformations of the soil mass and the pile are strongly interdependent as a result of their actions on one another at their common boundary. There is an analogy with the simple mechanical system depicted in Figure 1.4, in which it is not possible to determine the force and displacement in either spring without taking into account the influence of the other. Of course, this phenomenon is much more complex in the soil-pile system. While the behavior of the pile is to a very good approximation elastic, that of the soil mass is nonlinear and stress-history-dependent. Moreover, interaction takes place all along the pile and at its base.

Two of the important quantities which characterize the interaction between the pile and the soil mass as a function of depth are soil-pile shear stress acting in the axial direction and pile axial displacement. Letting z refer to distance along the pile, these quantities are represented by the functions $t(z)$ and $w(z)$, respectively. From equilibrium of the entire pile, an applied load F_a will be met by an oppositely-directed force of the same magnitude provided by the soil mass, a net force composed of the actions of shear stresses on the sides of the pile and normal stresses on its base. Two examples of the transfer of applied load from pile to soil mass are diagrammed in Figure 1.5 below. Note the general manner in which the distribution of shear stress along the pile sides, $t(z)$, and the proportion of the total applied load carried by the the pile base depend on the soil and pile properties.

The pile axial displacement $w(z)$ is equal to δ_a at the top of the pile. Elsewhere along the pile, the pile and soil mass displacements are closely related. If the possibility of sliding between soil and pile is disregarded, the deformations of the soil mass and pile are governed by the condition that their displacements must match at their common boundary. If sliding is taken into account, soil and pile displacements must differ by the sliding displacements. At every point τ on a loading path, the shear stress and displacement distributions along the length of the pile, $t(z,\tau)$ and $w(z,\tau)$, represent stress and displacement boundary conditions under which the pile and soil mass balance in equilibrium with one another.

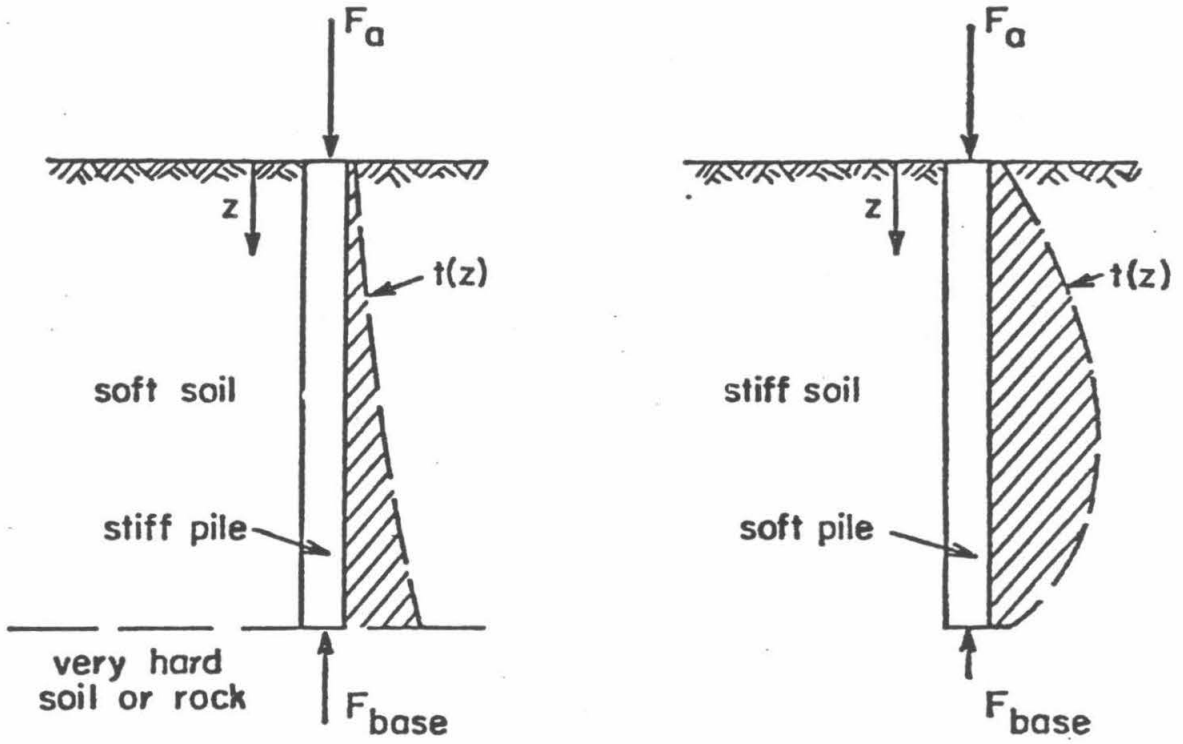

Figure 1.5 Examples of pile load transfer (Note: If the pile has length L and a circular cross-section of diameter D, then

$$\pi D \int_0^L t(\xi)\, d\xi = F_a - F_{base} \ .)$$

The nonlinear and history-dependent behavior of the soil mass and soil-structure interaction along the length of the pile are reflected significantly in the behavior of the soil-pile system. As a result of soil yielding, the soil-pile system exhibits permanent deformations and hysteresis. Soil yielding along the length of the pile produces "residual" forces in the pile; that is to say, non-zero, locked-in axial forces are present at system equilibrium under zero applied load. These forces are important in the interpretation of instrumented pile tests.

Both nonlinear and history-dependent aspects of soil behavior are reflected in the phenomenon of effective fatigue failure under cyclic loading. Suppose that a pile is subjected to persistent cycling from zero applied load to a value of compressive load F_a^{max}. Under usual conditions, a single application of monotonically increasing force causes yielding in the soil mass to progress downward from the top of the pile. For a sufficiently high value of F_a^{max}, say $F_a^{max^*}$, cycling will cause the gradual accumulation of soil strength loss, beginning at the top of the pile, spreading downward, and culminating in complete pile failure. $F_a^{max^*}$ may be as little as one-half of the bearing capacity of the soil-pile system in its original condition.

1.3 Current Purposes and Methods of Pile Analysis

The fundamental features of soil-pile systems have now been described, and the intrinsic complexities of analyzing these systems explained. Despite its formidable difficulties, the problem of pile analysis is the object of a large volume of current research. The accomplishments and shortcomings of this activity are best understood by reference to its practical objectives.

1.3.1 Ocean Structure Applications

The primary motivation for research into foundation pile behavior during the past decade has been the very significant use of piles in supporting offshore oil drilling and production platforms. The first offshore oil platform was constructed in 1947, off the coast of Louisiana. It is estimated that offshore production supplied 16% of the world's oil in 1970 and more than 30% (20,000,000 barrels per day) in 1980 [18]. Associated with this swift production growth has been a rapid increase in the depths of water in which platforms are constructed. Piles have proven an indispensable element in the

foundations for offshore platforms, serving to transfer to competent levels in the sea-floor soils forces due both to the weight of the platform and substructure and to wave action on the substructure.

Ocean structure applications present a great challenge to pile analysis. Severe performance requirements for these structures create a demand for knowledge of axial pile top response $\delta_a[F_a(\tau)]$ for a wide range of pile load levels and loading sequences. On land, piles are usually emplaced vertically and loaded only in compression, by the weight of the superstructure. Hence, traditional concerns of analysis have been with pile compressive bearing capacities and settlements under applied loads which are constant in time. In contrast, piles for ocean structures must sustain tensile axial loads as well as compressive ones, and loads varying considerably with time. One of the loading sequences very commonly of concern here is the cyclic axial pile loading which will be generated by the action of waves or ocean swells on a platform substructure.

Another challenging aspect of pile analysis for ocean structures applications is the comparative dearth of empirical data available in this regime. Because predicting the behavior of soil-pile systems on the basis of fundamental pile and soil characteristics has inherent difficulties related to the complexity of soil mass behavior and soil-structure interaction, extrapolation from observations of the performance of similar piles in similar soils has traditionally been the primary means of prediction. Terzaghi and Peck [51], in 1948, warn of the unreliability of formulas for bearing capacity based on driving records, discourage attempts at theoretical refinements such as application of the theory of elasticity, and praise the common practice of conducting pile load tests at the construction site. More recently Meyerhof [30], in his 1975 Terzaghi Lecture to the ASCE, "Bearing Capacity and Settlement of Pile Foundations", recommends the use of pile load tests and empirical correlations in a broad range of cases. However, empirical data is in very short supply in the offshore area. Foundation piles for ocean structures are typically on a different scale from those used on land; they may be 500 feet in length and 10 feet in diameter, three or four times the size of the largest land piles. As a result, the large body of empirical knowledge about the behavior of piles on land can be extrapolated to ocean piles only with great uncertainty. As yet, there have been few load tests of very large, offshore-scale piles, and little information is available concerning the performance of piles beneath existing ocean structures. Most

important of all, pile load testing at the construction site is severely limited. Preliminary or design-phase load tests are usually prohibited by the high costs of taking pile installation equipment to the ocean site at this stage. Even during construction operations, it may be a practical impossibility to test piles over more than a small interval of the full loading range of interest.

In summary, requirements for improved analysis of foundation pile behavior are today largely defined by the needs of ocean structure applications, as a result both of the significant technical challenge presented by this problem and the great economic rewards which its solution offers. Pile analysis for ocean construction is called upon for the characterization of axial pile behavior $\delta_a[F_a(\tau)]$ under a wide variety of loadings, while it works from minimal empirical information concerning the behavior of similar piles in similar soils under the relevant loadings. As a response to these requirements, analysis has turned to (a) computational models of pile-soil systems and (b) physical model testing. These two approaches will now be discussed in turn.

1.3.2 Computational Models

Certain simple computational models for bearing capacity merely divide the total action of the soil mass on the pile into components acting on the base of the pile and on its sides. An example of a model of this kind is the following formulation for preliminary estimation of the bearing capacity of land piles under compressive loading: Using the notation of Meyerhof [30],

$$Q_u = Q^p + Q_s = q_p A_p + f_s A_s$$

where Q_u is the ultimate bearing capacity, Q_p the total force on the pile base, Q_s the force on the pile sides, q_p the average soil resistance on the pile base per unit area, f_s the average soil resistance on the pile sides per unit area, and A_p and A_s the areas of the pile base and sides, respectively. In estimating the bearing capacity of a given pile at a given site, the quantities q_p and f_s are chosen on the basis of the soil mass characteristics as determined from both laboratory and field tests. Various empirical correlations have been drawn between measured soil properties and the quantities q_p and f_s [30,53,55]. However, because the observational basis for these correlations is composed almost entirely of land pile tests, this computation is far more satisfactory in applications on land than offshore. First, the

empirical correlations between q_p and f_s derived from the performance of land piles may be greatly in error if applied to the much larger ocean piles. In addition, only initial compressive bearing capacity is treated, of the entire range of soil-pile system behavior under load $\delta_a(F_a)$ which is of concern offshore.

Simple, highly empirical models such as the above bearing capacity formulation may be surpassed in effectiveness for offshore pile analysis by more detailed, mechanistic computational models, which distinguish the action of the soil mass at points all along the pile. By discriminating the particular features of a soil-pile system which determine its behavior, such models can filter the available empirical data and utilize this scarce commodity more efficiently. Accurate extrapolation from empirical observations is made possible over expanded ranges of variation in pile and soil mass characteristics, and installation procedures. For example, if thin lenses of dense sand at a certain construction site contribute a significant proportion of the total soil mass resistance, the effect on pile behavior of the presence or absence of such lenses at a given pile location can only be properly accounted for by a model which distinguishes soil-pile interaction as a function of depth. Another advantage of detailed mechanistic models in offshore applications lies in their ability to provide a unified picture of pile behavior $\delta_a[F_a(\tau)]$ under a variety of loadings. In such models, the same mechanisms will often operate in simulating the response of the soil-pile system to unloading, tensile loading, or cyclic loading as operate in describing the compressive loading response, so that from knowledge of system behavior under one kind of loading, behavior under other loadings can be inferred. In contrast, the above bearing capacity formulation $Q_u = Q_p + Q_s$ only speaks about the load at the end point of a path of monotonically increasing compressive loading. An analogous formulation to address displacements associated with single compressive loading, or $\delta_a[F_a(\tau)]$ behavior under other loading sequences, must be based on a completely different set of empirical data. The principal mechanistic computational models currently in use for the analysis of piles in axial loading will now be discussed.

The ideal computational model would accurately predict pile behavior from descriptions of the pile, soil mass, and installation procedures alone. Only soil investigation would be required for pile design analysis. There would be no dependence on empirical information about pile performance elsewhere or pile tests. Unfortunately, no such ideal models have been developed which are accurate over

a broad range of pile and soil types, and so on, because of the inherent analytical complexities of the soil-pile system: soil mass characterization and soil-structure interaction. (See section 1.2, above.) However, models based on fundamental soil mass and pile properties are under development along two main lines, the finite element method and a technique which will be referred to here as the "boundary integral" method.

The finite element method [20,56] holds great promise for modeling soil-pile system behavior from fundamental pile and soil mass characteristics, because it is well suited to the incorporation of complex soil material behavior. The method involves the division of the continuum consisting of the pile and the soil mass into a patchwork of elements. (Since the problem of a pile in axial loading is axisymmetric, the finite element mesh here is two-dimensional.) Each element exhibits its own individual material behavior, so that soil-pile interaction and soil mass inhomogeneity are incorporated in a natural way. Elements of the soil mass may show both nonlinear stress-strain behavior and changes in their properties as a result of loading, that is, history-dependent material behavior.

Many different workers have participated in the development of finite element models for pile behavior under axial loading. (See references 2, 3, 10, 14, 16, 17, and 19.) In addition to modeling the soil mass as a homogeneous, linearly-elastic body, spatial variations in the elastic moduli and non-linear stress-strain behavior have been introduced. However, no significant progress has been made in applying these models to loading-history-dependent behavior of the soil-pile system, or to extensive loading paths, beyond single loadings in compression or tension. A important difficulty is presented by uncertainty about the effects of pile installation procedures in changing the mechanical characteristics of soil near the pile and generating a system of residual stresses in the soil-pile system as a whole [3,11]. The most accurate and efficient representation of soil material behavior, the constitutive properties to be ascribed to the soil elements of the model, is another matter not fully resolved [9]. These difficulties prevent the prediction of soil-pile system behavior starting from fundamental information characterizing the soil mass and pile. In their present state of development, finite element models for general piles, soils, and installation procedures depend heavily on empirical observations of pile behavior [14].

The scope of "boundary integral" methods is narrower than that of finite element models because they are, in essence, capable of simulating the behavior of the soil mass only as an elastic body. The boundary integral method is based on the Mindlin solution for the stresses and displacements due to a point load acting within a homogeneous isotropic elastic half-space [31]. The soil mass deformations are calculated as the solution of an integral equation for which the Mindlin result provides the kernel. The domain of integration is the interface between the soil mass and the pile, S, the combined external surfaces of the pile walls and base. Adopting the index notation for vectors of Butterfield and Banerjee [7], the displacement U_i at any point B on the surface S is related to the traction T_j at any point A by the operator due to Mindlin, K_{ij}:

$$U_i(B) = T_j(A)K_{ij}(A,B)$$

Thus, the total displacement at B due to all the forces acting on the soil-pile interface is

$$U_iB = \int_S T_j(A)K_{ij}(A,B)ds \tag{1.1}$$

Displacement boundary conditions $U_i(B)$ on S are available in the case of a rigid pile, and the elastic half-space deformation is given directly by the numerical solution of equation (1.1). The behavior of a soil-pile system with a deformable pile may be found iteratively, alternating between the soil mass deformation computations just described and simple computations of the deformation of the pile as a one-dimensional elastic bar [7]. Banerjee [4] has placed this boundary integral method into perspective with regard to all uses of integral equation methods in elastostatics, and generalized it to apply to piecewise homogeneous elastic bodies. Using the more general boundary integral formulation, the soil mass can be represented as approximately a Gibson soil, an elastic medium in which Young's modulus increases linearly with depth [5,21,39].

Boundary integral models, because they depend directly on "elementary solutions" from the theory of elasticity, are applicable only to soil-pile systems and loading sequences such that the behavior of the soil mass is well characterized as elastic. Thus, these models are not suited to the simulation of pile system behavior which reflects the nonlinear stress-strain and stress-history-dependent behavior of

the soil. Compared to finite element models, they have little potential for development as general models for the prediction of soil-pile system behavior from fundamental soil mass and pile characterizations.

A third important class of mechanistic models for pile behavior under axial loading is that of "t-z" models. While finite element and boundary integral models have fundamental information about the soil mass, pile, and installation procedures as their independent variables and input parameters, and are oriented toward prediction of soil-pile system behavior independent of empirical data, t-z models are based directly on empirical observations of soil-pile system behavior. Their primary purpose is to improve the accuracy of extrapolation from empirical data by taking advantage of information about soil-pile interaction along the full length of the pile.

A significant capability of t-z models is the direct interpretation of soil-pile system behavior on the basis of the functions $t(z,\tau)$ and $w(z,\tau)$ measured in tests on instrumented piles. [The term "t-z" derives from the use of the symbols t and z to denote the functions t(z) and w(z) respectively.] Recall that $t(z,\tau)$ and $w(z,\tau)$ represent soil-pile shear stress and pile displacements, respectively, as functions of both depth along the pile and position within the loading sequence. Simple, exact formulas relate these two functions to a third function, $f(z,\tau)$, the most direct result of a load test on a pile instrumented with strain gauges along its length, as follows. The function $f(z,\tau)$ represents the axial force in the pile at depth z and stage τ in a given loading sequence. Introducing the additional notation, for the pile material,

$$\sigma(z) = \textit{axial normal stress},$$

$$\varepsilon(z) = \textit{axial normal strain},$$

$$E = \textit{Young's modulus}$$

and

A = *cross-sectional area.*

since the pile material remains elastic,

$$\sigma(z) = E\varepsilon(z) \tag{1.2}$$

In addition,

$$f(z) = A\sigma(z) \tag{1.3}$$

$$\varepsilon(z) = \frac{dw(z)}{dz} \tag{1.4}$$

so that

$$f(z) = EA\,\frac{dw(z)}{dz} \tag{1.5}$$

$$w(z) = \frac{1}{EA}\int f(\xi)d\xi \tag{1.6}$$

Denoting, furthermore, the circumference of the pile by S,

$$t(z) = \frac{1}{S}\,\frac{df(z)}{dz} \tag{1.7}$$

Instrumenting a test pile with strain gauges at points distributed along its length enables interpolation of the function $\varepsilon(z)$ at any point τ in the loading sequence. $f(z,\tau)$, $t(z,\tau)$, and $w(z,\tau)$ are then available immediately from the above relations.

A principal way in which t-z models are put to use is the "transfer function method". First proposed by Seed and Reese [49] in 1957, the transfer function method utilizes "t-z curves", plots of soil-pile shear stress (or "load transfer") $t(z,\tau)$ versus pile displacement $w(z,\tau)$ at a given depth z for τ traversing the loading path of interest. In order to predict the behavior $\delta_a[F_a(\tau)]$ of a given soil-pile system, a set of t-z curves pertaining to all intervals of depth along the pile is prepared from suitable records of load tests on similar piles in similar soils. The reaction of the soil to pile movements all along the soil-pile interface having been established in this way, the pile movements $w(z)$ associated

with any value of applied load F_a can be found from equations (1.5), (1.6), and (1.7), above, by iterative calculation procedures [12,49].

The transfer function method has proven useful for calculating the behavior $\delta_a(F_a)$ of piles for ocean structures. The study of Coyle and Reese [12] referred to in the 1980 American Petroleum Institute Recommended Practice bulletin [1] is a good example of the application of this method. Working from published results of three field load tests on driven steel piles in clay and a series of laboratory tests on small piles, Coyle and Reese established correlations between pile displacement $w(z)$ and the ratio of load transfer $t(z)$ to soil shear strength for three depth intervals: 0-10 feet, 10-20 feet, and below 20 feet. In Figure 1.6, below, the t-z curves corresponding to these depth intervals are A', B', and C', respectively. Having normalized soil properties with respect to shear strength, Coyle and Reese proposed the applicability of their t-z curves to all cases of driven steel piles in clay for depths up to 100 feet. In a separate, direct application of the transfer function method to piles for ocean structures, McClelland [28] achieved good correspondence with the observed $\delta_a(F_a)$ behavior of a steel pipe pile embedded to a depth of 333 feet in under-consolidated clay by normalizing soil properties with respect to a quantity involving both effective vertical stress $\bar{\sigma}_v$ and undrained shear strength, c_u, as illustrated in Figure 1.7, below.

While the use of t-z models in the transfer function method is simple and based on concrete empirical data, these models exhibit the general advantages of mechanistic computational models for the soil-pile system. First, variation in the characteristics of the soil mass with depth is taken into account. In combination with empirically derived t-z curves, Coyle and Reese [12] and McClelland [28] have employed expressions involving soil shear strength as a function of depth. An analogous expression for sands is $p\tan\varphi$, where p is the effective vertical stress, *i.e.*, the effective stress acting on horizontal planes, and φ the friction angle of the sand [13,53]. A second benefit of the mechanistic t-z model is that it can simulate system behavior for a variety of loadings, presenting a unified picture of the soil-pile system behavior associated with the extensive loading paths, including tensile and cyclic loading, of concern in offshore applications. The t-z studies discussed above treated only behavior under a single application of compressive load. However, t-z models are equally suitable for

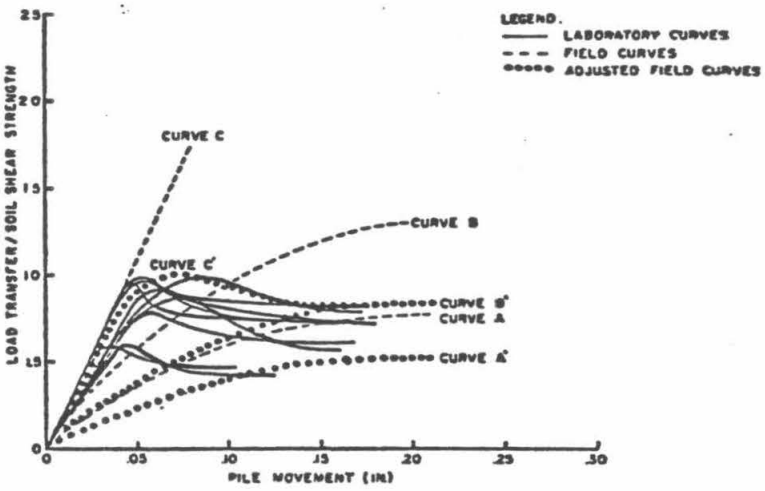

Figure 1.6 t-z curves (from reference 12)

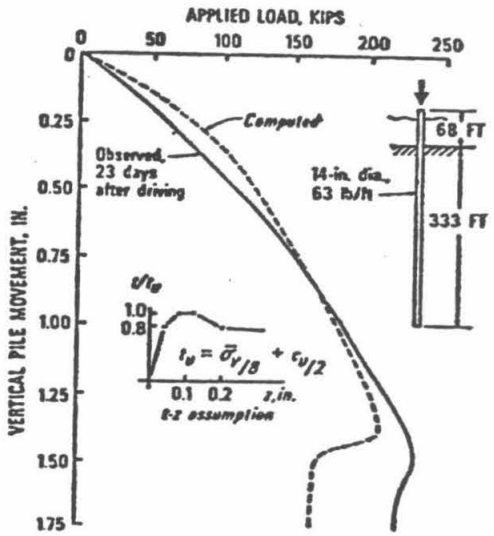

Figure 1.7 t-z analysis applied to a large ocean pile (from reference 28)

interpreting, simulating, and correlating observed axial soil-pile system behavior under general sequences of loading. Here, the models shed light on primary soil-pile interaction phenomena such as distributions of residual soil-pile shear stress.

A natural development from the use of t-z models for direct extrapolation from empirical data is the attribution of mechanical characteristics to the soil mass in these models. Indeed, the distribution of t-z curves along the pile developed to describe the reaction of the soil mass to pile movement at any depth can be likened to an ensemble of independent, general, black-box mechanisms, as illustrated in Figure 1.8, below. Meyer [29] and Matlock and Foo [24] have presented models in which the black-box mechanisms are identified with specific mechanical analogs composed of springs, dash-pots, and friction blocks. These models can simulate the nonlinear stress-strain and loading- history-dependent behavior of soil-pile systems under axial loading, including the degradation of system strength as a result of cyclic loading.

Significant insight can be gained into soil-pile system behavior by using simple force-displacement relations for the t-z mechanisms. Assuming t-z behavior to be represented by a distribution of linear springs gives a simple, useful model analogous to the classical Winkler treatment of surface subgrade reaction. Scott [48] has given a thorough discussion of both purely elastic Winkler models and models in which elastic-perfectly plastic behavior, as illustrated in Figure 1.9 below, is ascribed to the mechanical elements. He outlines solutions for a variety of distributions with depth of Winkler stiffness k and soil-pile interface yield stress t_y.

The primary purpose of t-z models is extrapolation from empirical data. Employed for this purpose, the t-z model has significant advantages over finite element and boundary integral models. First, it provides a simple and logical method for the prediction of pile behavior. When empirical information concerning the behavior of similar soil-pile systems becomes abundant the proper way of implementing the t-z model will be clear. Under these circumstances, well within the range of reliable extrapolation, the complexities and uncertainties of characterizing soil material behavior and soil-structure interaction for finite element and boundary integral models are minimized in applying the t-z model. Here the model is purely empirical, there are no assumptions. This is one important reason that t-z

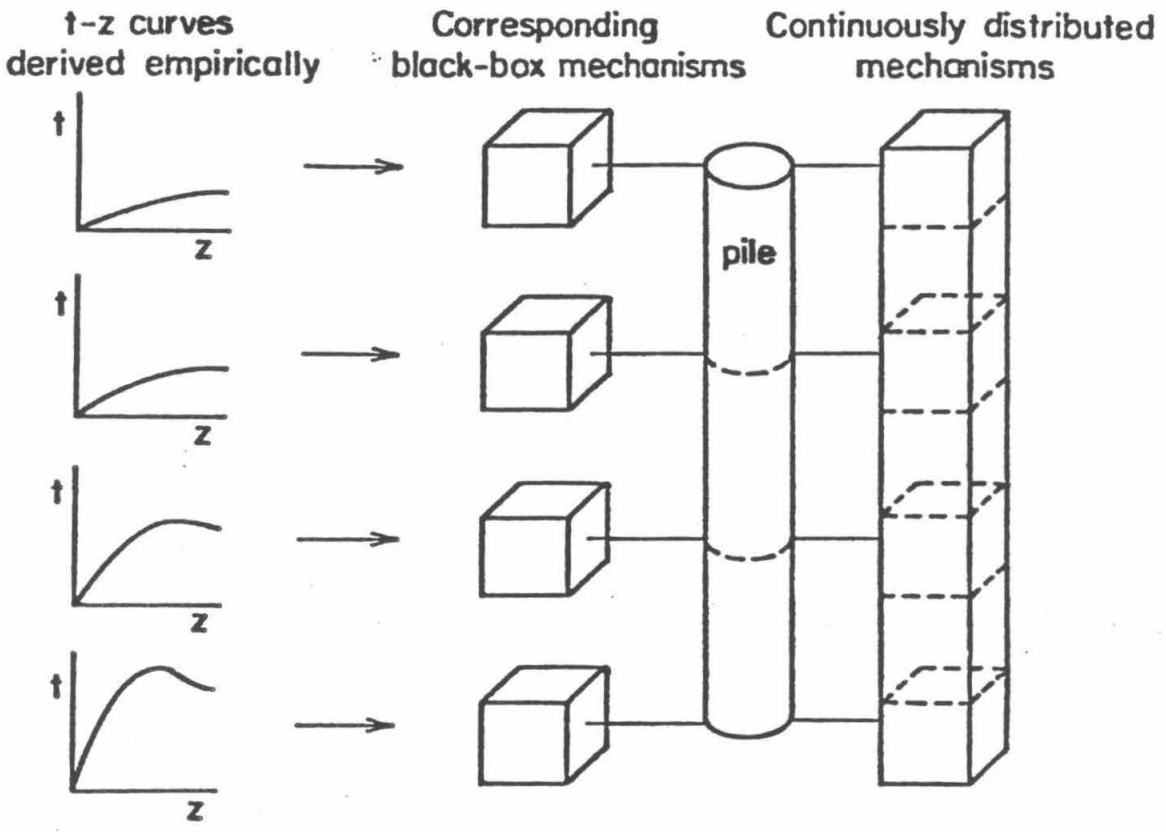

Figure 1.8 t-z curves as general mechanisms

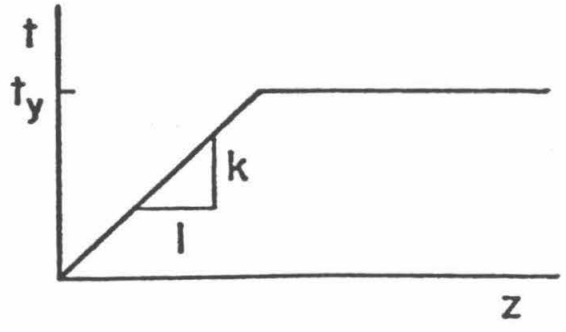

Figure 1.9 Elastic-perfectly plastic t-z behavior

models have already received wide application. Another significant capability of the t-z model is the thorough and veracious interpretation of pile test data. Just as $\delta_a[F_a(\tau)]$ is the complete result from a test in axial loading of a soil-pile system monitored at ground surface, the functions $t(z,\tau)$ and $w(z,\tau)$ are the essential results of a test on a pile instrumented with strain gauges. Beyond the direct predictive value of t-z analysis, it leads to improved understanding of the axial loading problem through the accumulation of detailed experimental results. In particular, the use of t-z models can contribute to the development of finite element models, both by indicating the primary soil-pile interaction mechanisms which these models should show, and, more generally, by providing direct information on shear stress and displacement conditions at the crucial boundary between the soil mass and the pile.

While t-z models provide simple and accurate means of predicting soil-pile system behavior when empirical data is abundant, when information concerning similar systems is scarce and extrapolation must be carried out over greater ranges of disparity in soil mass and pile characteristics, installation procedures, or loadings the simplicity advantage of t-z models gives way to concerns over diminished reliability. The following aspects of the t-z model limit its range of reliable extrapolation:

1. The behavior of the soil mass as a mechanical continuum is neglected. The deformational behavior at any point along the pile is treated as if it were independent of deformations elsewhere. Thus, for example, the deformation of the soil mass as a continuous elastic body is not accounted for. Recalling the conception of t-z relationships as independent black-box mechanisms, note that the displacement $w(z')$ at a point z' along the pile is attributed entirely to the corresponding shear stress $t(z')$. The elastic displacement at point z' in the soil mass due to the distribution of shear stresses $t(z)$ acting on the soil mass elsewhere along the pile is not taken into account.

2. Extrapolation of soil mass t-z behavior must be based on correspondences in soil mass properties measured by means of field and laboratory soil tests. As a result of the intense loading of the soil in the vicinity of the pile associated with pile installation procedures, there is great uncertainty concerning initial soil properties in this crucial region.

3. Because the soil mass is not represented as a continuum but as the more artificial ensemble of black box mechanisms, the relationship between its characterization in the soil-pile system and its properties as determined in soil tests is not well-defined.

The t-z model extrapolation limitations 1, 2, and 3 essentially represent limitations on the capability of the model to predict soil-pile system behavior on the basis of fundamental information describing the soil mass, pile, and installation procedures. The mechanistic computational models in which the soil mass is represented as a continuum, finite element and boundary integral models, share limitation 2. However, limitations 1 and 3 make t-z models inherently less suited to prediction from fundamental system specifications, and hence to broad extrapolation from empirical data, than finite element models.

1.3.3. Physical Model Testing

Pile analysis turns to physical model testing as well as computational models in an effort to satisfy the requirements of ocean structure applications for insight into pile behavior under axial loading. It is desired to extract information concerning the behavior of the very large piles used in ocean construction from tests on much smaller soil-pile systems which are carried out in the laboratory. However, direct scale modeling is not satisfactory. If the model soil mass is composed of material resembling the field site soil in density, homologous points in the field soil mass and its scale model are overlain by differing depths and weights of soil. The resulting significant difference in stresses causes significant deviation of the model soil-pile system behavior from that of a full-scale system. For example, because of the much smaller range of effective vertical stresses in the model soil mass, the frictional component of the soil's shearing resistance at the deepest intervals along the pile is much less in the model than in the corresponding prototype field system.

The best way of overcoming the problem of soil weight is by centrifugal modeling. This technique involves swinging the soil-pile model in a bucket in the centrifuge so that the accelerations downward along the model's vertical axis are greatly magnified from those which earth's gravity alone would produce. In this way, the "weight" of the soil may be increased and the associated stresses in a small model made to match those acting on a very large pile-soil system. Scale modeling in large

centrifuges has been applied to a wide variety of soil mechanics problems. Smith [50] presents an extensive review of this work to 1977.

It is easy to calculate the "gravitational" acceleration to be applied to the model using the centrifuge in order that the model vertical stresses associated with soil weight match those acting in a large soil-pile system. Using the notation

σ_p...vertical stress due to soil weight in the prototype soil-pile system,

σ_m...vertical stress due to soil weight in the model soil-pile system,

L_p...characteristic length in the prototype soil-pile system,

L_m...characteristic length in the model soil-pile system,

g_p...acceleration due to earth's gravity, g,

g_m..."gravitational" acceleration which acts in the model soil-pile system,

ρ_p...soil density in the prototype soil-pile system,

ρ_m...soil density in the model soil-pile system,

and

n...desired prototype-model length scaling factor, L_p/L_m,

$$\sigma_p = \rho_p g_p L_p \text{ and } \rho_m g_m L_m$$

Since the soil materials of the model and the prototype are the same ($\rho_p = \rho_m$),

$$\sigma_p = \sigma_m \text{ implies } g_p L_p = g_m L_m,$$

and

$$\frac{g_m}{g_p} = \frac{L_p}{L_m} (=n)$$

That is, an acceleration field of strength *n times* g must be applied to the model soil-pile system if its behavior is to match that of a prototype system greater in linear dimension by n times. Other important scaling relations for the interpretation of a model pile test at n g's, which can be determined

similarly, include those for forces, $F_p = n^2 F_m$, and for strains, $\varepsilon_p = \varepsilon_m$. Note that both stress and strain quantities are the same in the model and the prototype systems. Because of this fact, the stress-strain behavior of the soil at a field site can be directly matched by the use in the model of soils taken from the site.

Physical model testing using the centrifuge is capable of contributing significantly to the prediction of pile behavior under axial loading for offshore applications. Like mechanistic computational models, it will yield information on soil-pile system behavior for the wide variety of loadings which are of interest in ocean construction and it is applicable to systems featuring a broad range of piles, soil masses, and installation procedures, including the very large piles used offshore. Centrifugal modeling has a significant advantage over computational models in that it is not dependent on empirical data taken from field pile tests. The t-z, boundary integral, and finite element models have all been seen, at their current states of development, to depend significantly on empirical information because of the difficulties of identifying and representing complex soil mass behavior. In physical models, using soil samples taken from the construction site at relatively low cost, soil mass behavior is represented directly.

The process of load testing a model pile in the centrifuge is just like executing a load test in the field. The axial loading sequences which are of practical concern are applied to the top of the model pile and its behavior is expected to correspond directly, in accordance with the scaling relations, to the behavior of a definite field prototype. If it is desired to investigate soil-pile interaction along the length of the prototype pile, the model pile may be instrumented with strain gauges and its behavior interpreted using t-z analysis. Ideally, then, centrifugal modeling should produce the same information as the corresponding field load test, at greatly reduced expense.

The key obstacles to the broad, successful use of centrifugal modeling in piles analysis are (a) technical difficulties associated with carrying out load tests in the spinning centrifuge and (b) defects in the fidelity with which the soil-pile system model represents the assumed prototype. During testing, the model resides in a container at the end of the centrifuge arm, which is rotating at a constant speed. The experimenter can exert influence on the model and communicate with it, e.g., apply loads to the

pile top and take strain gauge readings, only by means of electrical and hydraulic sliprings. As a result of the severe constraints on manipulating the soil-pile system under these conditions, it is very difficult to emplace the model pile in the soil after the centrifuge has been set into motion. Therefore, emplacement is usually carried out under 1-g conditions, before centrifuging. When the model pile has been installed in this way, the installation procedure for the associated prototype system corresponds more closely to the drill-and-grout method of installing piles in the field than to driving methods, in that the pile does not displace soil material as it is emplaced. However, this correspondence is not precise, for the increase in "gravitational" forces as the centrifuge is brought up to test speed causes additional deformations of the model soil-pile system.

These technical constraints on the simulation of field pile installation cause uncertainty concerning the correspondence of the initial conditions of the soil masses in the model and prototype. Other features of the centrifugal modeling technique which may cast doubt on the essential assumption of model- prototype correspondence are the following:

1. **Construction of the model soil mass.** Reconstruction of the depth profile of soil materials at the construction site using prototype materials is straight-forward, but greater difficulties are encountered in seeking an appropriate match between the conditions of the soil mass *in-situ* in the field and remolded in the model. Proper packing of sands and consolidation of clays are important.

2. **Grain size scale effects.** The accuracy of the central modeling assumption that the model and prototype soil materials exhibit identical stress-strain behavior depends on the relative sizes of the model pile and the soil grains. It is assumed that the soil will act as a continuum and not express its particulate nature. But if, for example, a coarse sand is used in the model in conjunction with a small-diameter model pile, relatively few particles are in contact with the pile and the continuum assumption breaks down [41].

3. **Non-uniformity of acceleration field.** The strength of the acceleration field produced by the centrifuge is proportional to the radial distance from the centrifuge axis, that is, to depth in the soil-pile model. As a result, a cylindrical pile corresponds to a prototype pile the diameter of which increases with depth, as illustrated in Figure 10 below. The radial variation of accelerations is more

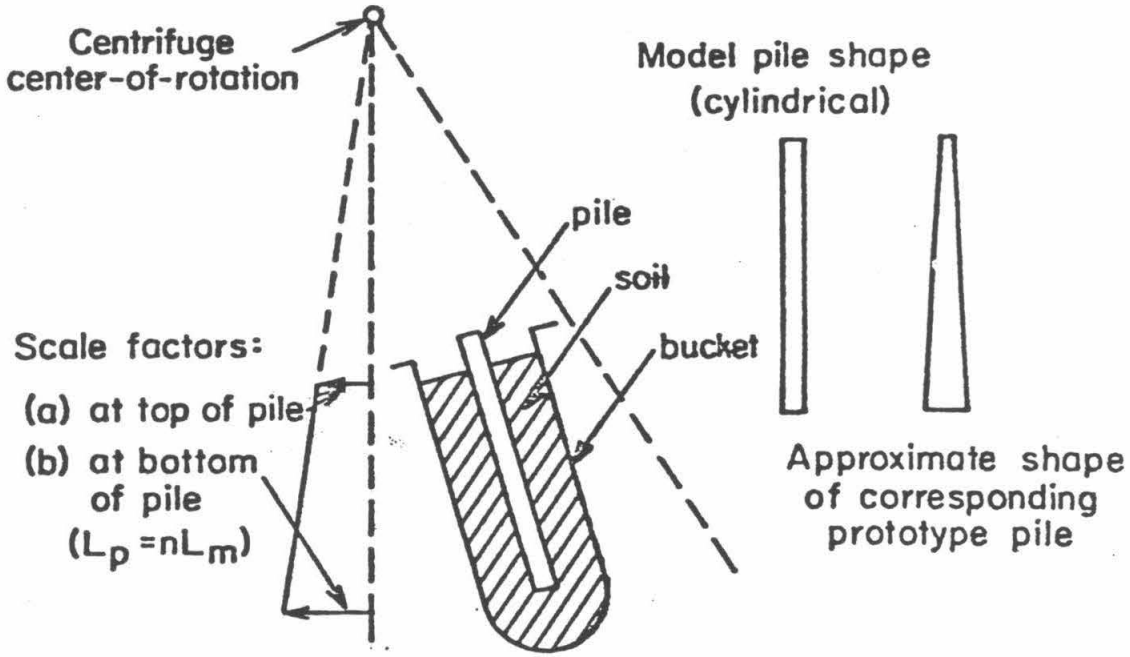

Figure 1.10 An effect of acceleration field non-uniformity

important in the centrifugal modeling of piles than other geotechnical structures because of the large vertical dimension of piles.

The influence of sources of disparity 2 and 3, above, between the centrifugal model and its assumed prototype can be reduced by employing larger centrifuges. The longer the centrifuge arm, the smaller the variation in scaling factor will be between the top and bottom of a model pile of a given length. In a centrifuge capable of bearing larger soil-pile models to a given level of accelerations, the continuum assumption applied to the soil material is accurate over a wider range of soil grain sizes.

Centrifugal modeling is useful for two kinds of pile axial loading investigations. The first of these is the direct investigation of the behavior of a given pile in a particular soil mass, for example, the assessment of pile behavior for the foundation of an offshore platform at a given site. In such an investigation the distribution of various soils and their conditions *in-situ* will be reproduced as faithfully as possible. The advantages and limitations of centrifugal modeling used in this way have been discussed. The second kind of investigation involves pile testing in common uniform soils. Because they provide information on soil-pile behavior in typical, ideal soils, the results of such centrifugal modeling tests are well suited to all of the following uses:

1. Serving as points of reference for the design of similar piles in similar soils by extrapolation.
2. Studying general principles of soil-pile system behavior and developing procedures for proper design extrapolation from field test results.
3. Providing data for refining finite element models for the calculation of soil-pile system behavior from fundamental (directly measurable) soil mass and pile characteristics.

1.4. Summary of the Current State of Analysis and Prospects for Advancements

Throughout the 1980's and beyond, the demands of ocean structure applications will continue to provide a major impetus to achieving improved understanding of the behavior of piles in axial loading. Pressure will therefore remain high to substitute the use of physical and computational models for expensive empirical data gathering, and to develop the reliability of these analytical tools. The

principal uses and limitations of those models which appear to be most useful and promising are now reviewed:

1. t-z Models—The transfer function approach is used to predict pile behavior by extrapolation from empirically-derived t-z curves. In addition, t-z analysis produces the essential data from load tests on strain gauge-instrumented piles. However, the range of extrapolation of t-z models is limited because of their complete dependence on empirical data.

2. Finite Element Models—Because their natural basis is in fundamental soil mass and pile characteristics, finite element models are potentially very powerful. Due to complexities in identifying and representing soil mass characteristics, especially in the crucial region in the vicinity of the pile, significant refinement of these models is required if they are to achieve broad usefulness.

3. Centrifugal Models—Ideally, centrifugal modeling in the laboratory will produce the same information as a field load test. It can be applied to specific site soil profiles or to ideal homogeneous masses. Uncertainties about the correspondence of model and prototype soil-pile systems represent the major limitations of centrifugal modeling.

The three modeling methods above have uses and limitations quite distinct from one another and they are based on different kinds of input information. Because of this distinctness, the use of each model complements that of the others. Combining in use two or three of these kinds of models yields increased accuracy in the prediction of the behavior of a given soil-pile system. Furthermore, such combination promotes the general understanding of pile behavior under axial loading and effective utilization of the individual models. For example, finite element models can be refined by checking the simulation of soil behavior which they produce against t-z behavior observed both in field load tests and in centrifuge models involving ideal homogeneous soils. The ranges of validity of the transfer function method and centrifugal modeling can each be investigated using the other in establishing reference points.

CHAPTER 2

GENERAL FEATURES OF THE CENTRIFUGE MODEL PILE EXPERIMENTS

The results of five centrifuge model pile tests on instrumented piles are reported. The model soil-pile systems in these tests correspond to the following prototype systems:

Test 1. A cylindrical steel pile of diameter approximately 4 feet, wall thickness 1.0 inch, and stiffness, EA, about 4 million kips, embedded to a depth of about 180 feet in dry fine sand.

Tests 3 and 4. Cylindrical steel piles of diameter approximately 1.5 feet, wall thickness 0.35 inch, and EA about 500,000 kips, embedded to depths of about 55 feet in dry fine sand.

Tests 5 and 6. The same piles embedded to depths of about 55 feet in saturated fine sand.

The five tests share many features of apparatus, model preparation, procedure, and interpretation. These common aspects are described in the present chapter, as a basis for the descriptions of the individual tests and their results in Chapters 3 and 4.

2.1. Apparatus

2.1.1. Centrifuge

These tests were run using the Caltech geotechnical centrifuge. A full description of this machine has been given by Scott [41]. Its most important features are the following:

1. The centrifuge is rated at 10,000 g-pounds payload capacity. Thus, for example, it can carry a 100-pound payload to 100 g's acceleration.

2. The payload, in the present case a cylindrical bucket containing the soil- and-pile model, is suspended from bearings located 36 in. along the arm of the centrifuge from its center of rotation. The centrifuge is shown in Figure 2.1, below, carrying other payload containers.

3. The soil and model pile are placed into the special container with the centrifuge at rest (1-g). As the centrifuge is brought up to test speed, the bucket rotates in its bearings at the end of the centrifuge arm so that the net acceleration applied to the model is always directed "downward" along the pile.

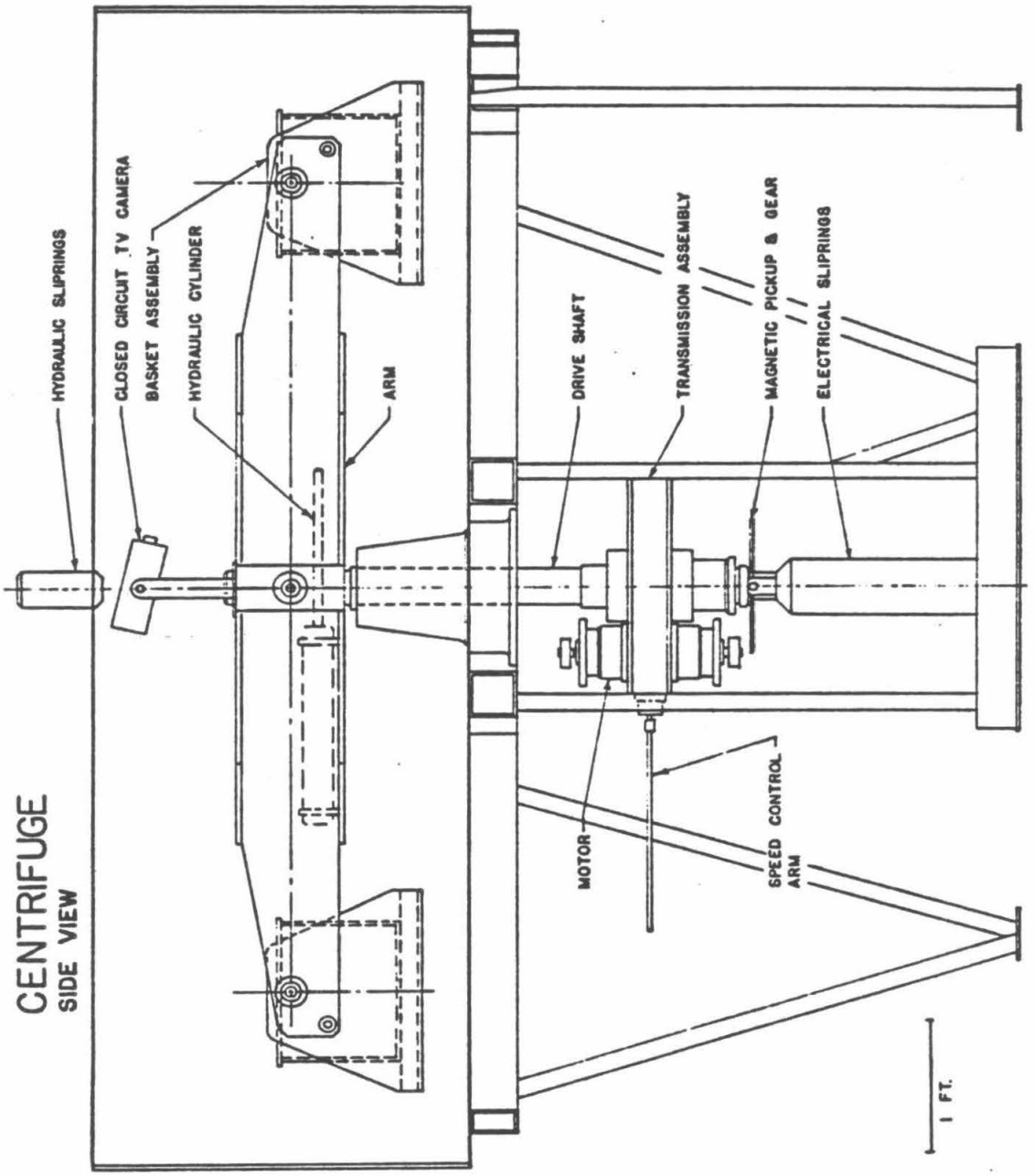

Figure 2.1 Side view of Caltech geotechnical centrifuge

4. Electrical power and signals are conducted to and from the rotating centrifuge arm by electrical sliprings. Hydraulic and air pressure are transmitted through rotary unions.

2.1.2. Model Soil-Pile System

The configuration of the complete model soil-pile system in its bucket container, including the loading mechanism and instrumentation, are illustrated by the view of a cross-section through the centerline in Figure 2.2, below. The most important aspects of this apparatus are now described.

1. The interior of the bucket is drawn to scale and marked with dimensions in Figure 2.3, below. The same cross-sectional view is presented as in Figure 2.2. The bucket interior is a right circular cylinder with an ellipsoidal bottom. For purposes of comparison, the sizes of the two model piles used in the present tests (see item 6, below) are also shown. The bucket walls represent essentially rigid outer boundaries of the model soil-pile system.

2. Lying along the centerline of the bucket, appearing in Figure 2.2, is the instrumentation, a vertical string of measurement elements topped by the ring-type load cell and extending to the pile bottom plug. The load cell, displacement platform, and pile top plug are held together by a threaded shaft which screws into both the load cell and the pile top plug. The plug fits snugly into the top of the pile tube and is held in place there by the pile top clamp. The bottom plug is simply pressure fit.

3. Hydraulic pressure generated outside the centrifuge is used in applying load to the top of the pile. As illustrated in Figure 2.2, above, a hydraulic ram alternately pushes and pulls on a loading beam which hinges from a fulcrum bolted to the opposite lip of the bucket. Compressive loads are applied directly to the load cell above the pile. Tensile loads are applied by means of a yoke linking the loading beam and the load cell.

4. Pile top displacements are measured using a set of three cantilever beam displacement transducers resting, via flexible plastic screws, on a platform located directly below the load cell in the pile assembly. One of these transducers appears in the section view of Figure 2.2. The three displacement transducers are clamped at equidistant points around the lip of the bucket, as illustrated in Figure 2.4a. This arrangement is used, with the sum of the three gauge signals giving an average pile top displacement, since tilting of the displacement platform may develop.

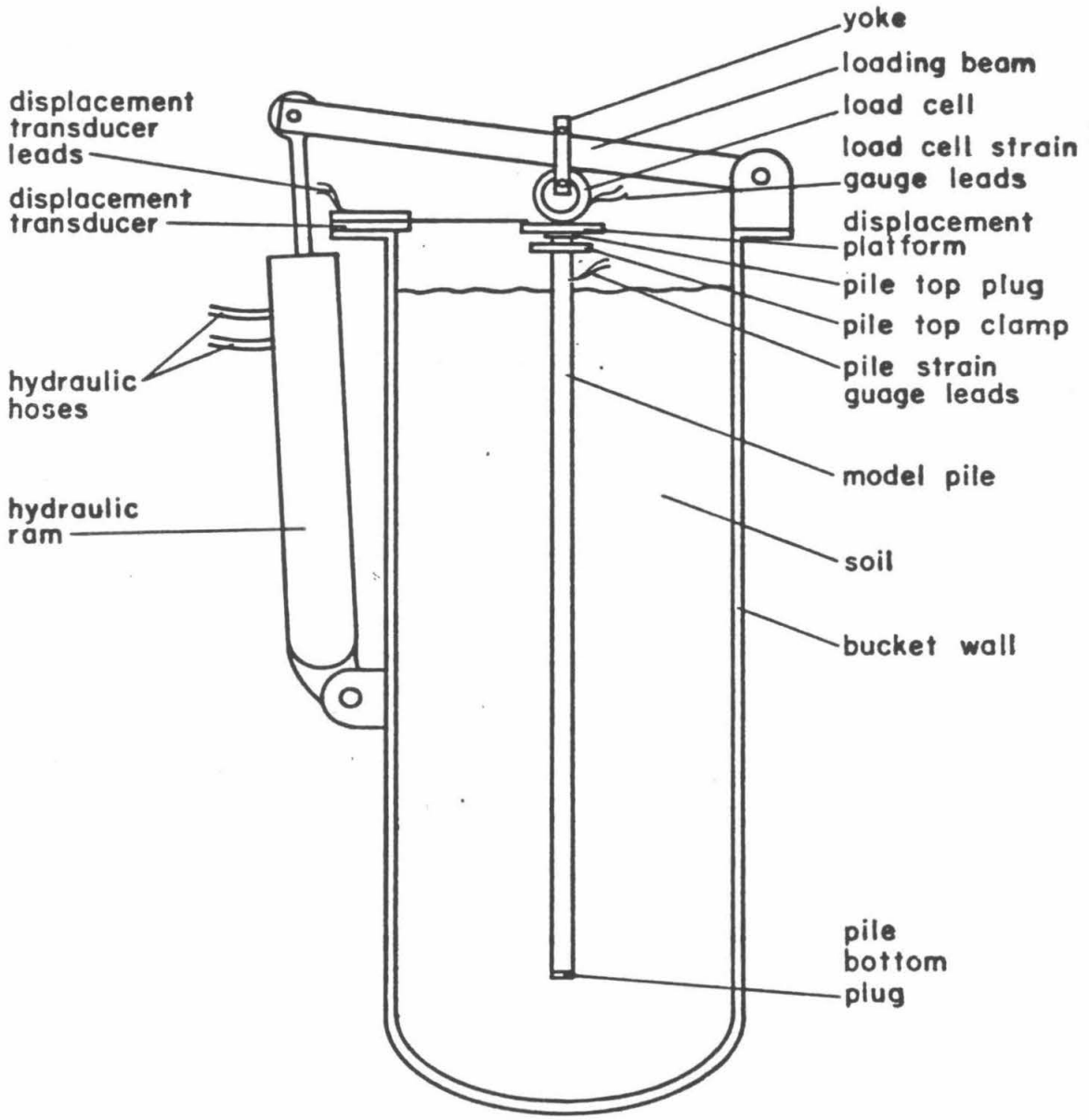

Figure 2.2 Model soil-pile system configuration

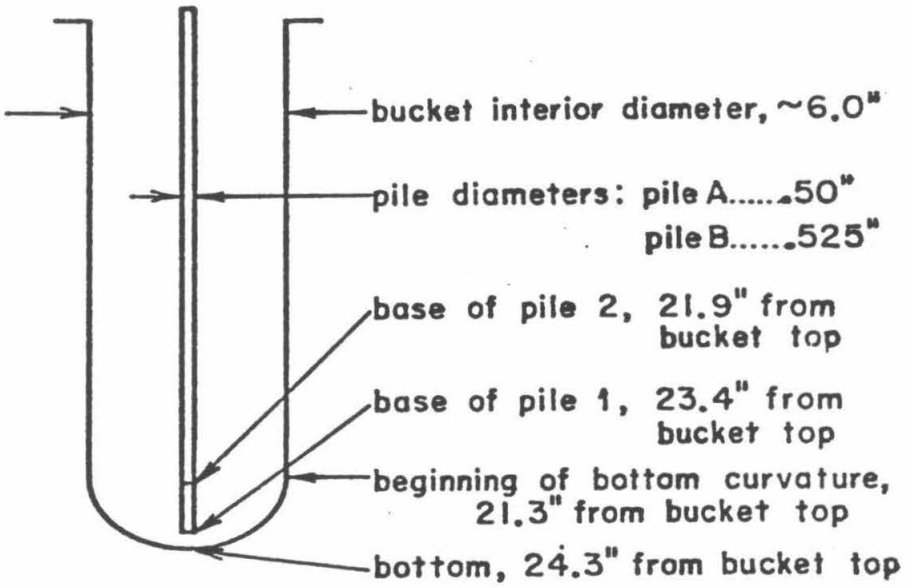

Figure 2.3 Pile and bucket dimensions

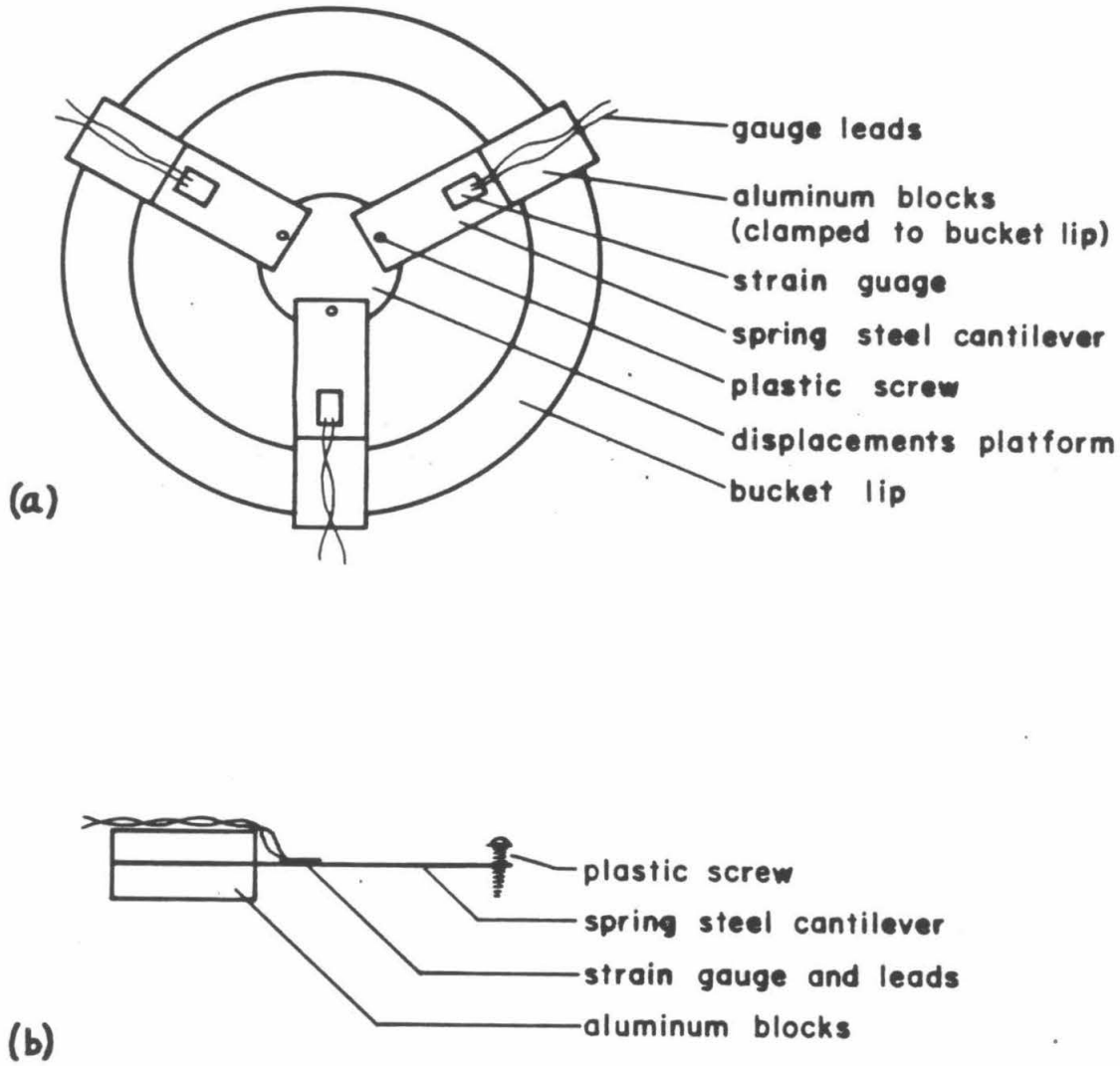

Figure 2.4 (a) Top view of displacement transducer system
(b) Side view of a single displacement transducer cantilever

5. The ring-type load cell is illustrated in Figure 2.5, below, at actual size. The locations of its four strain gauges are indicated. The cell is a proving ring, with a width perpendicular to this view of approximately 5/8 in. The hemispherical button on its peak bears against the loading beam.

6. Two model piles, which will be referred to as "pile A" and "pile B", were used in these experiments. The first was employed in Test 1, the other in Tests 3 through 6. Both were made from stainless steel tubing of outside diameter 0.50 in. and wall thickness approximately 0.010 in. Significant points along the lengths of these model piles are shown in the scale drawings, Figure 2.6, below. The decimal numbers here show distances from the top of the pile tubes in inches. A pair of strain gauges is used at each gauge point along the lengths of these pile tubes. The resistance changes in two gauges at diametrically opposite points on the tube wall are summed, automatically eliminating effects on the measured strains due to tube bending. The strain gauges are mounted on the interior surfaces of the tube in pile A and on the exterior surfaces in in pile B. The leads for the pile B strain gauges are conducted into the interior of the pile via small (1/32-in.) holes located about 0.75 in. above the measuring grid of each gauge. On both model piles, the leads from all the strain gauges are routed out of the tube interiors through a pair of somewhat larger (1/16-in.) holes near the top of the tube. Pile A was originally manufactured for the tests, but it buckled after prolonged use. Pile B was then made. The number of strain gauges on pile B and their distribution reflect experience gained with pile A.

Because the strain gauges are located on the outer surfaces of pile B, they require protection from moisture and soil abrasion. The outer surfaces of pile B--steel tube surface, strain gauges, and wires--were therefore coated with epoxy varnish.[1] This covering served satisfactorily in the tests in dry sand (Tests 3 and 4). However, the strain gauges were affected by moisture in a subsequent test in saturated soil (Test 5). This problem was solved by applying a supplementary coating of waterproofing material, the electrically insulating varnish GLPT.[2]

1. Epoxylite 6001, manufactured by The Epoxylite Corporation, Anaheim, CA.
2. Red GLPT Insulating Varnish, Catalog No. 90-2, GC Electronics, Rockford, IL.

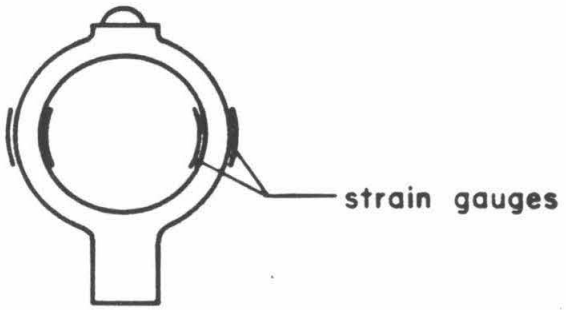

Figure 2.5 Load cell

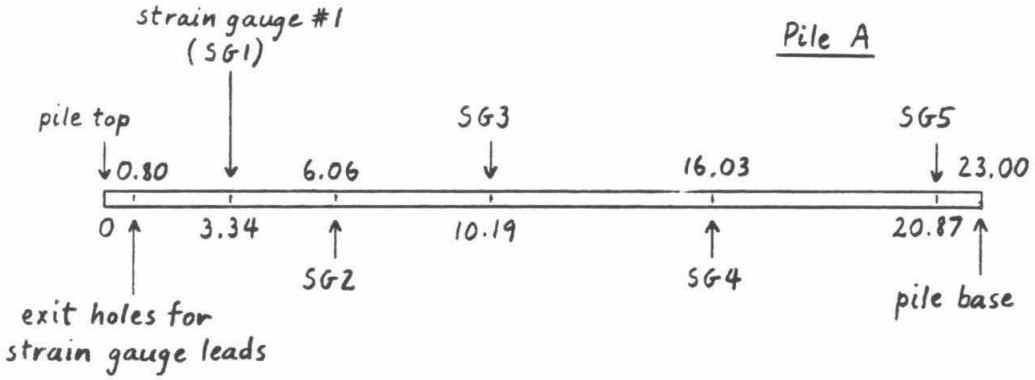

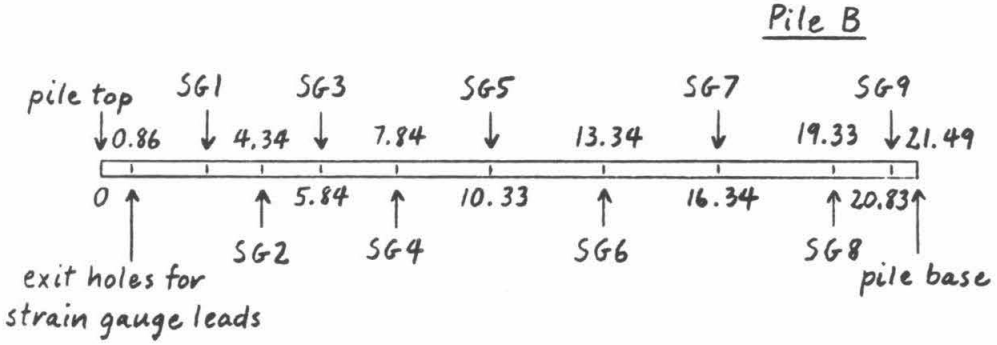

Figure 2.6 Strain gauge locations on the model piles (units : inches)

The stiffnesses, EA, of the model piles were measured by direct load testing. The values for pile A and pile B were found to be 431,000 and 465,000 pounds, respectively. With an E for stainless steel of 28 million psi, this indicates pile wall thicknesses of 0.0098 in. and 0.0106 in., respectively.

2.1.3. Electrical Instrumentation and Signal Recording Systems

Figure 2.7 shows the general configuration for all of the instrumentation systems used to monitor the behavior of the model soil-pile system--load cell, displacements transducer, and pile strain gauges. All of these systems utilize bridge circuits. A typical circuit of this kind, the bridge composed of the four load cell strain gauges, is depicted. A regulated direct current power supply on the centrifuge arm provides a stable 5.00V excitation voltage to the strain gauge circuits. In order to minimize the contamination of the gauge signals by ambient electrical noise, the signals are immediately boosted by 50 times with instrumentation amplifiers. They are also acted on by voltage followers before transmission off the moving centrifuge arm. These devices feature very low output impedances and give the signals a ground reference so that they can each be carried by a single centrifuge slipring.

A Hewlett-Packard 7045A X-Y recorder and a Honeywell Model 1858 CRT Visicorder were used together in recording the instrumentation system signals in all but one of the six soil-pile model tests. The X-Y recorder plots load applied to the top of the pile, $F_a(\tau)$, versus pile top displacement, $\delta_a(\tau)$, based on input signals from the load cell and displacements transducer. A typical plot produced by the X-Y recorder, the record of Test 3, is shown in Figure 2.8. This recorder is used both for recording a test and for monitoring its progress. The experimenter refers to it in directing the course of loading (see 2.5, below). The Honeywell machine is a strip-chart recorder capable of monitoring several signals. Here, light-sensitive paper is drawn past a recording bar where cathode ray tube beams follow the input voltages. This strip-chart recorder is used to record the signals from all the test instrumentation systems--load cell, displacement transducer, and multiple pile strain gauge readings. A sample segment of the strip chart record for Test 5 is shown in Figure 2.9.

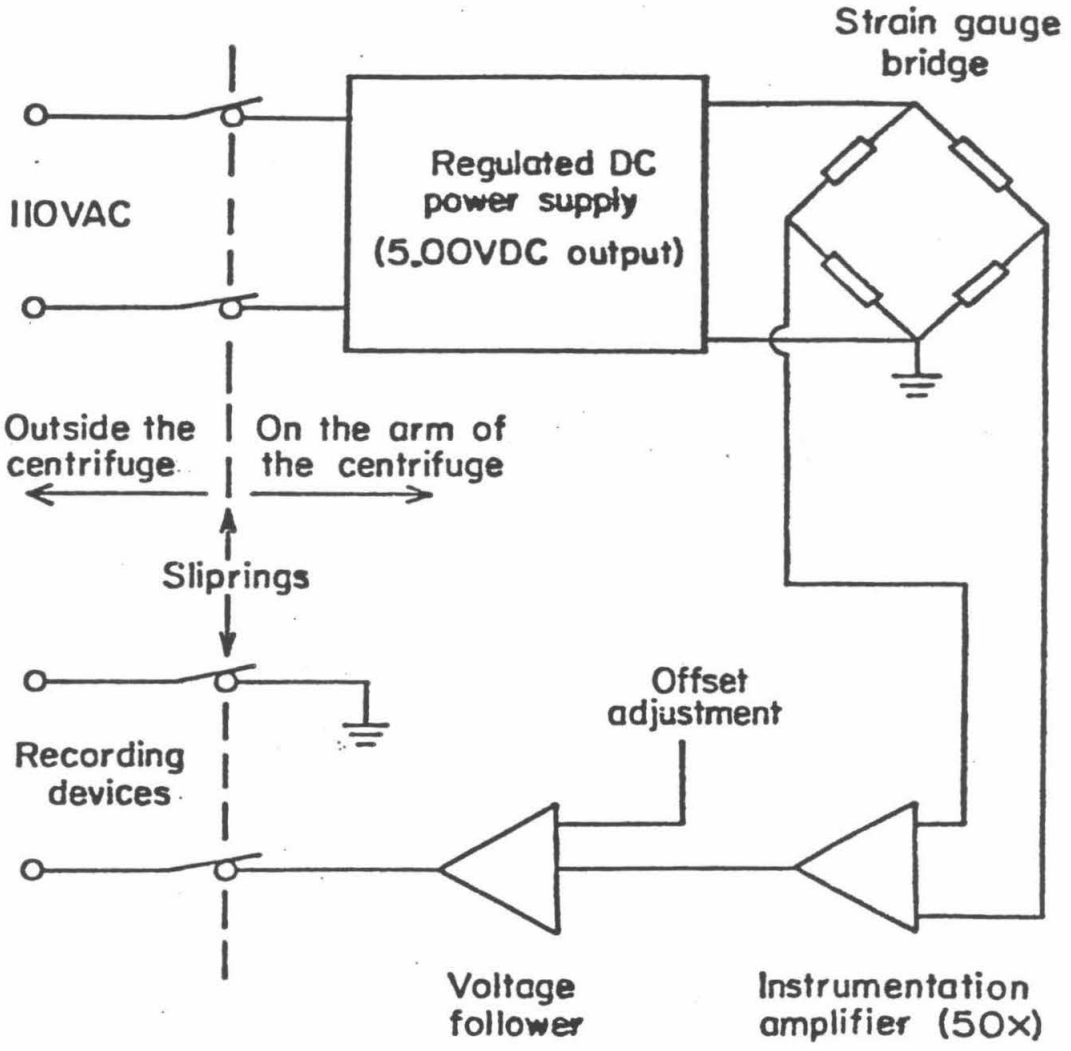

Figure 2.7 General configuration of electrical instrumentation systems

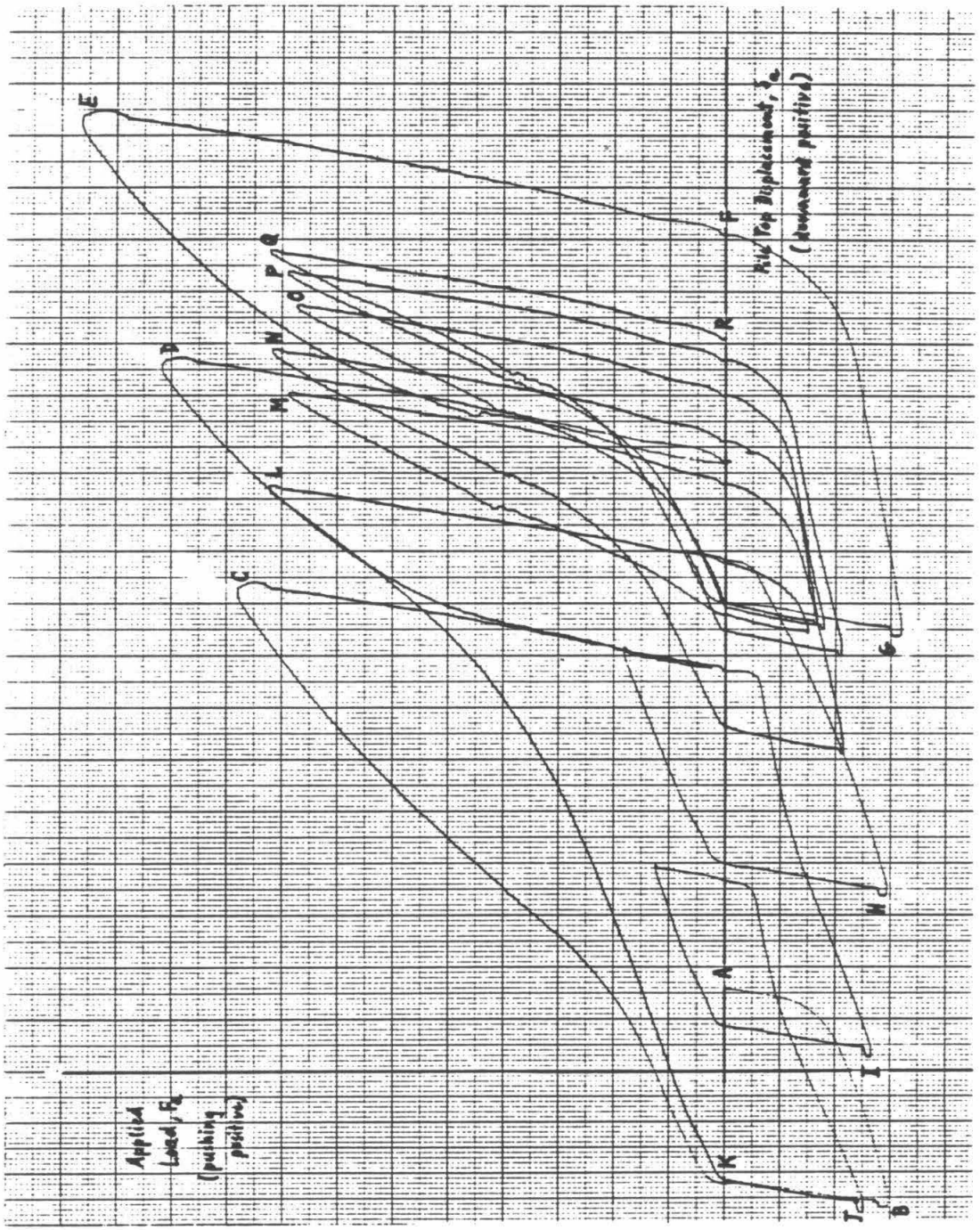

Figure 2.8 Typical X-Y recorder plot

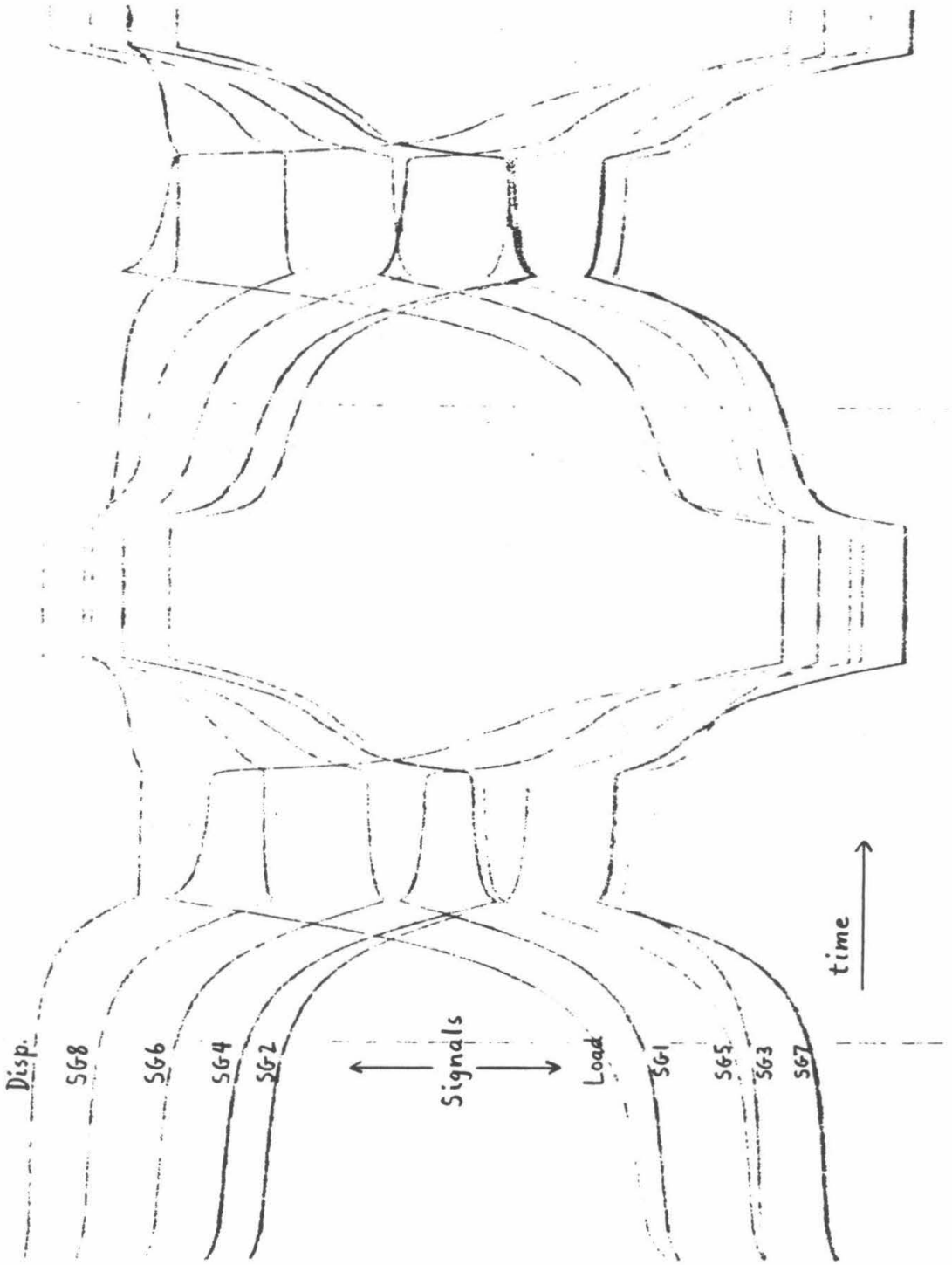

Figure 2.9 Sample segment of strip chart record

2.2. Calibration of the Instrumentation Systems

The relationships between the load cell, displacement transducer, and model pile strain gauges signals and the associated measured quantities--applied load [$F_a = f(0)$], pile top displacement [$\delta_a = w(0)$], and pile axial strains [$f(z_i)$], respectively--were established by direct observation. For example, rather than attempting to calculate the response of the ring-type load cell by consideration of the elastic deformations of the steel ring, strain gauge specifications, and bridge circuit and amplifier characteristics, the cell was subjected to a sequence of loads (represented by a stack of brass tester weights) and its output voltages read. In this load cell calibration test and in corresponding tests on the displacement transducer and pile strain gauges, the same excitation voltages, measurement circuits, sliprings, and recording devices were used in the calibration tests as in the model soil-pile system load tests.

In principle, the responses of the instrumentation systems are all linear. The linearly-elastic deformational behavior of the load cell ring, the displacement transducer cantilevers, and the model pile tube dictates that unvarying proportionality constants relate the strains measured by the strain gauges in these devices to the force and displacement quantities which they monitor. It is intended that this proportionality be preserved in the responses of the complete instrumentation systems. Direct calibration indicates in all cases that the linearity assumption is valid. The proportionality constants c_1, c_d, and c_{si}, for load, displacement, and strain at the i-th gauge are given by the slopes of plots of load, displacement, and strain versus the recorder trace deflections, respectively.

2.3. Soils Tested

A uniformly-graded, fine-grained soil named "Nevada Fine Sand" (NFS) was used in tests 1, 3, 4, 5, and 6. The grain-size distributions of these soils are shown in Figure 2.10. Further information concerning soil properties in specific test specimens, including unit weights and water contents, is given in the individual test descriptions of Chapters 3 and 4.

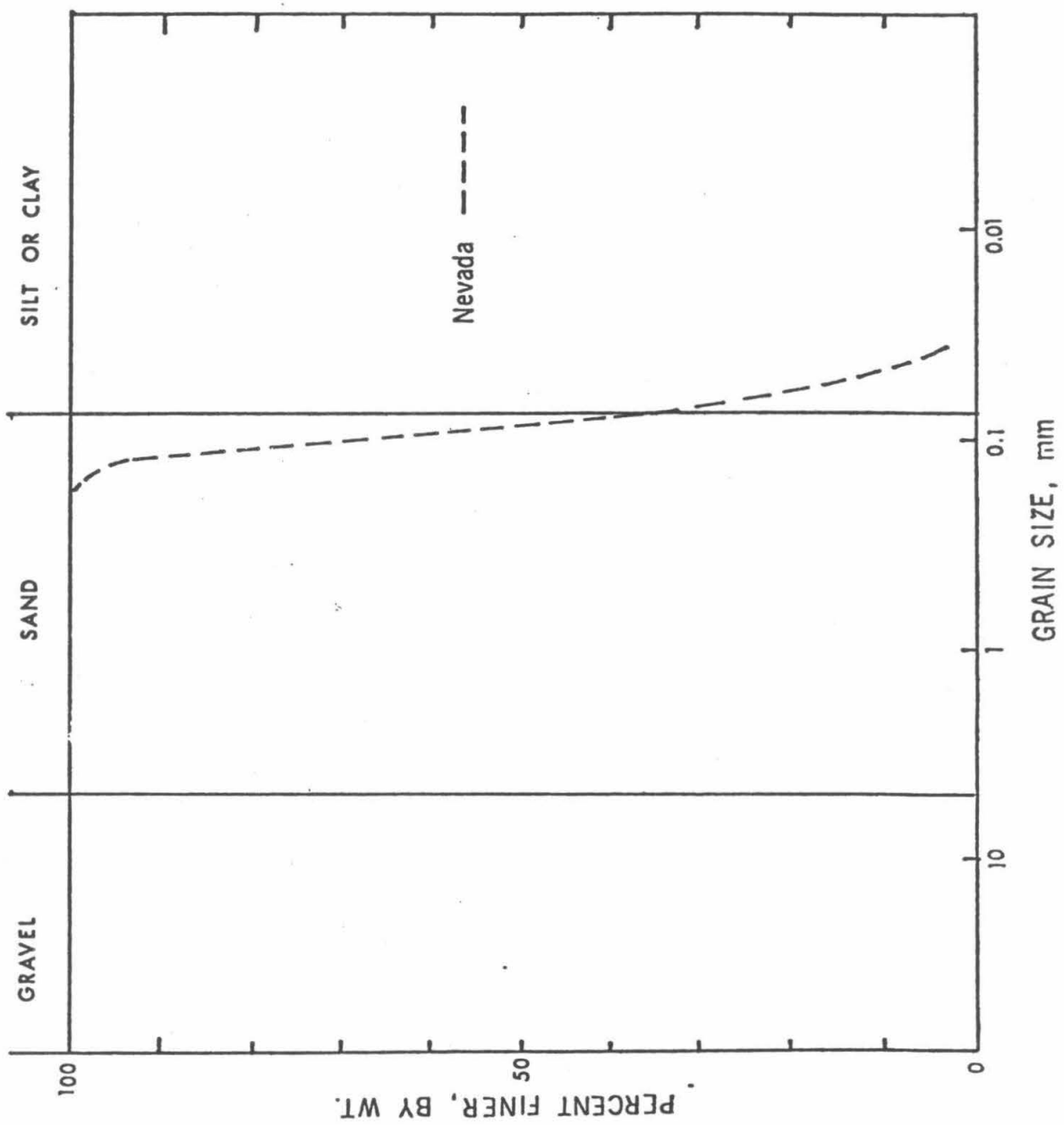

Figure 2.10 Grain size distribution curve for NFS

2.4. General Aspects of Soil-Pile Model Preparation

Assembly of the model soil-pile system in the centrifuge bucket, in the configuration shown in Figure 2.2, begins with placing the soil into the bucket and insertion of the model pile. A base layer of soil is first formed in the bottom of the bucket. Next, the tip of the pile is positioned at the center of this soil pad and the pile is pushed into the soil to a depth such that: (a) the pile tip is supported in its centered position, and (b) the top of the pile is at a proper level relative to the top of the bucket. The pile assembly is placed into position at this time as a complete unit, from the pile bottom plug to the load cell. The vertical position of the assembly is chosen by considering the level of the displacement platform relative to the location of the displacement cantilevers which will later be clamped to the bucket lip. The remainder of the soil mass is then put into place around the pile. In the case of sands, the soil is emplaced in layers of a few inches depth, with compaction procedures carried out at each layer. The procedures used in compacting sand specimens are explained in detail in the descriptions of the individual tests of Chapters 3 and 4, below. At this stage in the test on silt soil, the pile was held in position while the specimen was consolidated by centrifugation.

Upon completion of compaction (sand) and consolidation (silt), the centrifuge is stopped and the remainder of the apparatus depicted in Figure 2.2 is installed and adjusted. The displacement beams are clamped to the lip of the bucket and their cantilevers attached to the displacement platform. The loading beam and hydraulic ram are installed, and the beam linked to the load cell with the yoke. When the centrifuge is taken up to speed for the test, the massive loading beam will greatly increase in "weight". Significant loading of the soil-pile system would occur before the planned loading test sequence if the beam were not restrained. To prevent this, restraint is provided against the downward movement of the beam in the form of a hinged plate bolted to the lip of the bucket which fits into a notch in the loading beam. This device is illustrated in Figure 2.11, below. [After taking the centrifuge up to speed, the first action in the loading sequence is to raise the loading beam a short distance, allowing the restraining plate to fall out of the way (see 2.5, below).] Now the leads from the transducer bridges are connected to their respective amplifier circuits and to the power supply, and the bridges are nulled. The vertical position of the pile assembly and the level of the soil mass surface with

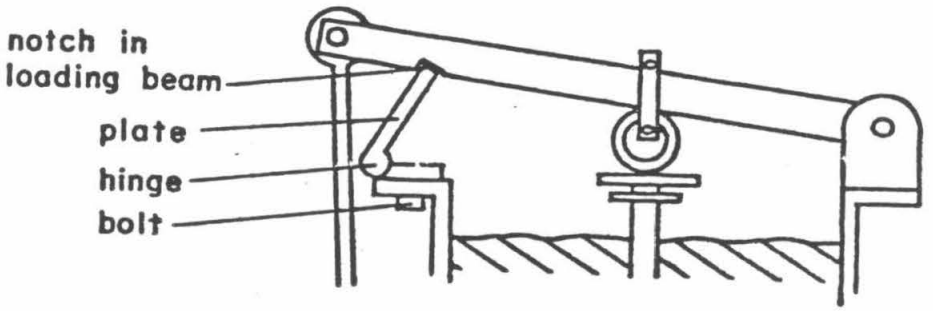

Figure 2.11 Diagram of hinged restraining plate

respect to the bucket top are recorded. This information will indicate the depth of embedment of the model pile for purposes of subsequent analysis.

2.5. Test Procedures

The experimenters monitor and control the progress of a test on the centrifuge from an instrumentation shed adjacent to the centrifuge building. Here are found the transducer signal recording devices, a control valve for the hydraulic loading system, and the centrifuge power control and speed indicator. The first step in running a model soil-pile system test is to bring the centrifuge up to test speed. Next, the initial positions of (a) the CRT traces on the recording bar of the strip chart recorder and (b) the X-Y recorder pen are set. Then the hydraulic fluid compressor is started. This is done immediately before loading of the model soil-pile system begins because the 3000-psi compressor will only run for about 15 minutes before it overheats and is automatically shut off. This consideration also determines the maximum duration of centrifuge tests involving hydraulic loading. The average duration of a pile loading test is about 10 minutes.

Loading is controlled by the experimenter through operation of a valve for the hydraulic fluid. He follows the current progress of load application and soil-pile system response on the X-Y recorder, which is producing a plot of load versus pile top displacement. The loading sequence begins with pulling on the top of the pile as the loading beam is raised to allow the hinged restraining plate to disengage. A typical loading sequence is illustrated in the X-Y recorder plot of Figure 2.8, the record of Test 3. The loading path begins at point A. The pulling associated with releasing the plate corresponds to the plot segment between points A and B. Now three compressive cycles of load test are carried out. The soil-pile system is subjected to successively higher values of pushing load at points C, D, and E, each followed by unloading to zero applied load. This brings the loading path to point F. Next, four tension tests are performed. Repeated pulling and unloading bring the system successively to the tension failure points G, H, I, and J. Finally, beginning from the condition of zero applied load at point K, five-and-one-half cycles of pushing and pulling to load levels somewhat less than failure are carried out. The maximum pushing loads in these cycles correspond to points L, M, N, O, P, and Q. The load test ends at point R. The loading sequence for this test can be summarized as follows:

1. three pushing (compression) tests to failure,

2. four pulling (tension) tests to failure, and

3. five-and-one-half pushing-pulling (compression-tension) cycles.

Note 1: In subsequent discussions of experimental loading test sequences in this report, there is frequent reference to "pushing" and "pulling" loads applied to the pile top. Use of this terminology often holds advantages in precision over the phrases "compressive loading" and "tensile loading" for describing portions of a complex and extensive loading path. For example, depending on the loading history of a soil-pile system, a pile may be in compression along varying proportions of its length when a given, moderate pulling load acts on its top, so that it is misleading to refer to this loading as "tensile".

Note 2: Both in the loading sequence descriptions above and in those of Chapters 3 and 4, loading to failure or near failure is referred to as "pushing to failure" or "pulling to failure", while lower intensities of loading are described simply as "pushing" or "pulling".

2.6. Procedures for Analyzing the Test Data

The load-displacement behavior, $\delta_a[F_a(\tau)]$, of the prototype soil-pile system associated with a model test is represented directly by the X-Y recorder plot of load cell reading versus displacements transducer reading. In order to interpret this plot, it is only necessary to determine the horizontal and vertical scales, taking into account (a) the calibration factors relating model pile top displacement to recorder pen X-deflection and pile applied load to pen Y-deflection, and (b) the centrifuge modeling scale factors relating model and prototype quantities.

In order to achieve a more detailed interpretation of the behavior of the prototype soil-pile system, a description of soil-pile interaction along the entire length of the pile by means of the functions $t(z)$, $f(z)$, and $w(z)$, and t-z curves, the model pile strain gauge readings must also be brought into the picture. The analysis begins with the identification of pile strain gauge readings with values of axial force in the model pile $f(z_i)$ by means of the gauge calibration factors. Next, a cubic polynomial is fit to these pile strain gauge axial force values, together with the load cell value $f(0)$. This function

serves as an approximation to the axial force distribution, $f(z)$, in the model pile. The model soil-pile shear stress and pile displacement functions for the model system, $t(z)$ and $w(z)$, are then derived by differentiation and integration of $f(z)$, respectively. When the functions $t(z)$ and $w(z)$ have been developed in this way at a sequence of points τ_j along the test loading path, t-z curves showing soil-pile interaction at various depths z_i are constructed by tying together points $[w(z_i,\tau_j),\ t(z_i,\tau_j)]$ for successive values of j. Finally, prototype-model scaling factors are applied to all force and displacement quantities, and the f, t, and w functions and t-z curves corresponding to the behavior of the prototype pile are plotted.

Details of the general application of this interpretation to the six model tests will now be described.

2.6.1. Data Reduction

The test loading sequence is reviewed by referring to the plot of load versus pile top displacement produced by the X-Y recorder and specific intervals of the test are chosen for t-z interpretation. In each test, 10-20% of the total data set was interpreted in this detailed way, in most cases including one loading sequence interval taken from near the beginning of the test, in which the pile was loaded first to failure in pushing and then to failure in pulling, and another interval from later in the test consisting of one-and- one-half cycles of pushing-pulling cyclic loading at load levels about one-half those of failure. Next, the segments of the strip chart or digital recorder records corresponding to these intervals are identified. For example, the partial X-Y and strip chart records of Test 5 shown in Figure 2.12, below, are associated with the same interval of the test. (Note: Records from the strip chart and digital recorders play the same role in these test interpretations and are treated very similarly. To simplify the presentation, it will be assumed in the remainder of this general description of the tests analysis that the strip chart machine was used.) The next step is to mark the strip chart record at a set of points, $\{\tau_j\}$ representing significant stages in the progress of the test, as shown in Figure 2.12b. Transducer readings at these loading path stations are the complete basis for the t-z interpretation. They include points separated by roughly equal increments of applied load, and applied load maxima, minima, and zeros. Finally, the simultaneous readings of the load cell, displacements transducer, and

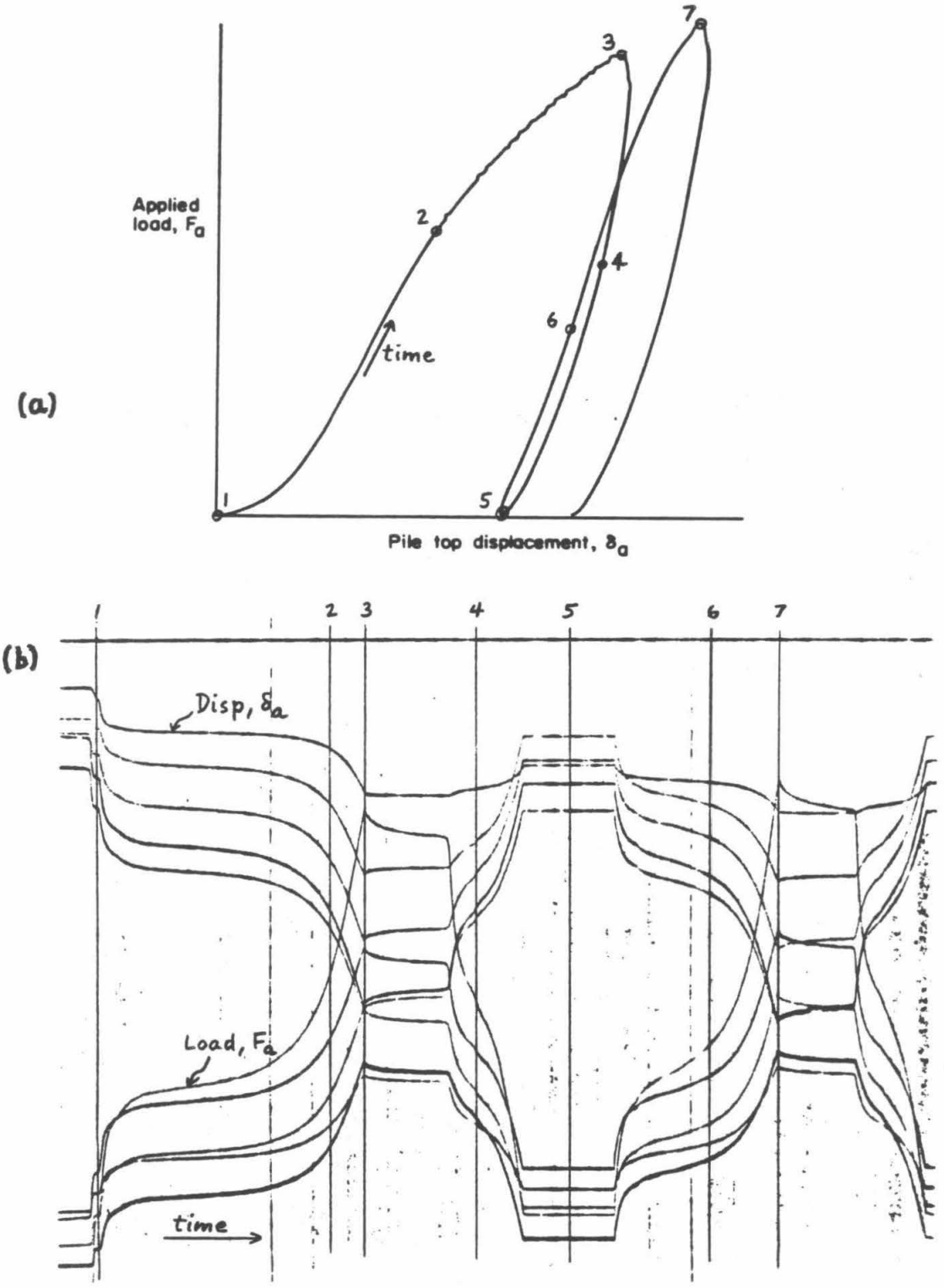

Figure 2.12 Corresponding record segments from (a) X-Y recorder and (b) strip-chart recorder

pile strain gauges at these 't-z basis stations', $\{\tau_j\}$, are measured from the strip chart record using a digitizer.

2.6.2. Conversion of Data Into Model Pile Force and Displacement Values

This is accomplished using the calibration factors described in section 2.2, above.

2.6.3. Construction of the Functions f(z), t(z), and w(z), For the Model Pile

For each of the loading path stations which form the basis for the interpretation of a particular test interval, values of axial force at the top of the model pile and at the strain gauge points are found. Since model pile A has five strain gauges and pile B nine, measured values of $f(z)$ are available at six z values (including z= 0) when pile A is used and at ten z values with pile B. The axial force function at all points along the model pile is now approximated by fitting a continuous curve to these experimental values.

Fitting the experimental data with the best cubic polynomial on a least squares basis has proven a satisfactory way of constructing the function $f(z)$. It is assumed that the distribution of model pile axial forces with depth has the form

$$f(z) = a_3z^3 + a_2z^2 + a_1z + a_0. \tag{2.7}$$

Though this assumption limits the degree of detail in pile behavior which shows up in the subsequent t-z interpretation, it has the converse advantage that smoothing is automatically applied to the experimental data. The use of higher order polynomials leads to spurious undulations in the fitted curves. The range of soil-pile system behavior which is revealed by this treatment includes many of the system's fundamental characteristics.

The relationships of soil-pile shear stresses $t(z)$ and pile displacements $w(z)$ to the derivative of $f(z)$ and its integral, respectively, were developed briefly in Chapter 1. A complete derivation of these relationships is now presented, demonstrating the notation, including sign conventions, which is utilized in the remainder of this chapter and in Chapters 3 and 4.

An elastic pile of circumference S, cross-sectional area A, and Young's modulus E is acted upon by the following forces, as illustrated in Figure 2.13a:

1. applied load

   $F_a[= f(0)]$, positive downward,

2. shear stresses given by the soil to the pile, $t(z)$, positive upward, and

3. tip load F_t, positive upward.

From the equilibrium of a differential section of the pile (Figure 2.13b):

$$f(z + \Delta z) + S\Delta z t(z) = f(z)$$

or

$$\frac{f(z + \Delta z) - f(z)}{\Delta z} = -St(z)$$

and in the limit as $\Delta z \to 0$,

$$t(z) = \frac{-1}{S} \frac{df(z)}{dz}. \tag{2.8}$$

As indicated in Figure 2.13a, downward movements of points along the pile represent positive pile displacements $w(z)$. Introducing $\sigma(z)$ = axial normal stress in the pile material, compressive stress positive, and $\varepsilon(z)$ = axial normal strain in the pile material, shortening positive, there appear

$$f(z) = A\sigma(z),$$

$$\varepsilon(z) = \frac{-dw(z)}{dz},$$

and from the pile's elasticity,

$$\sigma(z) = E\varepsilon(z).$$

Therefore,

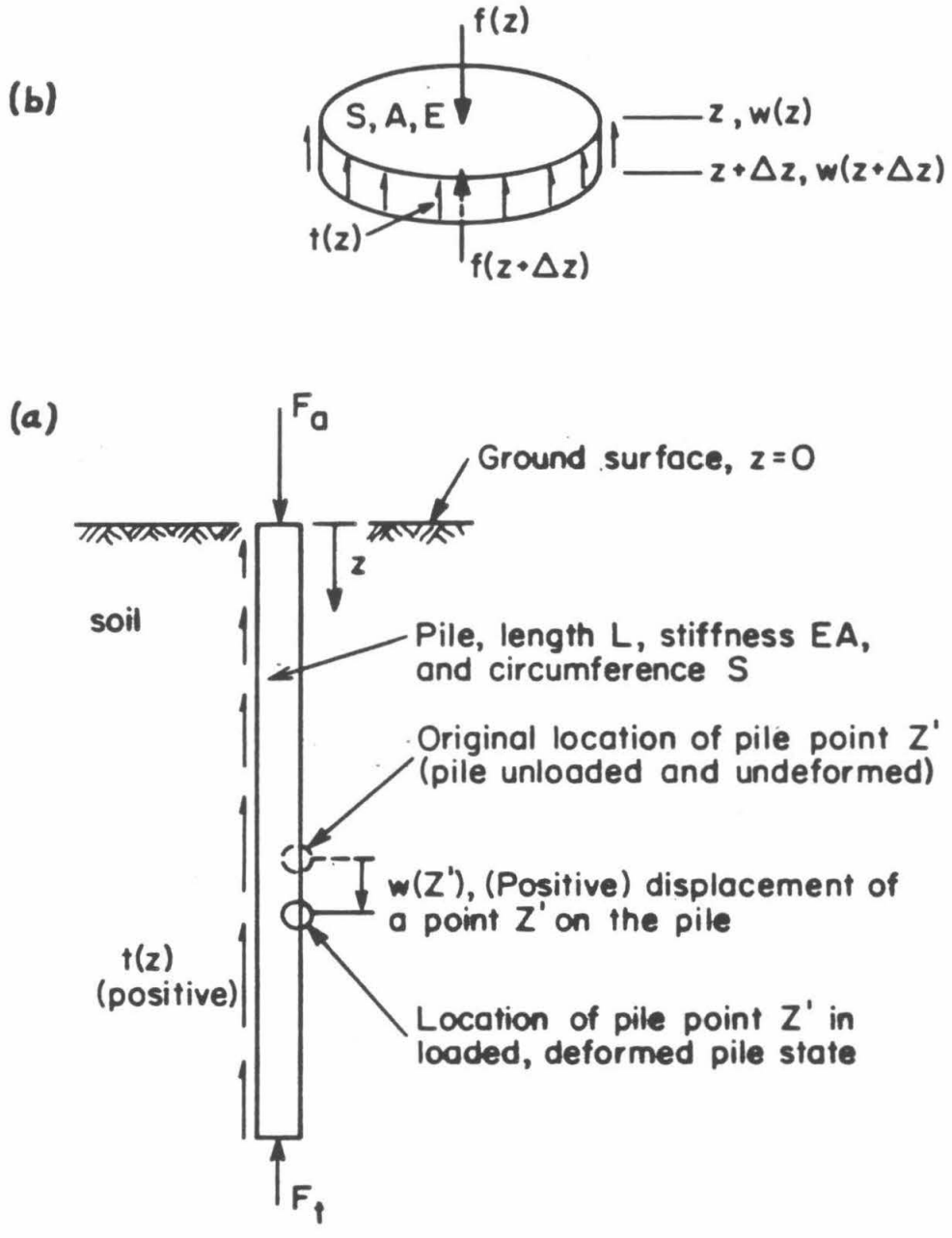

Figure 2.13 (a) Forces acting on the pile and pile displacements (b) Equilibrium of a differential section of the pile

$$f(z) = -EA \frac{dw(z)}{dz}$$

and

$$w(z) = \frac{-1}{EA} \int f(\xi) d(\xi) . \tag{2.9}$$

Equations (2.8) and (2.9) show the relationships of $t(z)$ and $w(z)$ to $f(z)$.

A useful constraint on the assumed form of the axial force function in equation (2.7) arises from the physics of the soil-pile system. The soil mass in nearly all of the model tests was composed of cohesionless sand. This material has no strength against shearing under the conditions of zero confining pressure which exist at ground surface, so that the soil-pile shear stresses $t(z)$ must satisfy the boundary condition

$$t(z) = 0 \quad at \quad z = 0 . \tag{2.10}$$

Since $f(z)$ has been assumed to have the cubic polynomial form of equation (2.7), from equation (2.8),

$$t(z) = \frac{-1}{S} \frac{df(z)}{dz} = \frac{-1}{S} (3a_3z^2 + 2a_2z + a_1) .$$

Boundary condition (2.10) implies that $a_1 = 0$, so that

$$t(z) = \frac{-1}{S} (3a_3z^2 + 2a_2z) \tag{2.11}$$

and

$$f(z) = a_3z^3 + a_2z^2 + a_0 . \tag{2.12}$$

The value of axial force F_a measured by the load cell is imposed on $f(z)$ as a boundary condition, namely,

$$f(z) = F_a \quad at \quad z = 0 .$$

Therefore, from equation (2.12), $a_0 = F_a$ and

$$f(z) = a_3 z^3 + a_2 z^2 + F_a \,. \tag{2.13}$$

Thus, the curve $f(z)$ is constrained to pass through the load cell measurement, while the pile strain gauge measurements are taken into account only by means of the least squares formulation. This procedure has the advantage of simplifying the curve fitting calculations.

The function $f(z)$ describing axial forces everywhere along the model pile is given, at last, by determining the coefficients a_2 and a_3 in equation (2.13) which best fit the pile strain gauge data in the sense of least squares. The associated distribution of soil-pile shear stress $t(z)$ is then available immediately from (2.11). The model pile displacements $w(z)$ are related to $f(z)$ as indicated in equation (2.9),

$$w(z) = \frac{-1}{EA} \int f(\xi) d\xi = \frac{-1}{EA} \left[\frac{a_3}{4} z^4 + \frac{a_2}{3} z^3 + F_a z \right] + w_0 \,.$$

The integration constant C is determined by the boundary condition that at the soil surface the pile displacement is a known quantity w_0. From

$$w(z) = w_0 \quad at \quad z = 0 \,.$$

it follows that $C = -EAw_0$ and

$$w(z) = \frac{-1}{EA} \left[\frac{a_3}{4} z^4 + \frac{a_2}{3} z^3 + F_a z \right] + w_0 \,.$$

The quantity w_0 is calculated by deducting the change in length of the model pile tube between the displacements platform and the soil surface, Δ_{ps}, from the measured movement of the platform, w_{dp}. The axial force in this segment of pile tube is the applied load, F_a. If its length is l_{ps}, then

$$\Delta_{ps} = \frac{F_a l_{ps}}{EA}$$

and

$$w_0 = w_{tp} - \Delta_{ps} .$$

2.6.4. Construction of t-z Curves for the Model Pile

In the manner described above, the functions $f(z)$, $t(z)$, and $w(z)$ are constructed from experimental data at each of the stations τ_j in a given loading path interval. A t-z diagram showing the course of soil-pile interaction at depth z_i during this interval is now produced from the set of ordered pairs $[w(z_i,\tau_j), t(z_i,\tau_j)]$ by connecting these points with line segments in loading path sequence.

2.6.5. Conversion from Model to Prototype Pile Force and Displacement Values

According to centrifugal modeling principles, as discussed in Chapter 1, the prototype-model scaling factor for length quantities, such as depths z along the pile and pile displacements $w(z)$, is given by the multiple, n, of earth's gravitational acceleration, g, applied to the model soil-pile system. The applied centrifugal acceleration at any point in the model is related to the distance from that point to the centrifuge center of rotation. In the present tests, the length of the model pile, typically about 20 inches, is of the same order as the distance from the top of the pile to the centrifuge center of rotation, about 25 inches. Therefore, the accelerations applied to the model vary significantly along the length of the pile. The acceleration value near the model pile midpoint was used as the basis for the prototype-model length scaling factor n in interpreting these tests. The specific values of n used in the six tests are indicated in the individual test descriptions of Chapters 3 and 4. The prototype-model scaling factor for force quantities, including pile axial force $f(z)$ and pile stiffness EA, is n^2.

CHAPTER 3

CENTRIFUGE MODEL TEST 1

Test 1 provides information concerning the behavior of very large piles in Nevada Fine Sand. The level of accelerations at mid-pile applied to the model soil-pile systems in this test is 100 g's, so that its behavior corresponds to that of systems with piles with embedded length about 175 feet. Of the centrifuge pile tests presented in this thesis, Test 1 was performed earliest. Because the testing procedures were still in a state of development at this time, this test shows the following complications and deficiencies, which are not present in Tests 3-6:

No precise determination was made of the properties of the soil composing the model soil mass specimens.

2. Difficulties encountered in recording the force and displacement transducer signals led to slight deviations from the procedures for analyzing the test data outlined in Chapter 2. (See "Special aspects of the analysis", sections 3.1.5 and 3.2.5, below.)

3.1. Specific Procedures and Results of Test 1

3.1.1. Apparatus

A detailed description of the apparatus was given in section 2.1, above. Model pile A was used here. The main record of transducer signals was made with the strip chart recorder.

3.1.2. Features of the model soil-pile system

a. The soil mass was composed of dry Nevada Fine Sand (NFS).

b. The soil was poured around the pile in 6-inch layers and lightly compacted by tamping with a metal rod.

c. The average unit weight of the sand in the soil mass specimen was not measured here, as it was for Tests 3-6. However, based on comparison with the dry unit weights of the soil

masses for Tests 3 and 4, in which greater compactive effort was expended (see 4.2.2, item b), the dry average unit weight of the Test 1 specimen is estimated to have been 100 pcf.

d. The friction angle of dry NFS was 33.2°. The coefficient of friction between the stainless steel of the pile tube and NFS was found to be 0.295.

e. The surface of the soil mass was 1.4 inches from the top of the centrifuge bucket.

f. The embedded length of the model pile was 22.0 inches.

3. The prototype-model scaling factor, n, is taken as 100.0, the value of the acceleration applied to the system 9.7 inches above the model base, 39.1 inches from the centrifuge center of rotation. With this scaling factor, the prototype pile specifications are:

a. embedded length . . . 183.3 feet,

b. diameter . . . 4.17 feet, and

c. EA . . . 4,310,000 kips.

4. Loads were applied to the top of the pile in the following sequence:

a. pushing to failure,

b. pulling to failure,

c. pushing to failure,

d. pulling to failure,

e. seven pushing-pulling cycles.

The following two loading path intervals were interpreted using t-z diagrams:

a. **Interval 1**--*The initial pushing and pulling loadings, a and b, above. Fifteen stations in the interval formed the basis for the t-z curves.*

b. **Interval 2**--*The fifth of the seven pushing-pulling cycles of e. Here, the t-z basis was composed of 11 stations.*

5. Special aspects of the analysis

a. The load cell and pile strain gauge readings at the t-z basis stations were digitized from the strip chart record. However, the response sensitivity of the strip chart recorder displacement transducer trace had been set too high, so that this trace went off scale very soon after the test began. The pile top displacements at the basis stations were found from the X-Y recorder plot of load cell versus displacement transducer readings.

b. A special procedure was used in forming the data basis for the second loading path interval. Load application during the pushing-pulling cycles part of the test had been erratic, and no interval of pushing followed by pulling near the end of the cycling sequence was satisfactory for direct analysis. The data basis for such a loading sequence was therefore constructed based on the record of an interval of pulling followed by pushing.

The load cell trace on the related portion of the strip chart record appeared as shown in Figure 3.1a. It is the path (A, BC, D) of Figure 3.1b which was constructed from the sub-paths (A, B) and (C, D) marked in Figure 3.1a to serve as the basis for a pushing-pulling loading path interval. The pile top displacement readings associated with stations in sub-path (C, D) were augmented by the quantity (displacement at B minus displacement at C) to give continuous displacements in the interval. This patching procedure was possible because the readings at the load cell and all the pile strain gauges at point B in Figure 3.1a precisely coincided with those at point C. The periodic nature of the loading sequence in this part of the test accounts for the matching of these readings, and gives the procedure validity.

6. The plotted results of Test 1 appear in Figures 3.2a through 3.2j, as indicated in the table below.

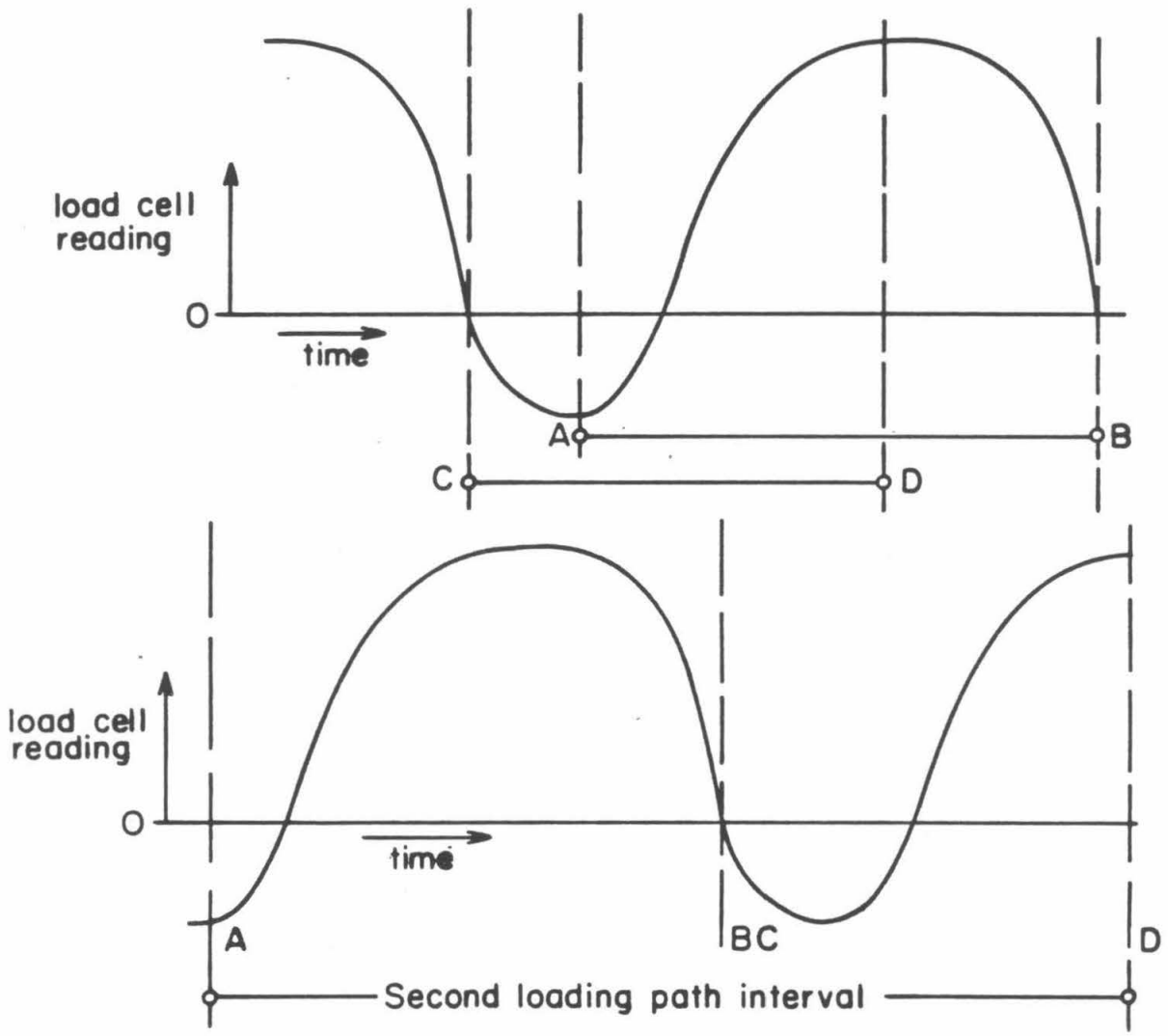

Figure 3.1 (a) Portion of original strip-chart record
(b) The second loading path interval of Test 3 composed for t-z analysis

TABLE 3.1. Figure Numbers for the Results of Test 1

Graphs	Interval 1	Interval 2
Applied load versus pile top displacement	Figure 3.2a	Figure 3.2f
Pile axial force, $f(z)$	Figure 3.2b	Figure 3.2g
Soil-pile shear stress, $t(z)$	Figure 3.2c	Figure 3.2h
Pile displacement, $w(z)$	Figure 3.2d	Figure 3.2i
t-z diagrams	Figure 3.2e	Figure 3.2j

3.2. Remark Concerning the Plotted Results of Test 1

No additional interpretation will be placed on the results of Test 1, though the graphs presented above compose a detailed account of soil-pile system behavior which can be used as the basis for a wide variety of interpretations and analyses, including t-z analysis. In the next chapter, the same types of graphs form a record of the more carefully planned and executed Tests 3-6. Some of the aspects of soil-pile behavior which these graphs can reveal are discussed there. (See section 4.4.)

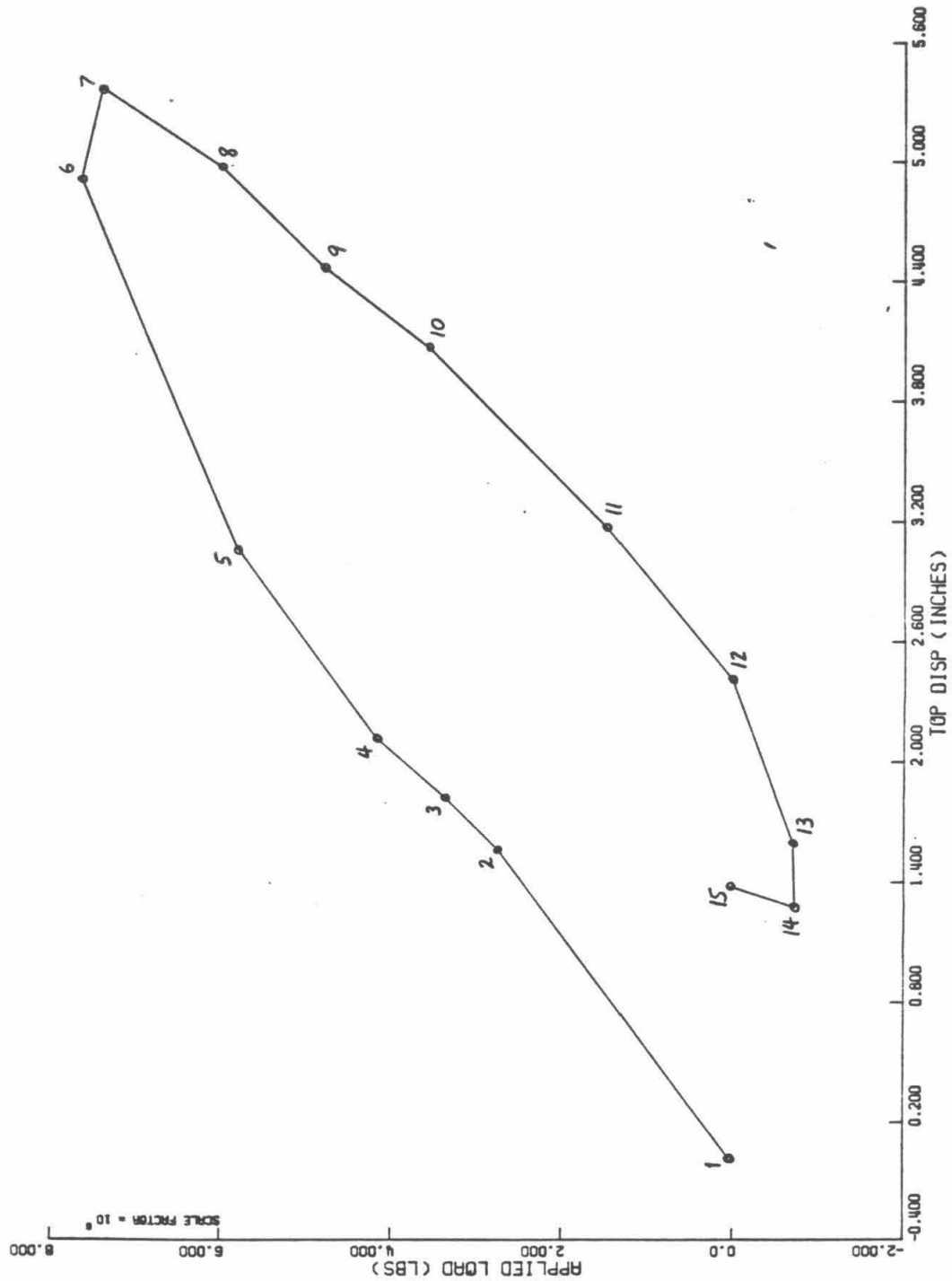

Figure 3.2a. Applied load vs. pile top displacement--Interval 1, Test 1

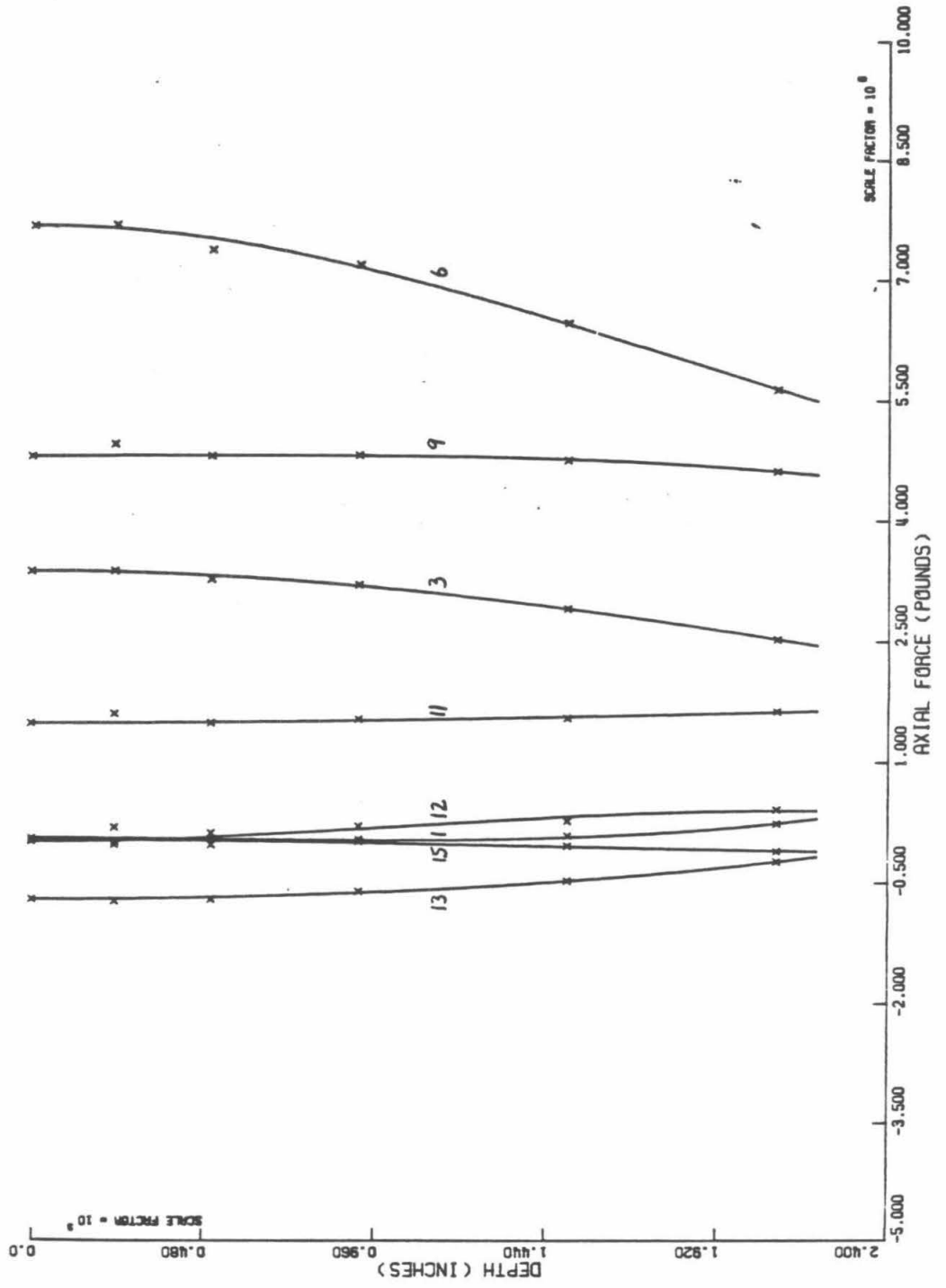

Figure 3.2b. Pile axial force, f(z)—Interval 1, Test 1

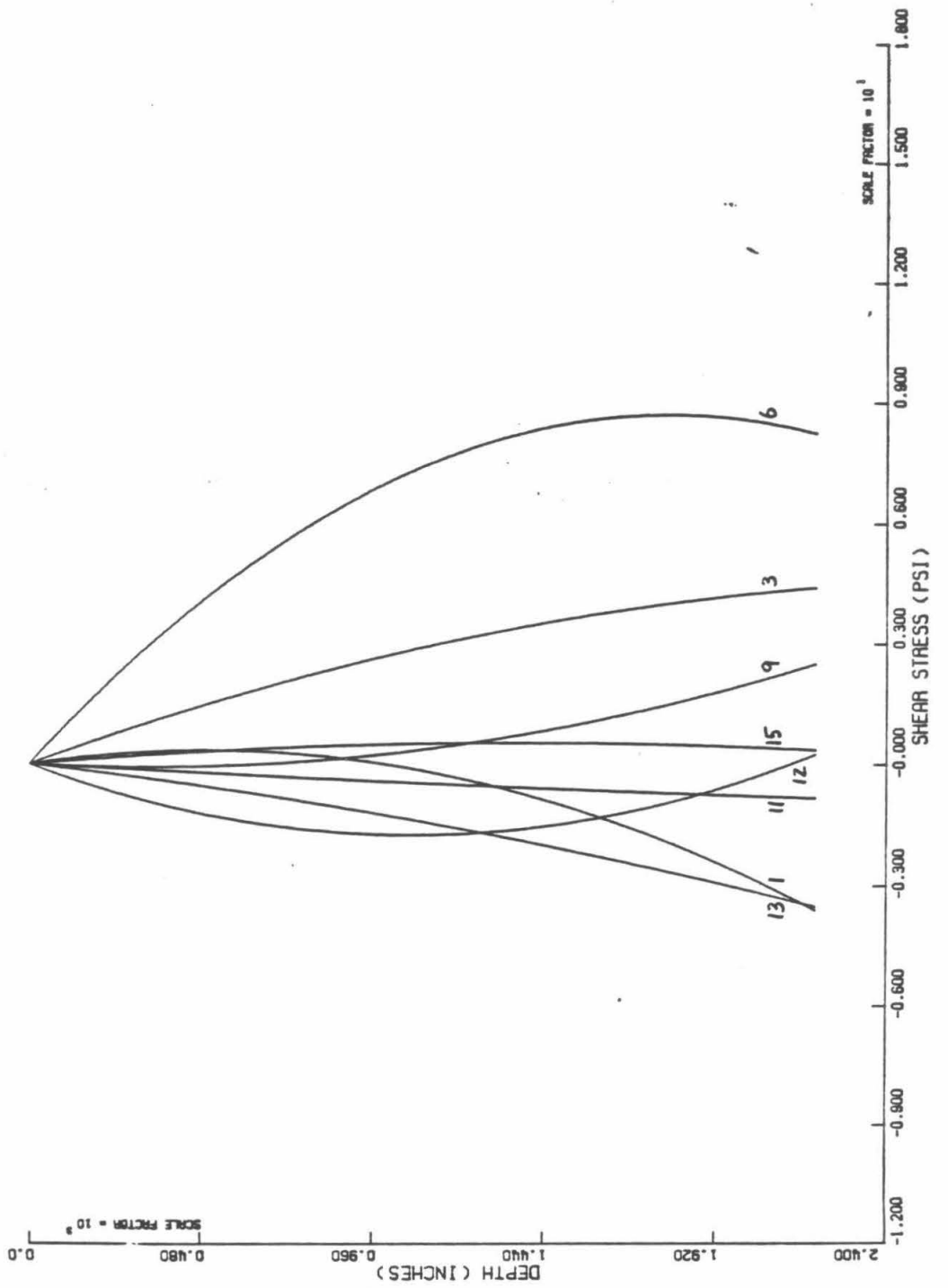

Figure 3.2c. Soil-pile shear stress, t(z)--Interval 1, Test 1

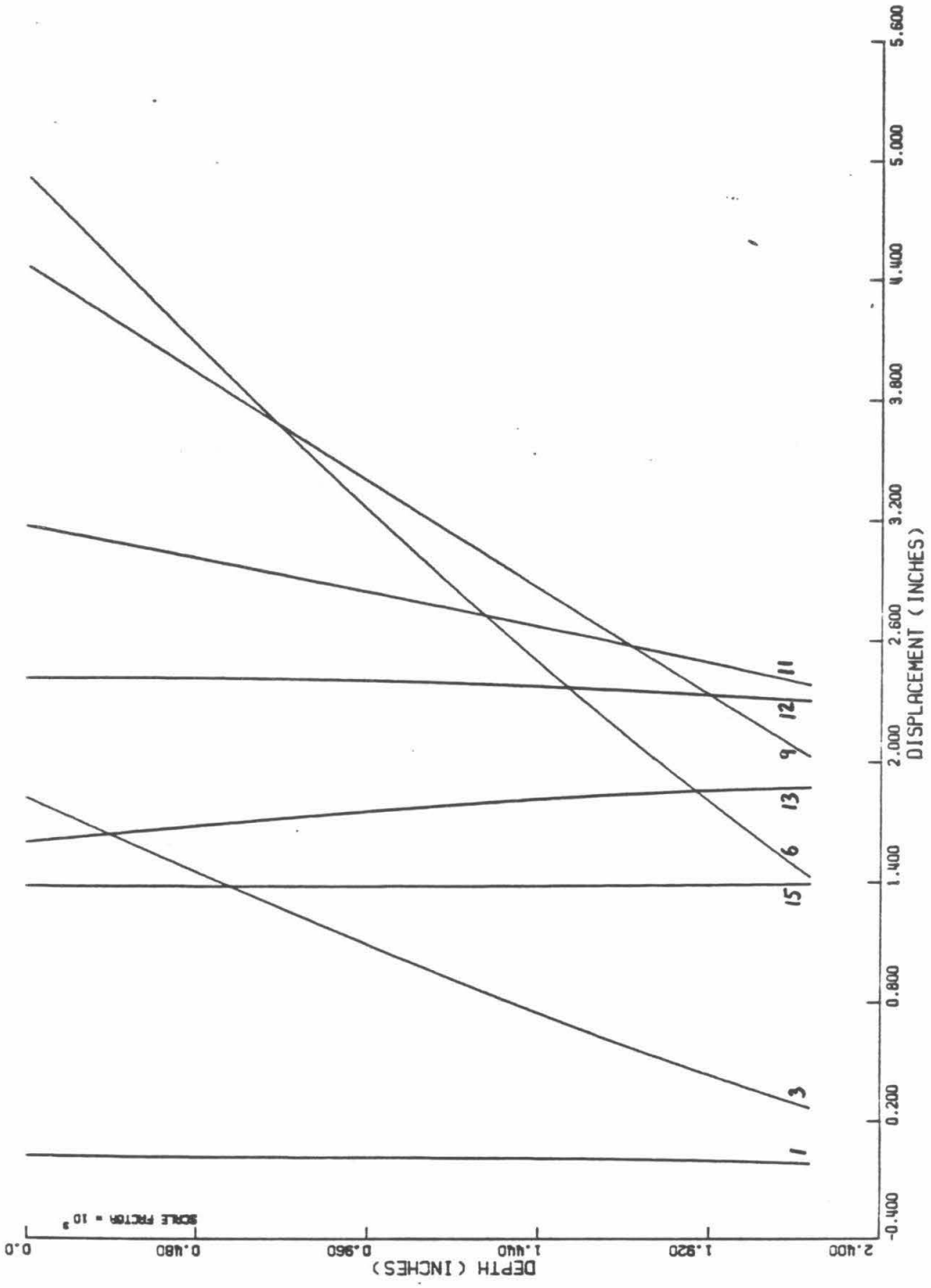

Figure 3.2d. Pile displacement, w(z)--Interval 1, Test 1

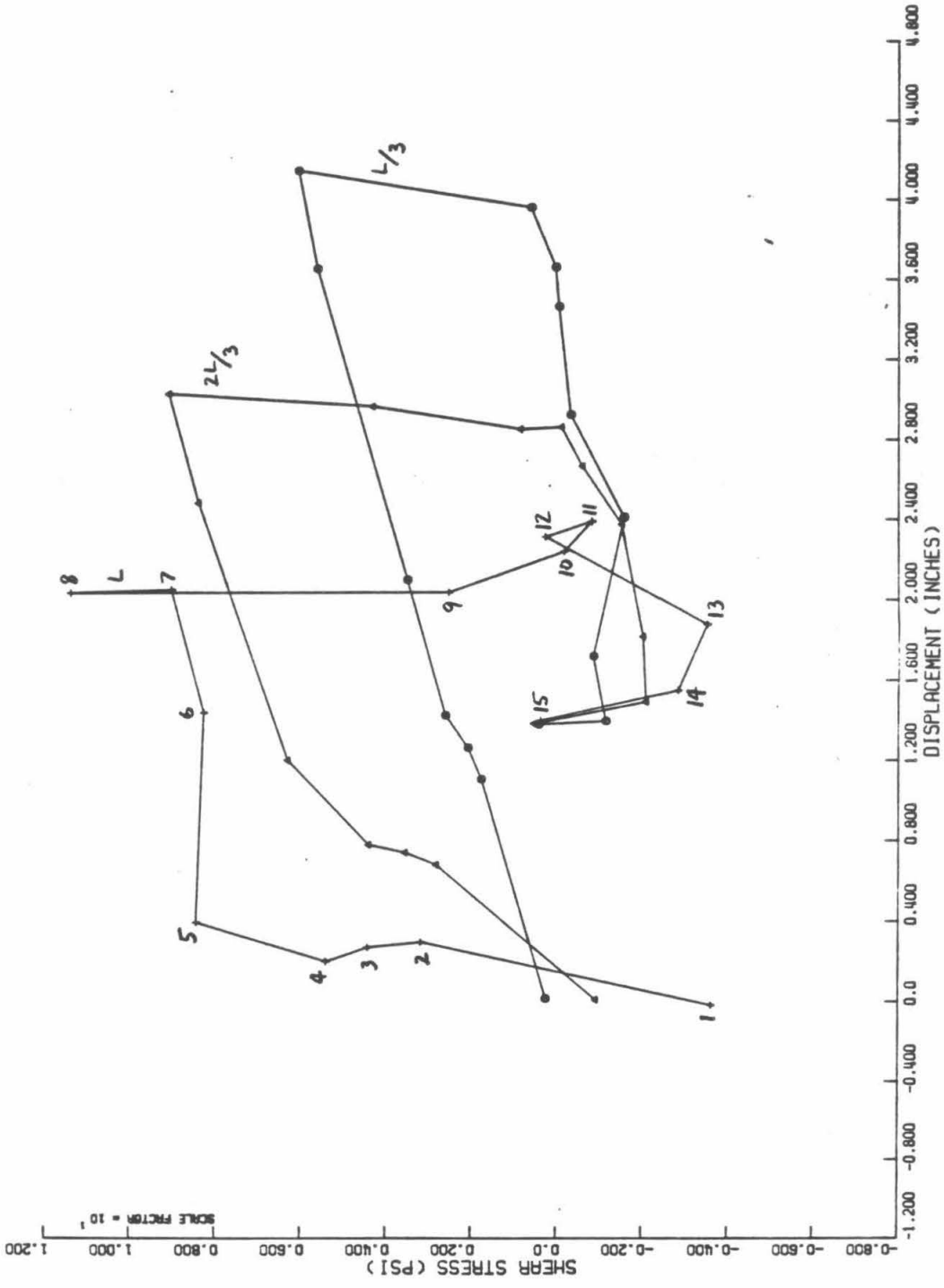

Figure 3.2e. t-z diagrams—Interval 1, Test 1

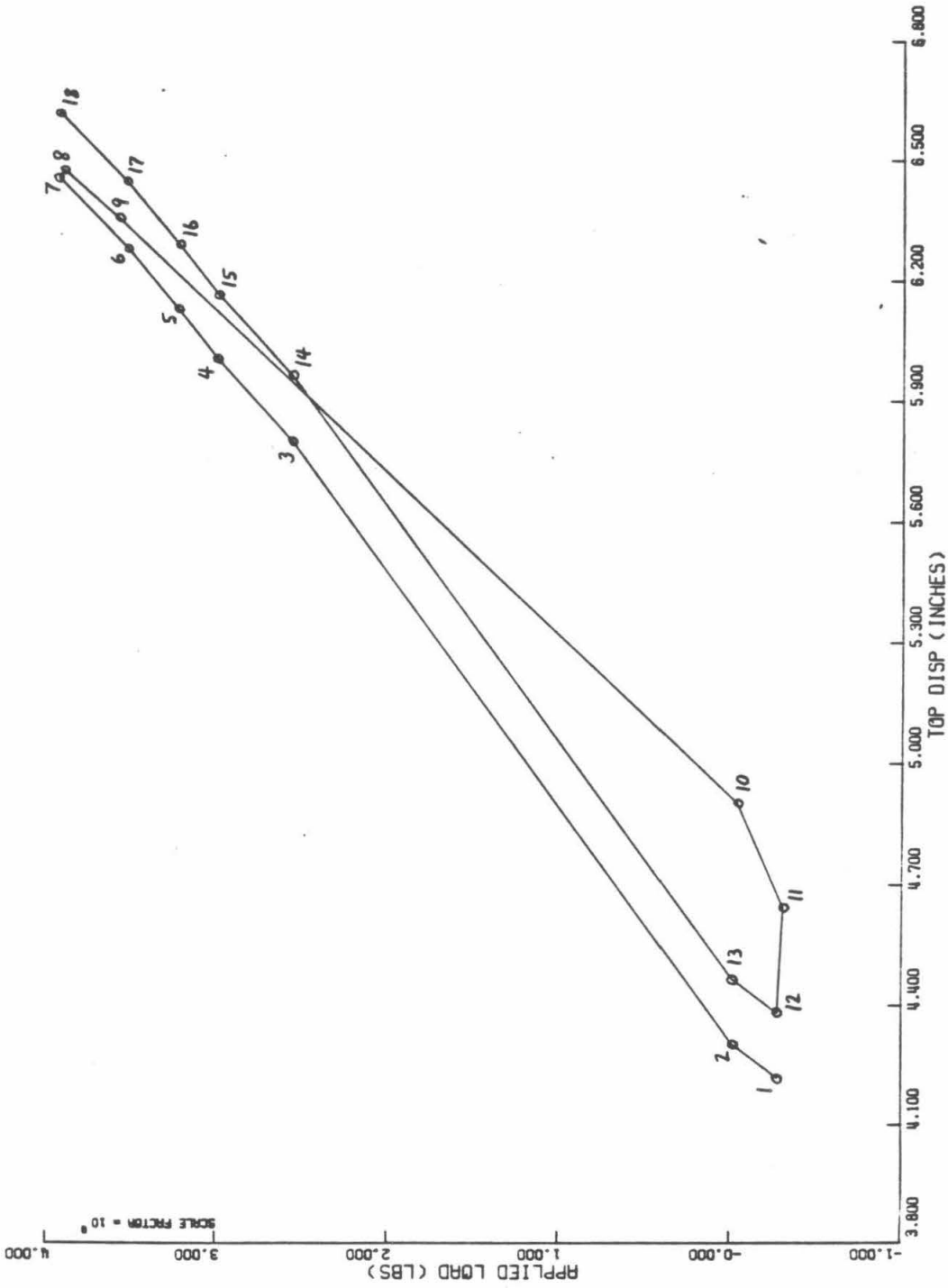

Figure 3.2f. Applied load vs. pile top displacement--Interval 2, Test 1

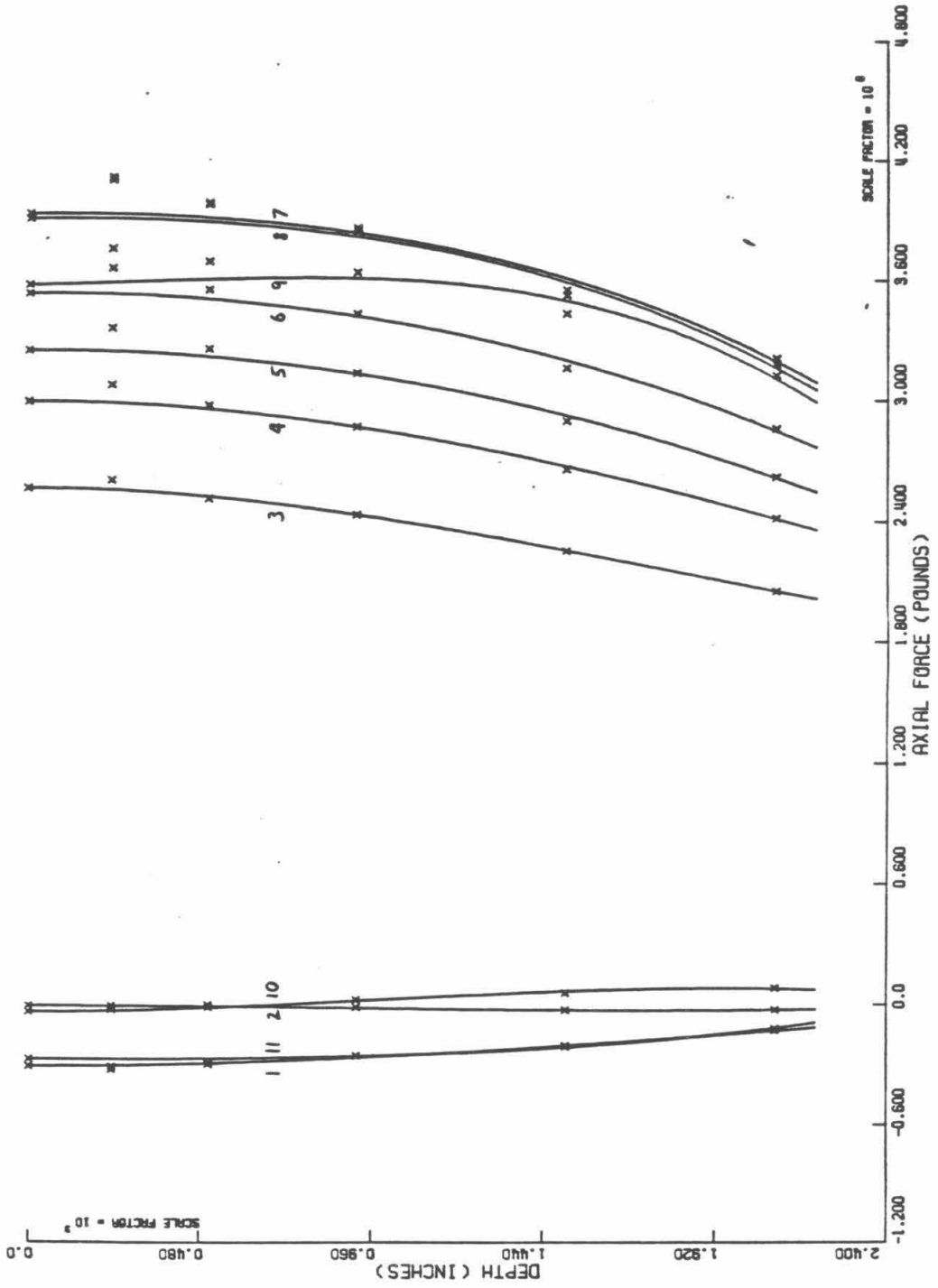

Figure 3.2g. Pile axial force, f(z)--Interval 2, Test 1

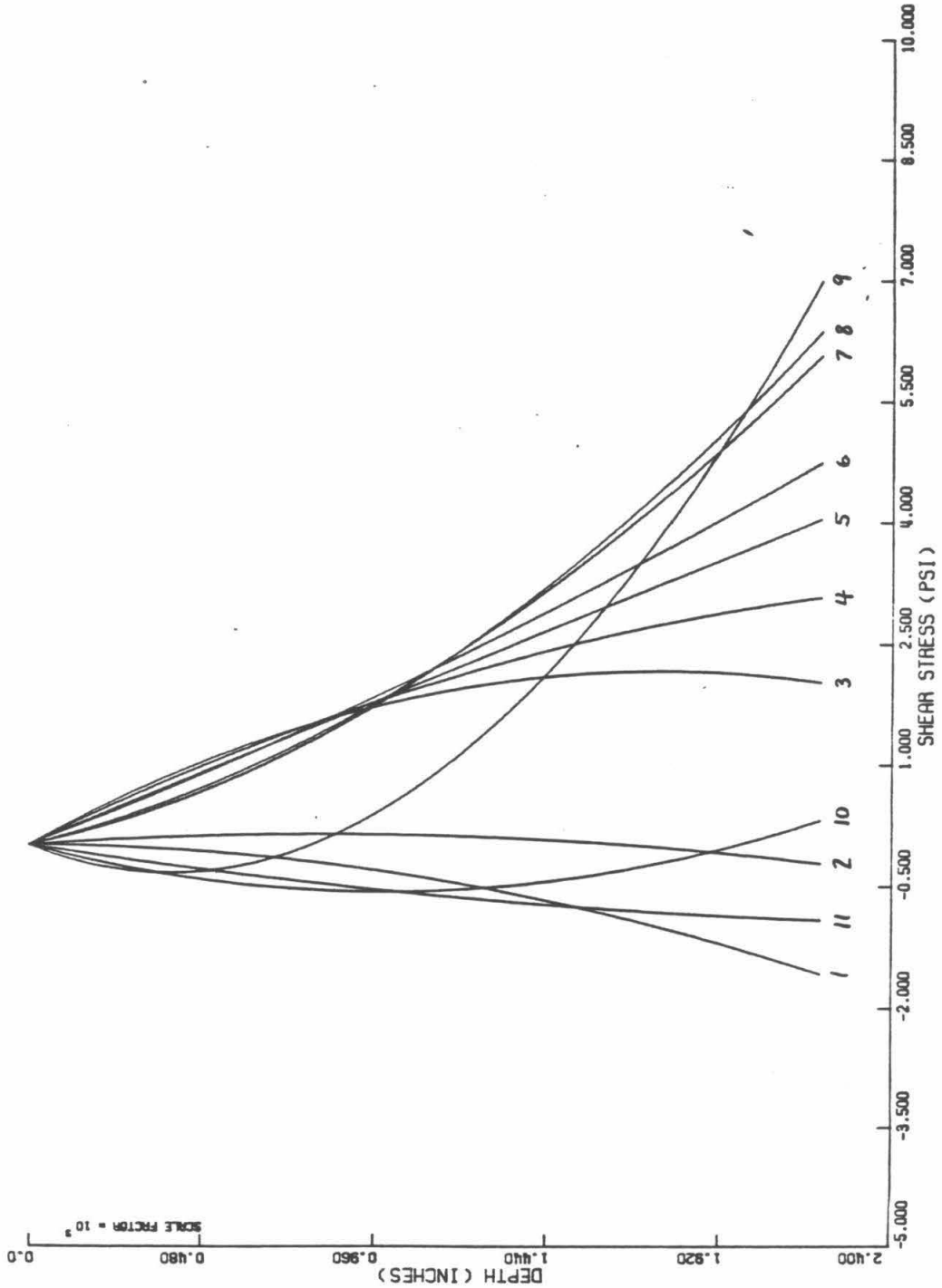

Figure 3.2h. Soil-pile shear stress, t(z)--Interval 2, Test 1

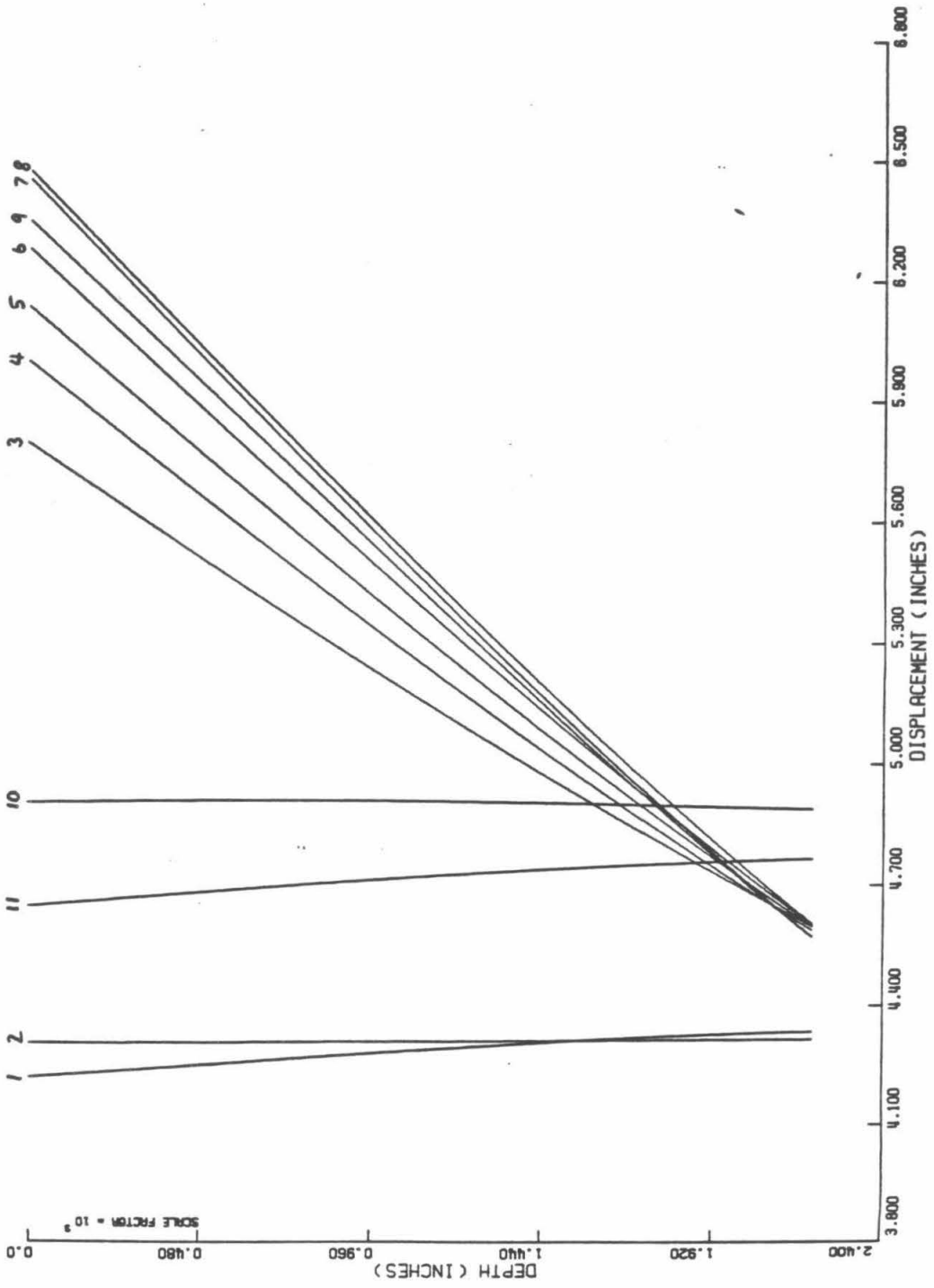

Figure 3.2i. Pile displacement, w(z)--Interval 2, Test 1

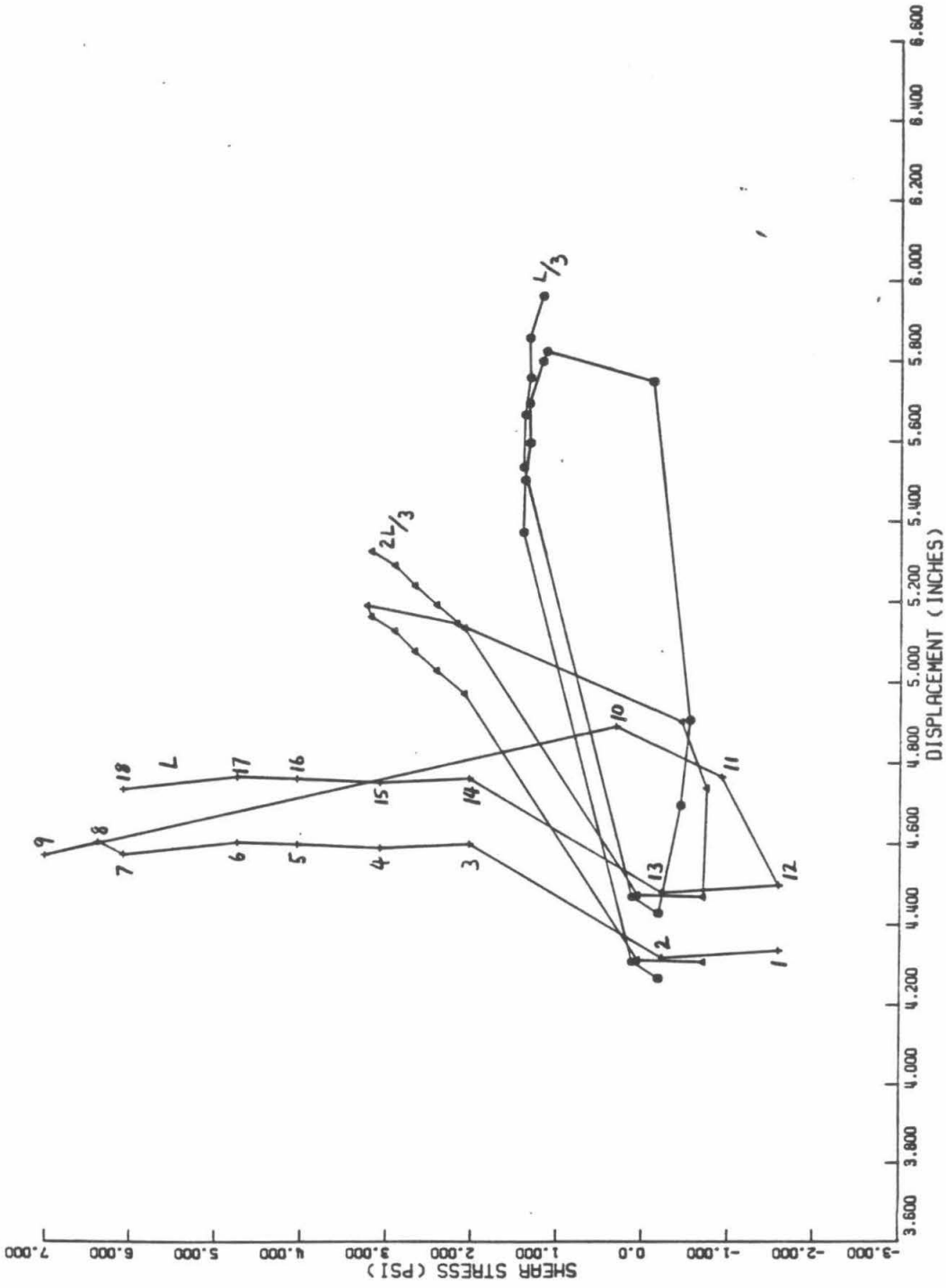

Figure 3.2j. t-z diagrams--Interval 2, Test 1

CHAPTER 4

CENTRIFUGE MODEL TESTS 3-6

4.1. Introduction

Tests 3-6 produced information concerning the behavior of piles embedded to a depth of about 55 feet in Nevada Fine Sand. The model soil mass is composed of dry NFS in Tests 3 and 4, and in Tests 5 and 6 the sand is saturated. These tests have two main purposes. First, as in Test 1, the behavior of certain prototype soil-pile systems, featuring ideal, homogeneous soil masses, is investigated under a variety of loadings. In particular, Tests 3-6 afford the opportunity to compare the behavior of systems differing primarily in the presence of groundwater. The second major purpose of these tests is to shed light on the accuracy of results obtained from the present centrifuge model tests. The prototype soil-pile system associated with Tests 5 and 6 is very similar to some of the full-scale field systems tested in connection with the Arkansas River Navigation Project [31]. Full scale and centrifuge model pile load testing results are compared in Chapter 5.

Tests 3 and 4 are nearly identical in their broad features, as are Tests 5 and 6. This duplication was performed to ensure that a clear picture was gained of model soil-pile system behavior in the dry and saturated soil mass cases. Since the procedures for the duplicate test pairs are nearly alike, these pairs of tests will be described together. Any significant disparities which existed between the matching tests will be noted in the course of the descriptions.

4.2. Specific Procedures and Results of Tests 3 and 4

4.2.1. Apparatus

Model pile B was used in these tests. Readings were not taken at strain gauge 3, which had produced very erratic signals in the preliminary calibration tests. The strip chart recorder was used in making the primary record of the remaining transducer signals.

4.2.2. Features of the Model Soil-Pile System

a. The soil mass was composed of dry NFS.

b. Special care was taken to achieve a high degree of compaction of the sand in the soil mass specimen. The following procedures were used in preparing the soil-pile model:

i. A base layer of sand of depth about 5-1/2 inches at its center was emplaced in the bottom of the bucket. This material was compacted by means of (a) probing and tamping with a metal rod and (b) vibration. Vibration was applied by striking the outside of the bucket with a hammer. To enhance the resulting compaction, three wedge-shaped lead plates (see Figure 4.1, below) with a combined weight of 11.3 pounds rested on the surface of the soil during the vibration.

ii. The model pile was placed in the center of this sand base by pushing its tip into the soil to a depth of about three inches.

iii. The remainder of the soil mass was packed around the pile in 2-3-inch layers, each such layer being compacted using the same methods applied to the base layer.

c. The degree of saturation of the sand in the soil specimen was 0%. Its average unit weight was 104 pcf and its porosity 0.37 in both Tests 3 and 4.

d. The friction angle of dry NFS was 33.2°. The coefficient of friction between the epoxy varnish with which the pile was coated and NFS was found to be 0.392.

e. The surface of the soil mass was 1.5 inches from the top of the centrifuge bucket.

f. The embedded length of the model pile was 20.4 inches.

4.2.3. The prototype-model scaling factor is taken as 33.0, the value of the acceleration applied to the system 10.2 inches above the model pile base, 37.1 inches from the centrifuge center of rotation. The prototype pile specifications are the following:

a. embedded length . . . 56.1 feet,

b. diameter . . . 17.3 inches, and

c. EA . . . 506,000 kips.

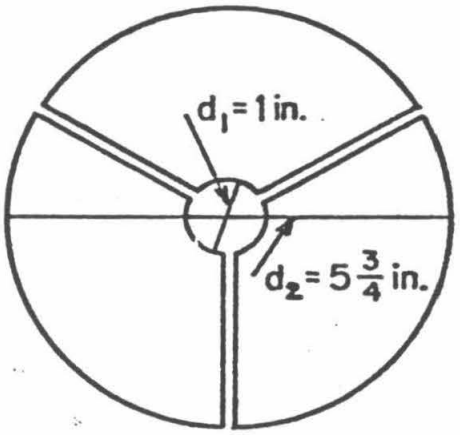

Figure 4.1 Lead plates used during compaction procedures of Tests 3-6

4.2.4. In Test 3, loads were applied to the top of the pile in the following sequence:

a. pulling to failure,
b. pushing to failure, unloading,
c. pushing to failure, unloading,
d. pushing to failure,
e. pulling to failure, unloading,
f. pulling to failure, unloading,
g. pulling to failure, unloading,
h. pulling to failure,
i. five-and-one-half pushing-pulling cycles.

The following two loading path intervals of Test 3 were interpreted using t-z diagrams:

a. Interval 1--From the unloaded condition following c, above, to the unloaded condition following e. The t-z curves for interval 1 were based on 12 digitized stations.

b. Interval 2--From the point of maximum pulling load in the third of the five-and-one-half pushing-pulling cycles of i, to the point of maximum mushing load in the fifth cycle. The t-z curves for interval 2 were based on 15 digitized stations.

4.2.5. The loading sequence in Test 4 was the following:

a. pulling to failure,
b. pushing to failure, unloading,
c. pushing to failure, unloading,
d. pushing to failure,
e. pulling to failure, unloading,
f. pulling to failure, unloading,
g. pulling to failure,
h. pushing to failure,
i. pulling,
j. four-and-one-half pushing-pulling cycles.

The following two loading path intervals of Test 4 were interpreted with t-z diagrams:

a. Interval 1--From the unloaded condition following c, above, to the unloaded condition following e. The t-z curves for interval 1 were based on 15 digitized stations.

b. Interval 2--From the point of maximum pulling load in the third of the four-and-one-half pushing-pulling cycles of j, to the point of maximum pushing load in the final half-cycle. The t-z curves for interval 2 were based 16 digitized stations.

4.2.6. The plotted results of Tests 3 and 4 appear in Figures 4.2a through 4.3j, as indicated in the table below.

TABLE 4.1. Figure Numbers for the Results of Tests 3 and 4

Graphs	Test 3		Test 4	
	Interval 1	Interval 2	Interval 1	Interval 2
Applied load versus pile top displacement	Fig. 4.2a	Fig. 4.2f	Fig. 4.3a	Fig. 4.3f
Pile axial force, $f(z)$	Fig. 4.2b	Fig. 4.2g	Fig. 4.3b	Fig. 4.3g
Soil-pile shear stress, $t(z)$	Fig. 4.2c	Fig. 4.2h	Fig. 4.3c	Fig. 4.3h
Pile displacement, $w(z)$	Fig. 4.2d	Fig. 4.2i	Fig. 4.3d	Fig. 4.3i
t-z diagrams	Fig. 4.2e	Fig. 4.2j	Fig. 4.3e	Fig. 4.3j

4.3. Specific Procedures and Results of Tests 5 and 6

4.3.1. Apparatus

Model pile B was used in these tests. Readings were not taken at strain gauges 3 and 9, which were not functioning correctly. The strip chart recorder was used in making the primary record of the remaining transducer signals.

4.3.2. Features of the Model Soil-Pile System

a. The soil mass was composed of saturated NFS.

b. The same procedures were used in preparing the soil-pile models for these tests as for Tests 3 and 4. During the layer-by-layer process of emplacement and compaction of the soil mass, the water level in the specimen was maintained just below the rising level of the soil surface.

c. The degree of saturation of the sand in the soil specimen was 100%. In both tests 5 and 6 the average total unit weight of the soil was 126 pcf and its porosity 0.37; thus its water content was 22%.

d. The coefficient of friction between the GLPT varnish with which the pile was coated and dry NFS was found to be 0.555.

e. The surface of the soil mass was 2.0 inches from the top of the centrifuge bucket in Test 5. In Test 6 this distance was 1.9 inches.

f. The embedded length of the model pile was 19.8 inches in Test 5 and 20.0 inches in Test 6.

4.3.3. Just as in Tests 3 and 4, the prototype-model scaling factor is taken as 33.0. The prototype pile specifications are the following:

a. embedded length . . . 54.6 feet in Test 5, 54.9 feet in Test 6,

b. diameter . . . 17.3 inches, and

c. EA . . . 506,000 kips.

4.3.4. In Test 5, loads were applied to the top of the pile in the following sequence:

a. pulling to failure,
b. pushing to failure, unloading,
c. pushing to failure, unloading,
d. pushing to failure,
e. pulling to failure, unloading,
f. pulling to failure, unloading,
g. pulling to failure,
h. pushing to failure,
i. pulling,
j. six pushing-pulling cycles.

The following two loading path intervals of Test 5 were interpreted with t-z diagrams:

a. Interval 1--From the unloaded condition following c, above, to the unloaded condition following e. The t-z curves for interval 1 were based on 14 digitized stations.

b. Interval 2--From the unloaded condition following the second of the pushing-pulling cycles of j, to the point of maximum pushing load in the fourth cycle. The t-z curves for interval 2 were based on 17 digitized stations.

4.3.5. The loading sequence in Test 6 was the following:

a. pulling to failure,
b. pushing to failure, unloading,
c. pushing to failure, unloading,
d. pushing to failure,
e. pulling to failure, unloading,
f. pulling to failure, unloading,
g. pulling to failure,
h. pushing to failure,
i. six pushing-pulling cycles.

The following two loading path intervals of Test 6 were interpreted with t-z diagrams:

a. Interval 1--From the unloaded condition following c, above, to the unloaded condition following e. The t-z curves for interval 1 were based on 17 digitized stations.

b. Interval 2--From the point of maximum pulling load in the second of the six pushing-pulling cycles of i, to the point of maximum pushing load in the fourth cycle. The t-z curves for interval 2 were based on 17 digitized stations.

4.3.6. The plotted results of Tests 5 and 6 appear in Figures 4.4a through 4.5j, as indicated in the table below.

TABLE 4.2. Figure Numbers for the Results of Tests 5 and 6

Graphs	Test 3		Test 4	
	Interval 1	Interval 2	Interval 1	Interval 2
Applied load versus pile top displacement	Fig. 4.4a	Fig. 4.4f	Fig. 4.5a	Fig. 4.5f
Pile axial force, $f(z)$	Fig. 4.4b	Fig. 4.4g	Fig. 4.5b	Fig. 4.5g
Soil-pile shear stress, $t(z)$	Fig. 4.4c	Fig. 4.4h	Fig. 4.5c	Fig. 4.5h
Pile displacement, $w(z)$	Fig. 4.4d	Fig. 4.4i	Fig. 4.5d	Fig. 4.5i
t-z diagrams	Fig. 4.4e	Fig. 4.4j	Fig. 4.5e	Fig. 4.5j

4.4. Remarks on the Plotted Results of Tests 3-6

4.4.1. Plots of applied load versus pile top displacement

These plots show $\delta_a[F_a(\tau)]$ for the loading path of a given test interval. Each plot is based on the Honeywell recorder load cell and displacements transducer readings at the t-z loading path basis stations, τ_j. A contour is formed by joining the data points for the successive stations by line segments, and the points are numbered.

The same plotting scales, both horizontal and vertical, have been used for all test intervals, so that the loading paths can be easily compared. As has been described above (see 2.6.1), loading path interval 1 includes pushing and pulling loading to near failure. The second loading path interval is

one-and-one-half-cycles taken from a series of pushing-pulling cycles later in the test. Pushing and pulling load levels about half those of interval 1 are reached here. In each test, the same displacement transducer reading--the reading at station 1 in the first interval--was taken as corresponding to zero displacement in both intervals 1 and 2. Thus, the relative vertical positions of the pile in the two loading intervals are represented correctly; their relationship on the X-Y recorder plot is reproduced.

The nonlinear and irreversible force-displacement behavior of the soil-pile system is evident in the $\delta_a(F_a)$ plots. Hysteresis associated with the dissipation of energy in soil yielding is seen in both the failure and cyclic loading intervals. Larger hysteresis loops are formed in the interval 1 failure loadings because yielding is more extensive here. The development of failure at high levels of pushing and pulling force is associated with the approach of the $\delta_a(F_a)$ curve to the horizontal, reduction of the effective stiffness of the system to zero. Complete failure, in this sense, was approached more closely in the pulling loadings of interval 1 than in pushing. The model soil- pile system was brought somewhat closer to complete pushing failure in the tests on saturated soils, 5 and 6, than in the dry soil tests.

4.4.2. Plots of Axial Force in the Pile as a Function of Depth

The function $f(x,\tau)$ is displayed at the t-z basis stations τ_j. Each curve is marked with the number of the station to which it corresponds. Thus, the axial force values $f(0)$ at the top of each curve match the force values of the corresponding station data point on the $\delta_a(F_a)$ plots. A single set of scales is used in plotting the interval 1 curves for all of Tests 3-6, and another for the interval 2 curves. In addition to the graphs of the constructed cubic polynomial functions $f(z,\tau)$, there are plotted the strain gauge data points on which these curves are based.

One important piece of information provided by the $f(z,\tau)$ curves is the tip load, the force exerted by the soil on the base of the pile. This is given by the value of the axial force at the bottom of each $f(z,\tau)$ curve. The proportions of the applied load carried by the wall and the tip of the pile at pushing failure in each of the tests on dry and saturated sand are indicated in Table 4.3, below. (At failure in pulling, the force acting on the base of the pile is negligible.) There is no substantial difference in the tip loads at pushing failure in the dry and saturated cases. The extra 30 kips measured

in the latter case may be attributed to the following facts: (a) the dry sand system was not brought as close to complete failure as the saturated system, and (b) the pile tip carried a greater proportion of the total applied load in the saturated case. The wall loads and their distributions with depth will be discussed in detail in section 4.4.4.

TABLE 4.3. Total Applied Loads and Tip Loads at Pushing and Pulling Failure

Tests	Pushing Failure Loads (kips)			Pulling Failure Loads (kips)
	Total	Tip	Wall	Total
3 and 4 (dry NFS, average)	452	264 (59%)	188 (41%)	106 (100% wall)
5 and 6 (sat. NFS, average)	454	294 (65%)	160 (35%)	57 (100% wall)

The shapes of the axial force curves shed light on the detailed behavior of the soil-pile system. For example, the sequence of $f(z,\tau)$ curves corresponding to stations 6, 7, 8, 9, 10, and 11 in interval 1 of Test 4 (Figure 4.3b) provide an interesting account of system behavior during unloading from pushing failure. The shape of curve 7 is nearly the same as that of 6, but at station 8, $f(z,\tau)$ has developed double curvature as the relaxation of compressive force at the top of the pile leaves a pocket of higher axial forces stranded, locked-in, in the lower reaches of the pile. The same double curvature is present to a milder degree at station 9. At station 10, the axial force lump has been eliminated and the reductions in applied load appear to be simply pulling the remainder of the $f(z,\tau)$ along. The

shape of the curve is little changed from this at station 11, where unloading is complete but a tip load remains. Unloading from failure in pushing develops similarly in several of the other loading path intervals of Tests 3-6, *e.g.*, interval 2 of Test 4 (Figure 4.3g).

4.4.3. Plots of Pile Axial Displacement as a Function of Depth

Graphs of the functions $w(z,\tau_j)$ are marked with their t-z basis station numbers. As with the curves of $f(z,\tau_j)$, one set of plotting scales and ranges is used for the $w(z,\tau_j)$ curves from the interval 1 loading paths, and another for the interval 2's, with the exception of the second interval of Test 3, in which loading was conducted in a slightly different displacement range. Net lengthening and shortening of the pile, which is represented by the difference between the values of $w(z,\tau_j)$ at the top and bottom of the pile, does not exceed 20 percent of the complete range of pile displacement in any loading path interval. Most of the pile displacement is due to the movement of the pile as a whole.

4.4.4. Plots of Soil-Pile Shear Stress as a Function of Depth

The graphs of the functions $t(z,\tau_j)$ at t-z basis stations are numbered, just as are the $f(z,\tau_j)$ and $w(z,\tau_j)$ curves. Again, one plotting scale combination is used for the interval 1's of Tests 3-6, and another for the second loading path interval of each test. As a result of the cohesionless soil boundary condition of zero shearing stress at ground surface (see 2.6.3), the functions $t(z,\tau_j)$ have in common the value zero at z = 0.

A form of inaccuracy present in the $t(z,\tau_j)$ curves for many of the test intervals should be noted. It is exemplified in the curves for interval 2 of Test 4 (Figure 4.3h). In this loading path interval, stations 6, 7, and 8 are successive stages in the course of unloading from pushing failure. Two kinds of flaw are exhibited by the $t(z,\tau_j)$ curves for these stations:

a. The value of $t(z,\tau_6)$ at the bottom of the pile is greater than the corresponding value at station 5. However, from basic energy considerations for the soil-pile system, no increase in soil-pile shear stress acting upward on the pile can be associated with a decrease in pushing load.

b. In roughly the upper third of the pile, $t(z,\tau_7)$ and $t(z,\tau_8)$ both show values significantly greater in magnitude than the stresses in this region along the pile at failure in pulling, yet the shear stresses in this region should be bounded by those developed at pulling failure.

These types of inconsistency may be observed in the $t(z,\tau_j)$ results from other loading path intervals of Tests 3-6, *e.g.*, interval 1 of Test 5 (Figure 4.4c). They are associated with unloading from pulling as well as from pushing. One possible explanation for these flaws is that the functions $t(z,\tau_j)$ are only quadratic polynomials and therefore have relatively little capacity for representing the measured pile behavior. [Recall that $t(z)$ is related to the derivative of the cubic polynomial $f(z)$, as expressed in equations (2.8) and (2.11).] At the same time, these inaccuracies may be attributed to the fact that measurement errors in the constructed function $f(z,\tau_j)$ will be magnified in its derivative.

It was tacitly assumed in item b, above, that the soil-pile shear stresses acting in a certain interval on the pile attain their maximum negative values when the pile is at failure in pulling. Indeed, on the basis of the reasonable working premise that the soil-pile yield strength at any point along the pile is independent of conditions elsewhere, it may be assumed that the maximum positive and negative values of $t(z)$ are achieved everywhere along the pile at pushing and pulling failure, respectively. Review of the $t(z,\tau_j)$ curves corresponding to these failure loading conditions indicates that yield strength distributions $t_{ys}(z)$ can be approximated by straight lines passing through the origin. That is, for a constant α,

$$t_{ys}(z) = \alpha z \tag{4.1}$$

Values of α corresponding to pushing and pulling failure in both dry and saturated sand are tabulated below.

TABLE 4.4. Linear Approximations to Yield Strength Distributions

Tests	Pile Length (feet)	Pushing Failure		Pulling Failure	
		$t_{ys}(L)$ (psi)	α (psi/ft)	$t_{ys}(L)$ (psi)	α (psi/ft)
3 and 4 (dry NFS)	56.1	10.3	.183	5.8	.103
5 and 6 (sat. NFS)	54.7	9.0	.164	3.2	.058

Since there is little variation in soil strength with radial distance from the model pile, the shearing stresses are a maximum at the pile wall, and it is at the soil-pile interface that soil shear failure occurs. Therefore, the yield strength at all points along the pile is directly related to the coefficient of friction, f_{sp}, between the soil and pile materials, according to

$$t_{ys}(z) = f_{sp}\overline{\sigma}_r(z)$$

where $\overline{\sigma}_r(z)$ is the normal stress exerted by the soil on the pile wall, the lateral soil pressure, at failure. Linear distributions of lateral soil pressure with depth, corresponding to the yield strength distributions described by equation (4.1), are given by

$$\overline{\sigma}_r(z) = \frac{t_{ys}(z)}{f_{sp}} = \frac{\sigma}{f_{sp}} z = \beta z \qquad (4.2)$$

The values of β corresponding to pushing and pulling failure in Tests 3-6 are given in Table 4.5, below.

TABLE 4.5. Linear Approximations to Lateral Soil Pressure Distributions at Pushing and Pulling Failure

Tests	Soil-pile Friction Coefficient, f_{sp}	Pushing Failure		Pulling Failure	
		α (psi/ft)	β (psi/ft)	α (psi/ft)	β (psi/ft)
3 and 4 (dry NFS)	.392	.183	.467	.103	.263
5 and 6 (sat. NFS)	.555	.164	.295	.058	.105

A more meaningful comparison can be made of the soil-pile shear stresses, $t(z)$, measured in tests on dry and saturated sand by taking into account the reduced effective stresses in the saturated soil due to buoyancy. Assuming that in all cases the vertical effective stress, $\overline{\sigma}_z$, increases with depth in accordance with the effective unit weight of the soil, in Tests 3 and 4,

$$\overline{\sigma}_z(z) = \gamma_d z = 104 \frac{pcf}{ft} z = 0.722 \frac{psi}{ft} z = \eta z$$

and in Tests 5 and 6,

$$\overline{\sigma}_z(z) = \gamma' z = (\gamma - \gamma_w) z = (126 - 62.4) \frac{pcf}{ft} z = 0.442 \frac{psi}{ft} z = \eta z$$

The lateral earth pressure coefficients in the tests on dry and saturated soil can now be calculated as

$$K = \frac{\overline{\sigma}_r}{\sigma_z} = \frac{\beta}{\eta}$$

The resulting values of K at pushing and pulling failure are tabulated below.

TABLE 4.6. Lateral Earth Pressure Coefficients at Pushing and Pulling Failure

Tests	η (psi/ft)	Pushing Failure		Pulling Failure	
		β (psi/ft)	K	β (psi/ft)	K
3 and 4 (dry NFS)	.722	.467	.647	.263	.364
5 and 6 (sat. NFS)	.442	.295	.667	.105	.238

The effect of buoyancy on effective stresses in the saturated soil accounts very well for the observed differences in lateral soil pressure at pushing failure in the the dry and saturated systems. However, the presence of water appears to reduce pulling resistance more than would be indicated by effective stress considerations alone.

5. t-z Diagrams

For each loading path interval, the t-z diagrams corresponding to depths L/3, 2L/3, and L are presented. To avoid cluttering the plots, only the points making up the diagram corresponding to depth L are numbered. For each test interval, the coordinate axes span the same ranges of soil-pile shear stress and pile displacement as were used in the plots of $t(z)$ and $w(z)$ for this interval.

The t-z diagrams have roughly the same shapes as the corresponding graphs of applied load versus pile top displacement. Maximum soil-pile shear stress magnitudes--both for stresses acting upward and downward on the pile--increase with depth, reflecting increases in soil yield strength. On the other hand, maximum displacement magnitudes decrease with depth because the lower parts of the pile are in some sense buffered from loads and displacements applied at the surface. For the same reason, conditions at increasing depth increasingly lag applied load events. An example of this is provided by the t-z diagrams for interval 1 of Test 3: At loading path station 8, the maximum value of shear stress acting downward on the pile has already been reached at depth L/3. At depth 2L/3 the stress level has moved about half way from its maximum positive (upward on the pile) to its maximum negative values. At the bottom of the pile, $z = L$, the soil-pile shear stress remains, at station 8, near its maximum positive value.

Certain anomalous features are produced in the t-z diagrams by the $t(z)$ inaccuracies discussed in item 4, above. Odd loops are generated near the point of maximum positive shear stress in the $z = L$ diagrams for all the loading path intervals of the tests on dry sand. These loops are not present in the t-z diagrams for the tests on saturated sand because the soil-pile yield strength, $t_{ys}(z)$, is lower in these tests, and less capacity exists for the maintenance of locked-in axial forces.

The initial stiffnesses at corresponding depths in the dry and saturated systems are similar, increasing approximately linearly with depth. However, while abrupt yielding at the soil-pile interface is observed in the saturated sand, in the dry sand the t-z stiffness falls off only gradually. In fact, at the highest values of pushing load applied to the piles in dry sand, the pile walls appear to retain significant additional strength.

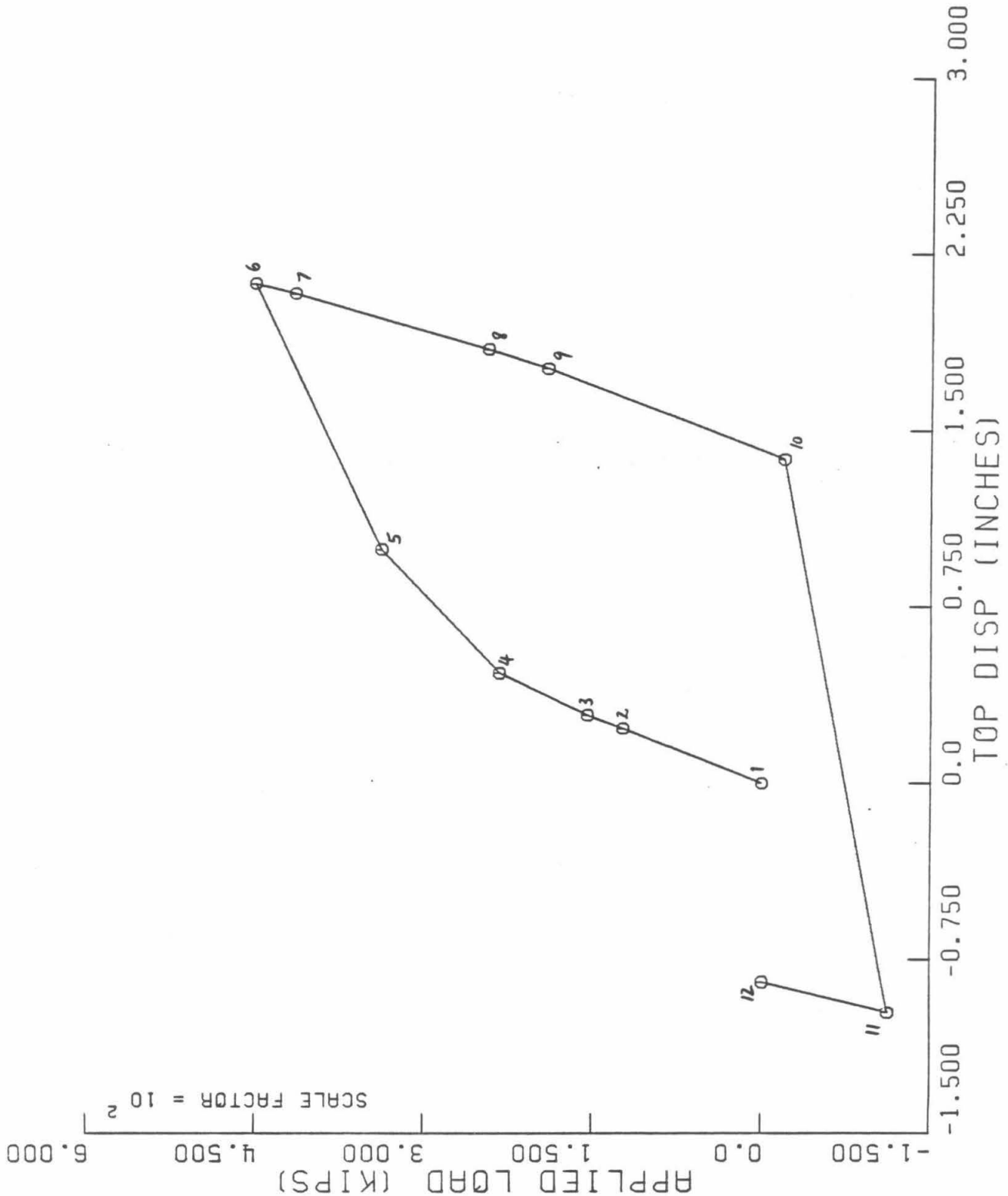

Figure 4.2a. Applied load vs. pile top displacement--Interval 1, Test 3

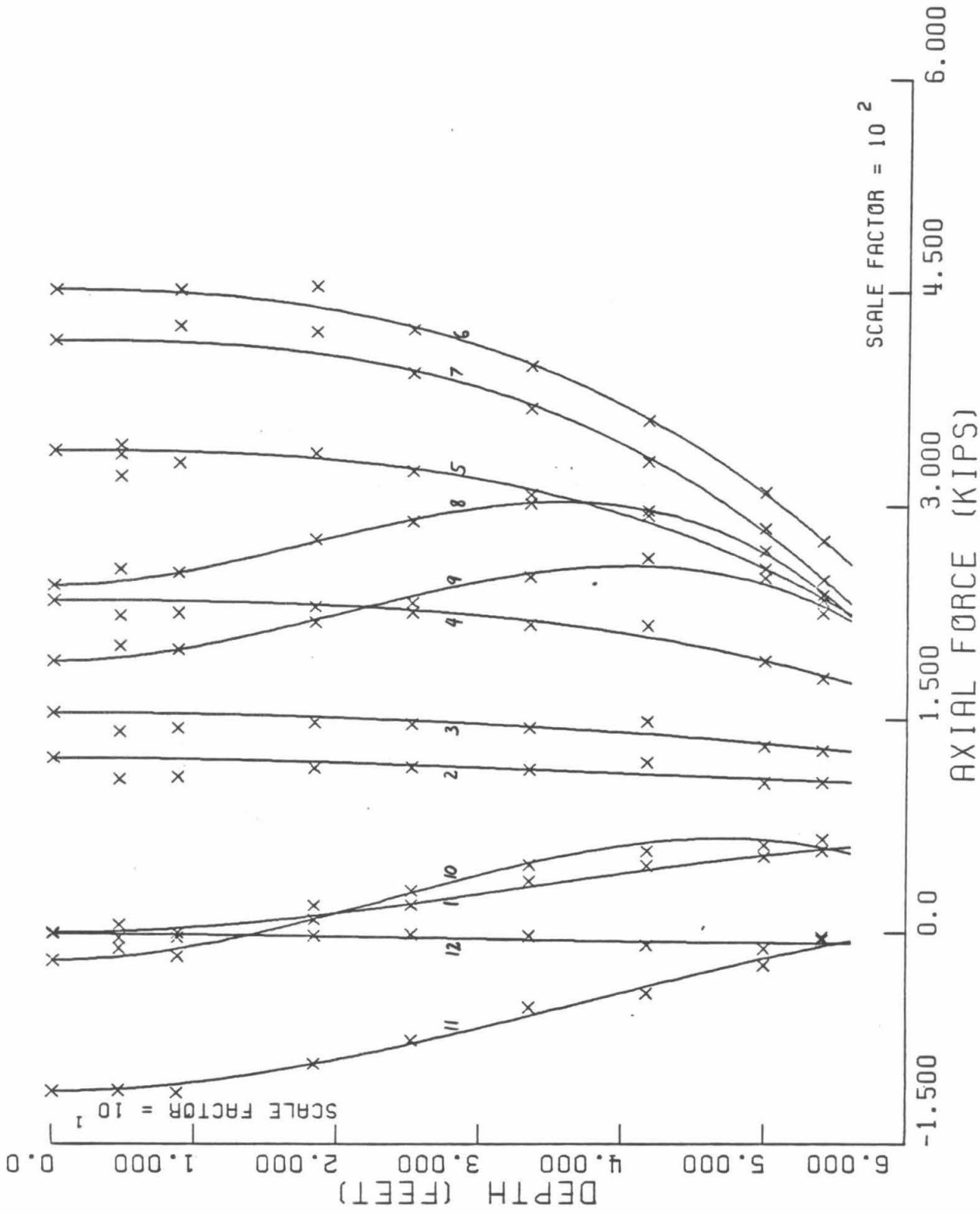

Figure 4.2b. Pile axial force, f(z)—Interval 1, Test 3

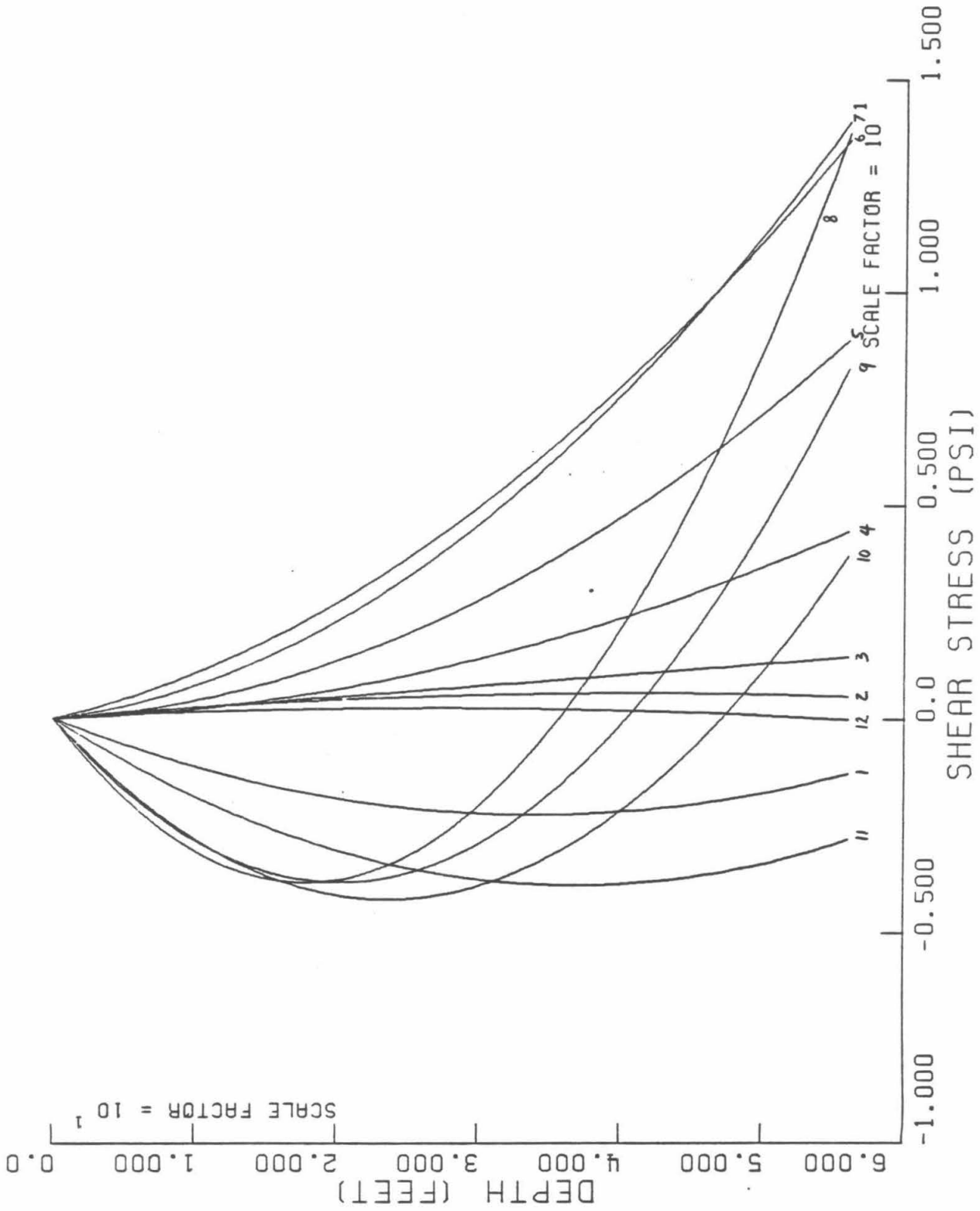

Figure 4.2c. Soil-pile shear stress, t(z)--Interval 1, Test 3

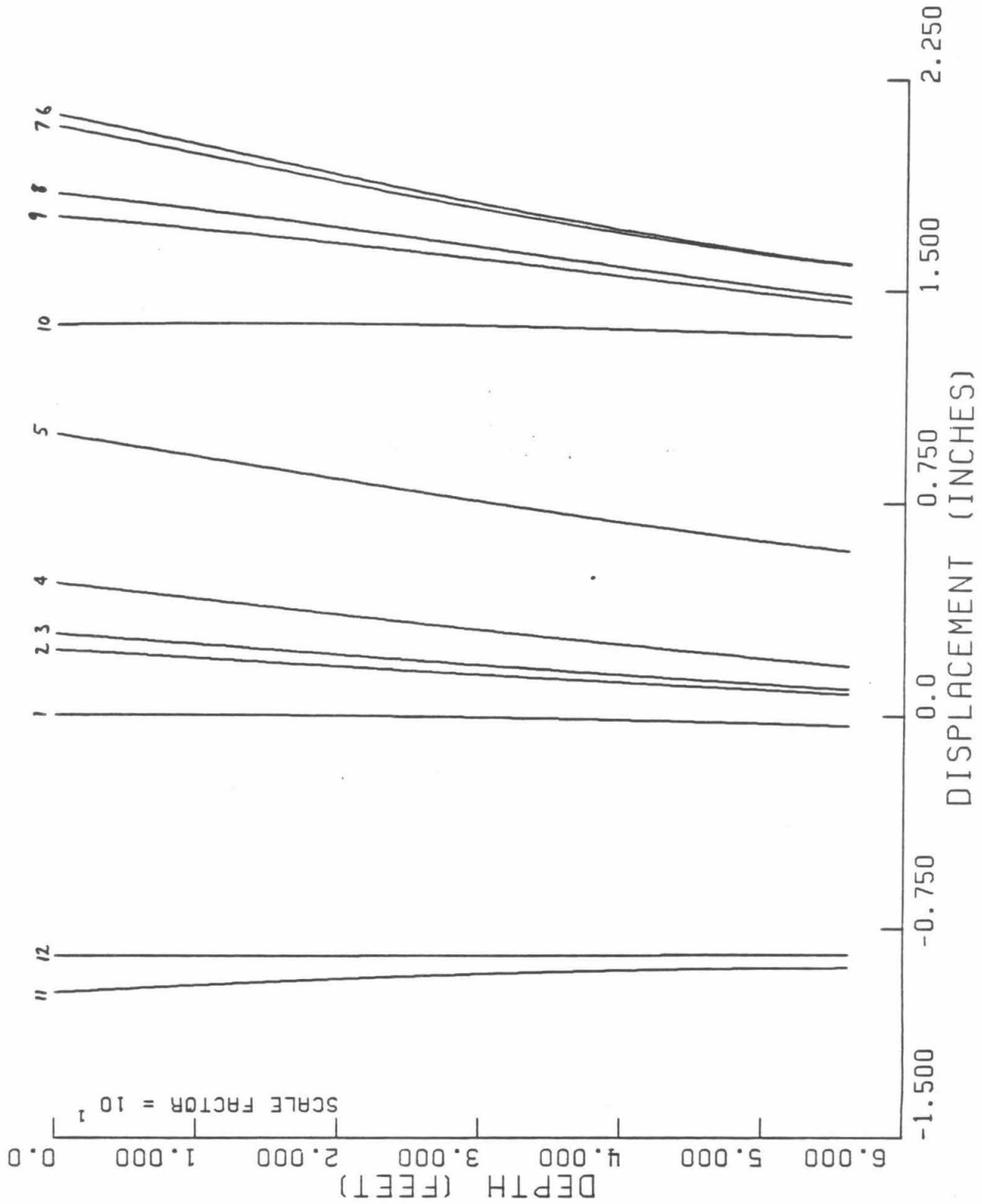

Figure 4.2d. Pile displacement, w(z)—Interval 1, Test 3

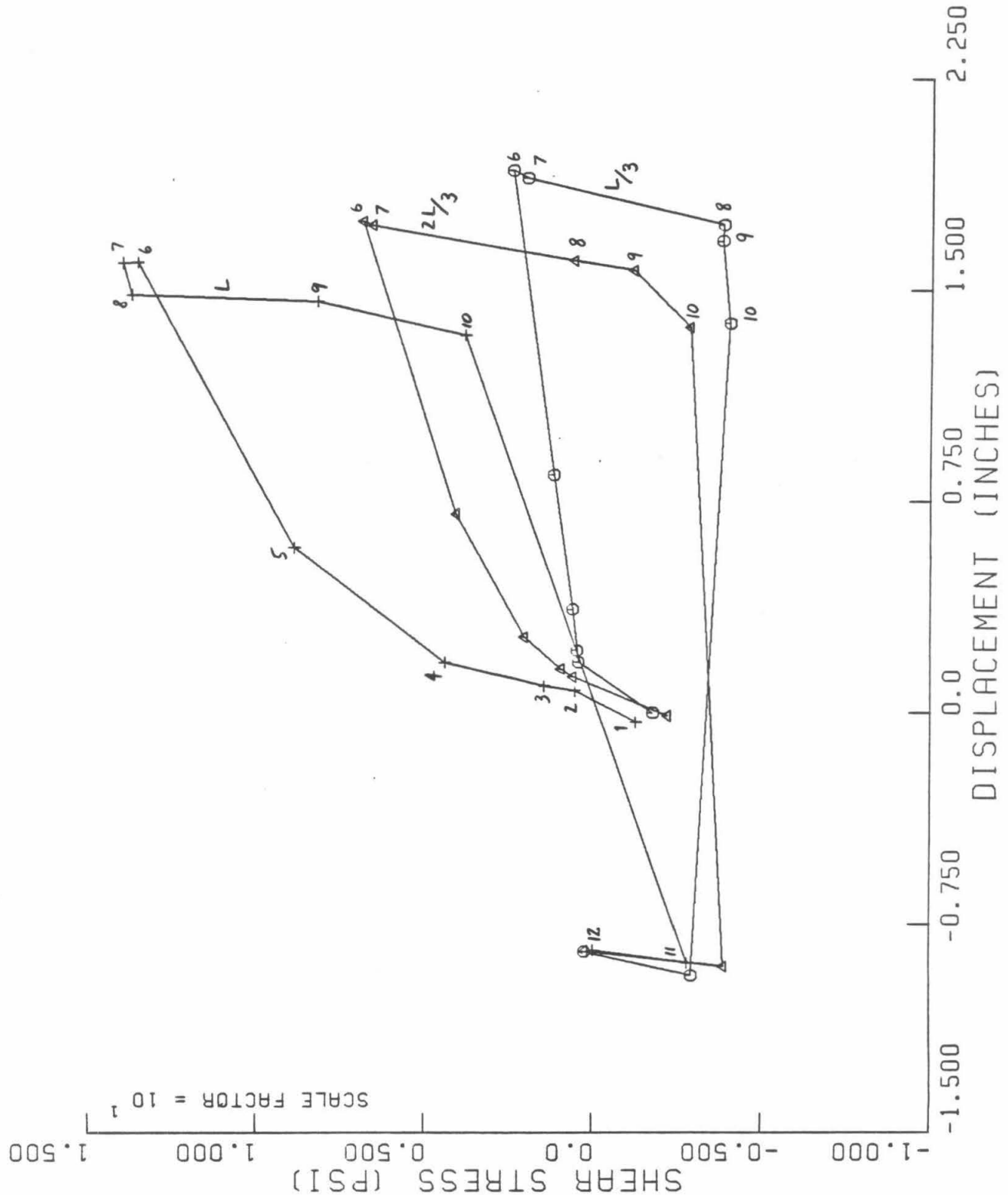

Figure 4.2e. t-z diagrams--Interval 1, Test 3

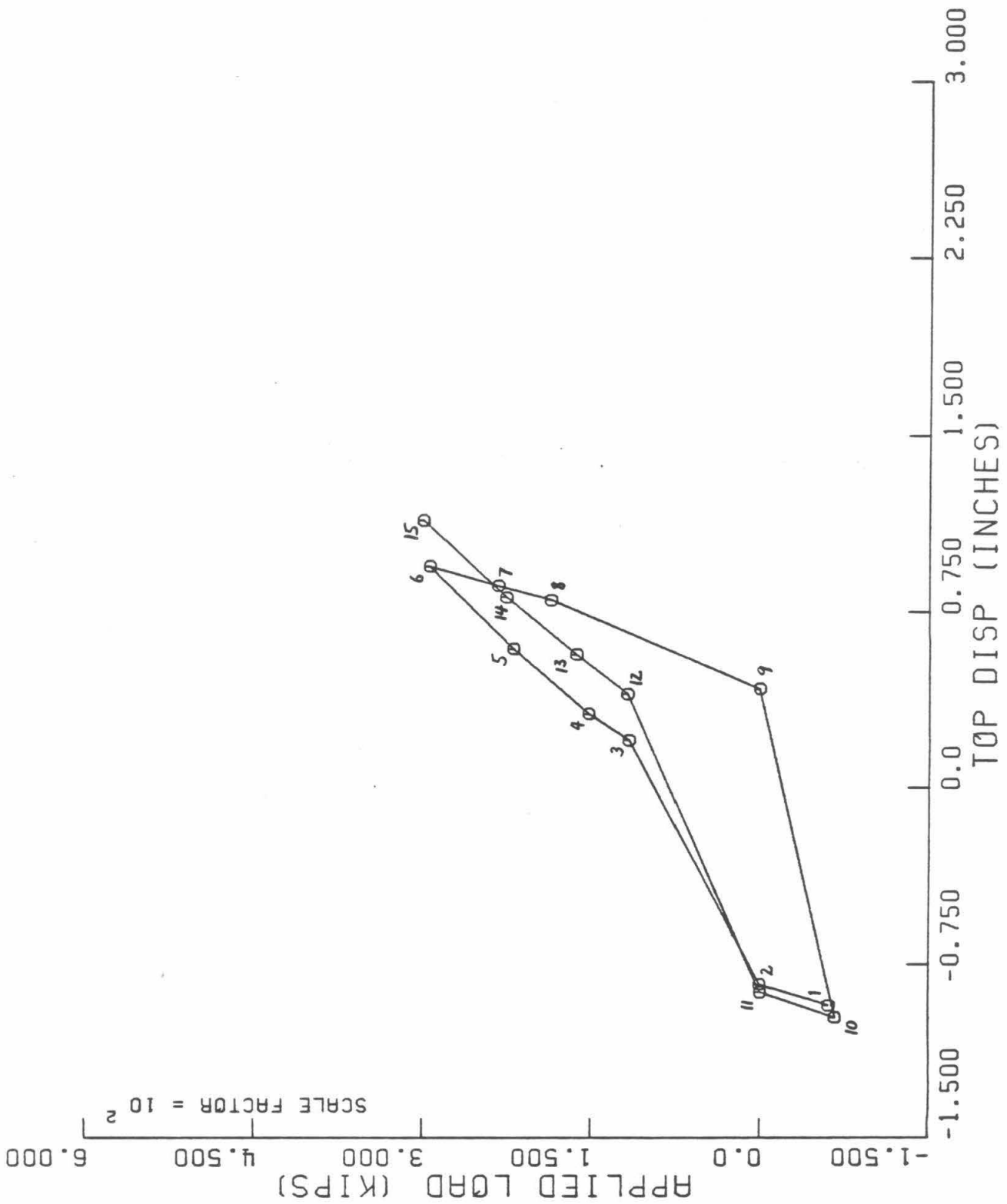

Figure 4.2f. Applied load vs. pile top displacement--Interval 2, Test 3

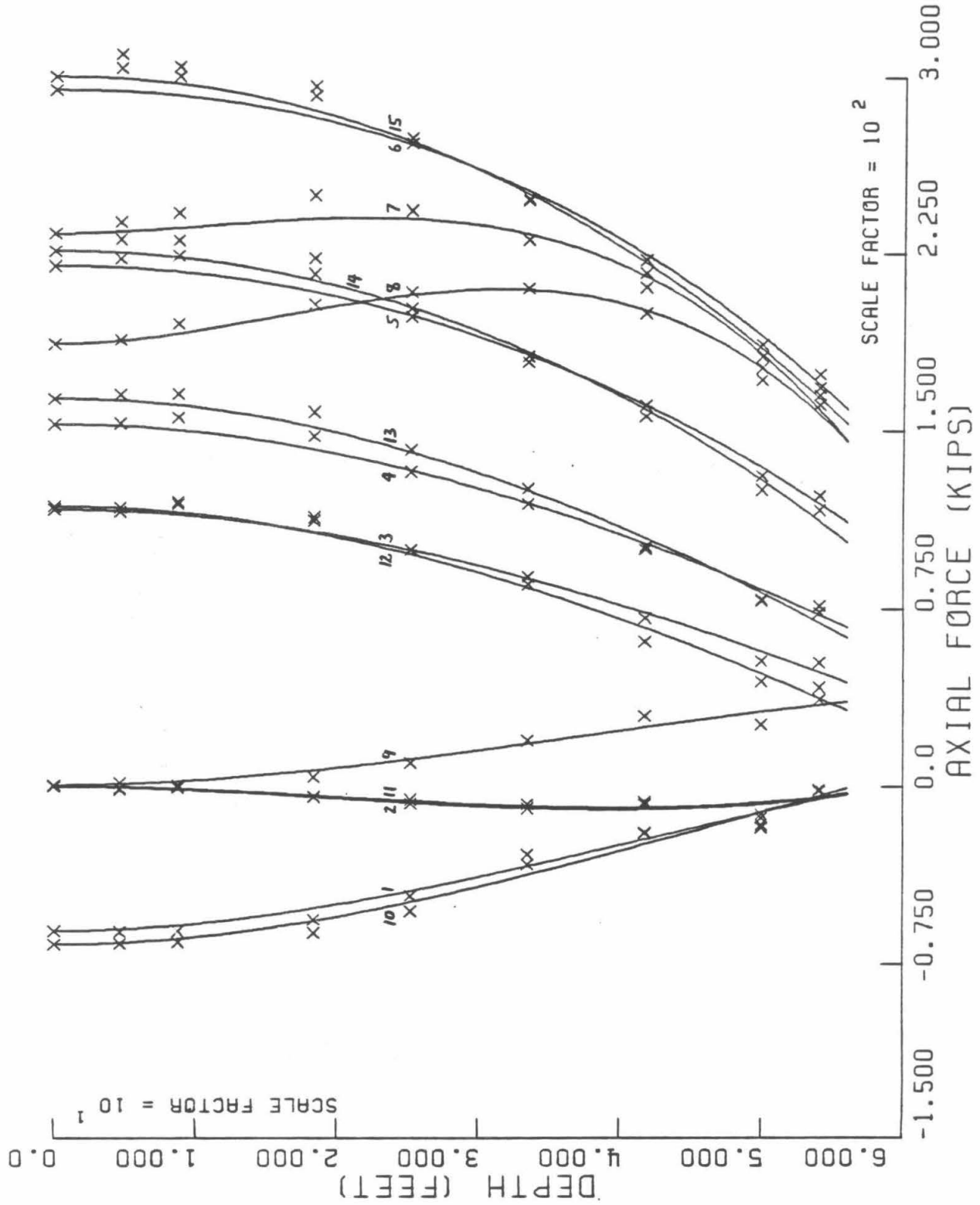

Figure 4.2g. Pile axial force, f(z)--Interval 2, Test 3

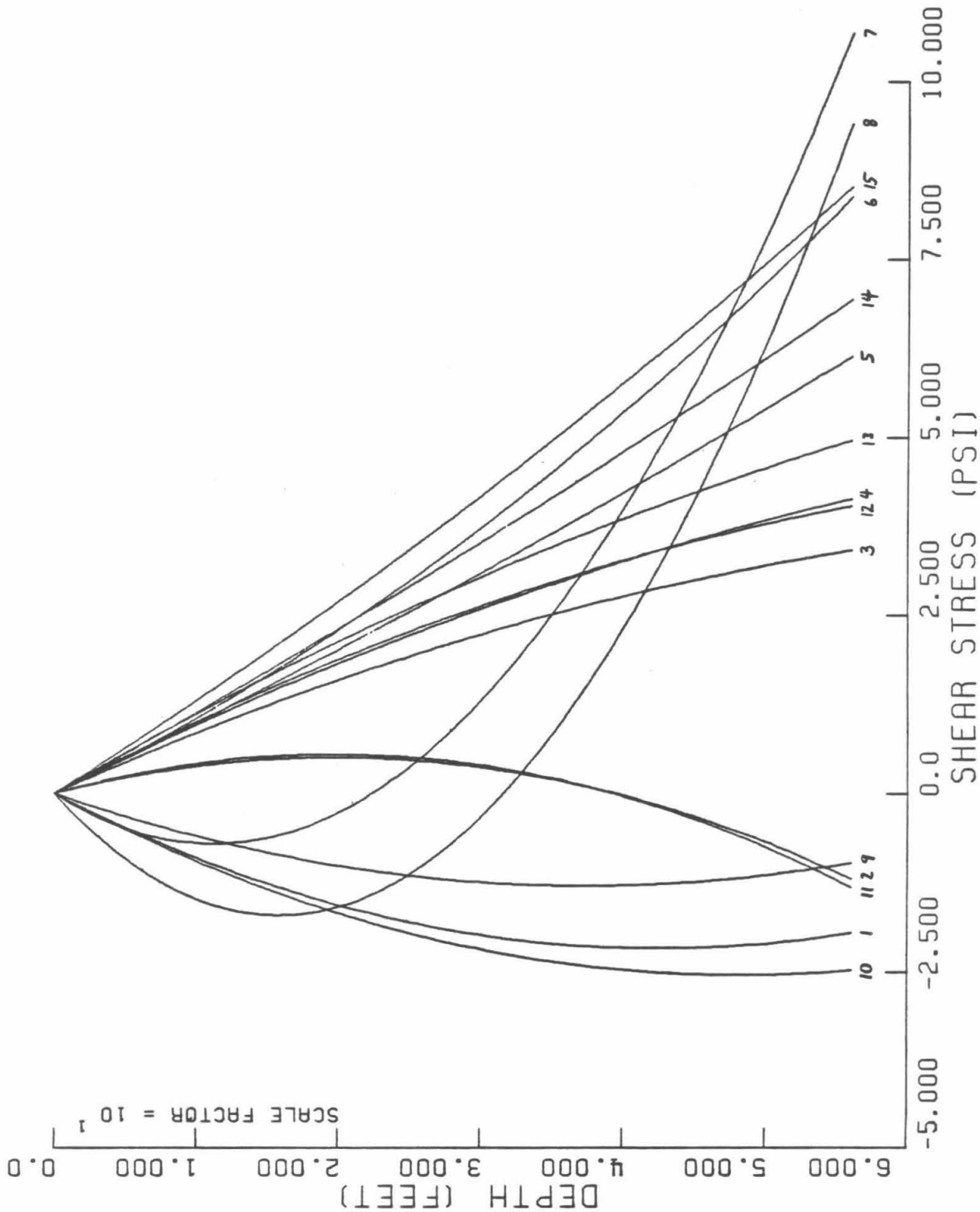

Figure 4.2h. Soil-pile shear stress, t(z)--Interval 2, Test 3

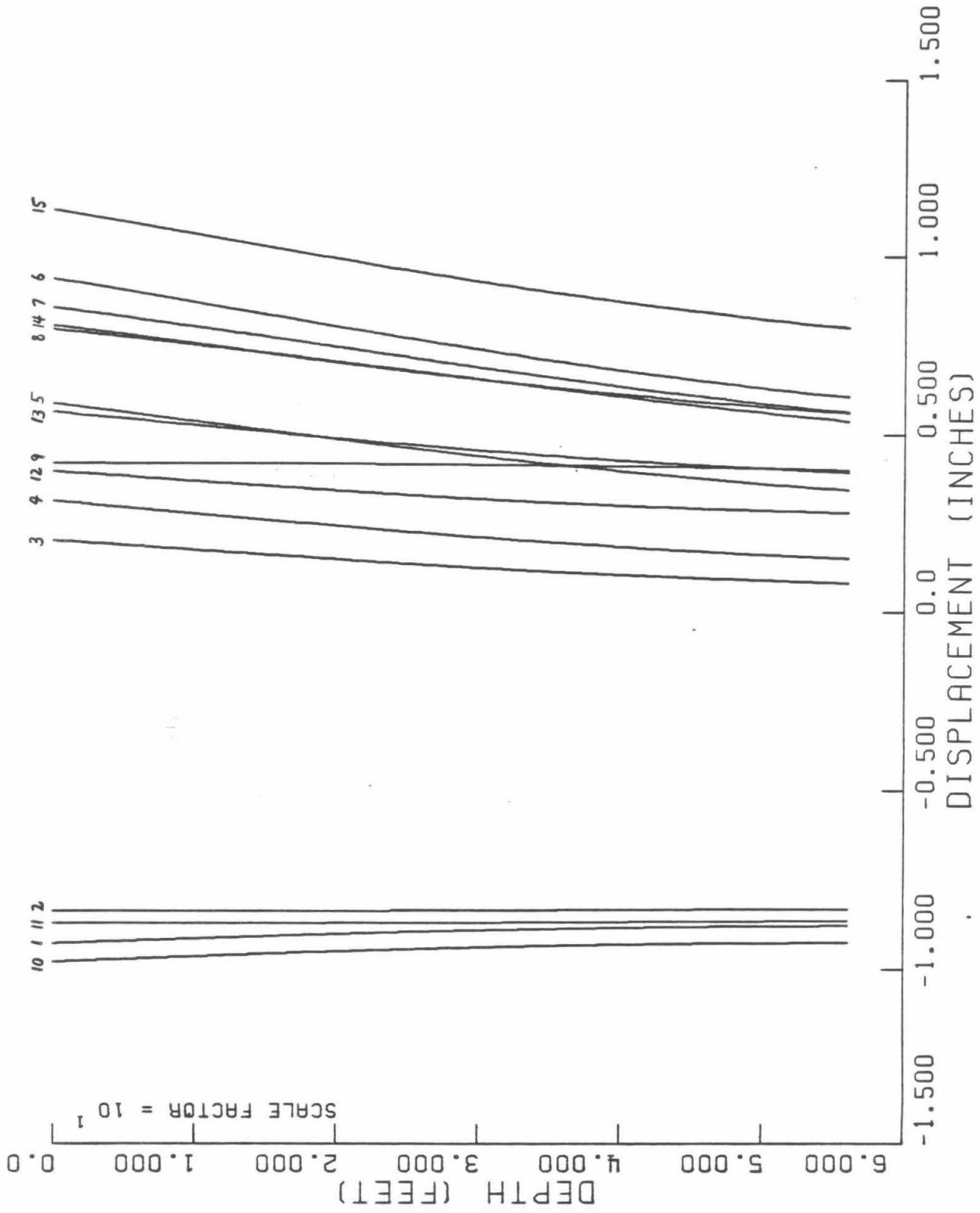

Figure 4.2i. Pile displacement, w(z)--Interval 2, Test 3

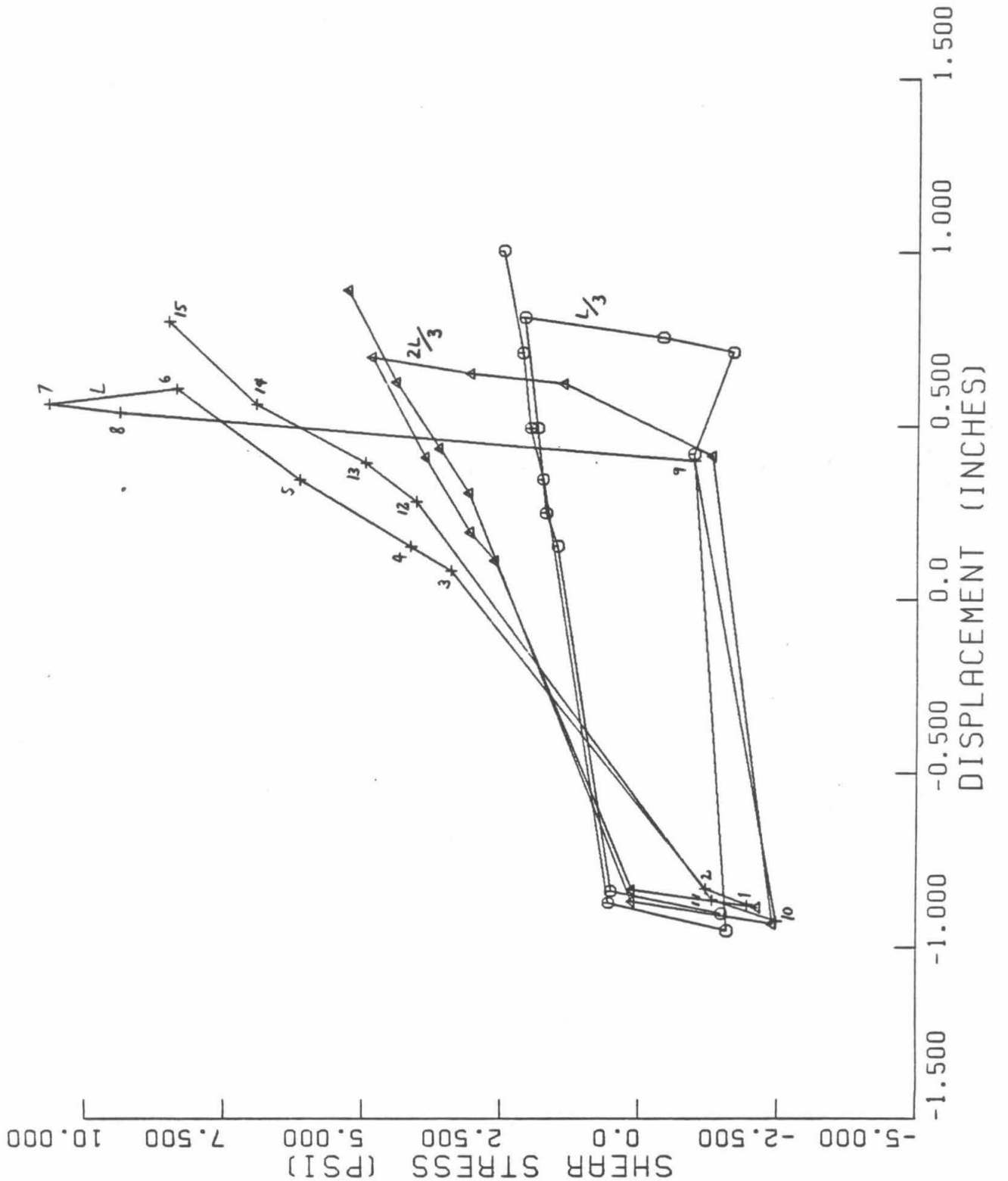

Figure 4.2j. t-z diagrams—Interval 2, Test 3

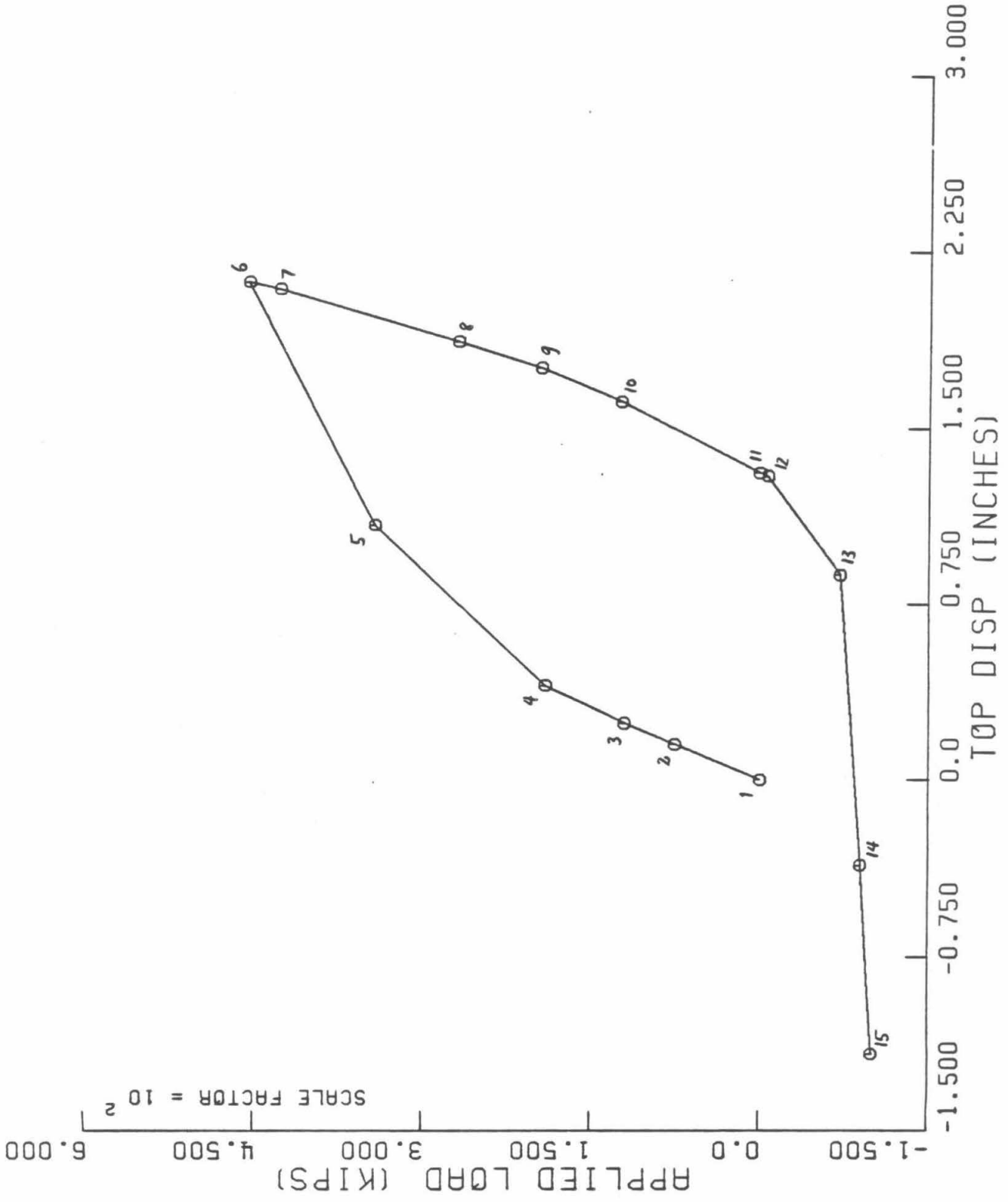

Figure 4.3a. Applied load vs. pile top displacement--Interval 1, Test 4

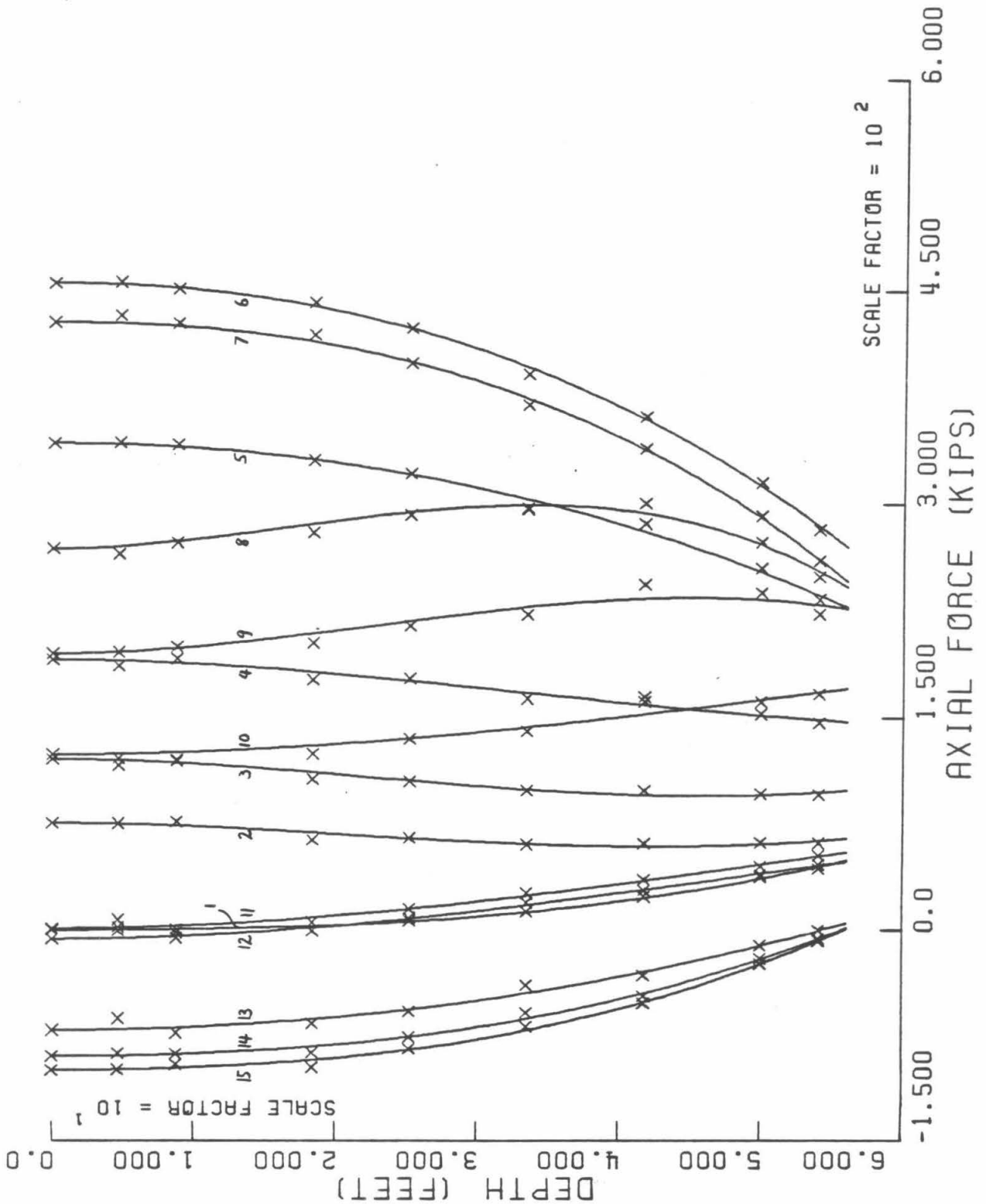

Figure 4.3b. Pile axial force, f(z)—Interval 1, Test 4

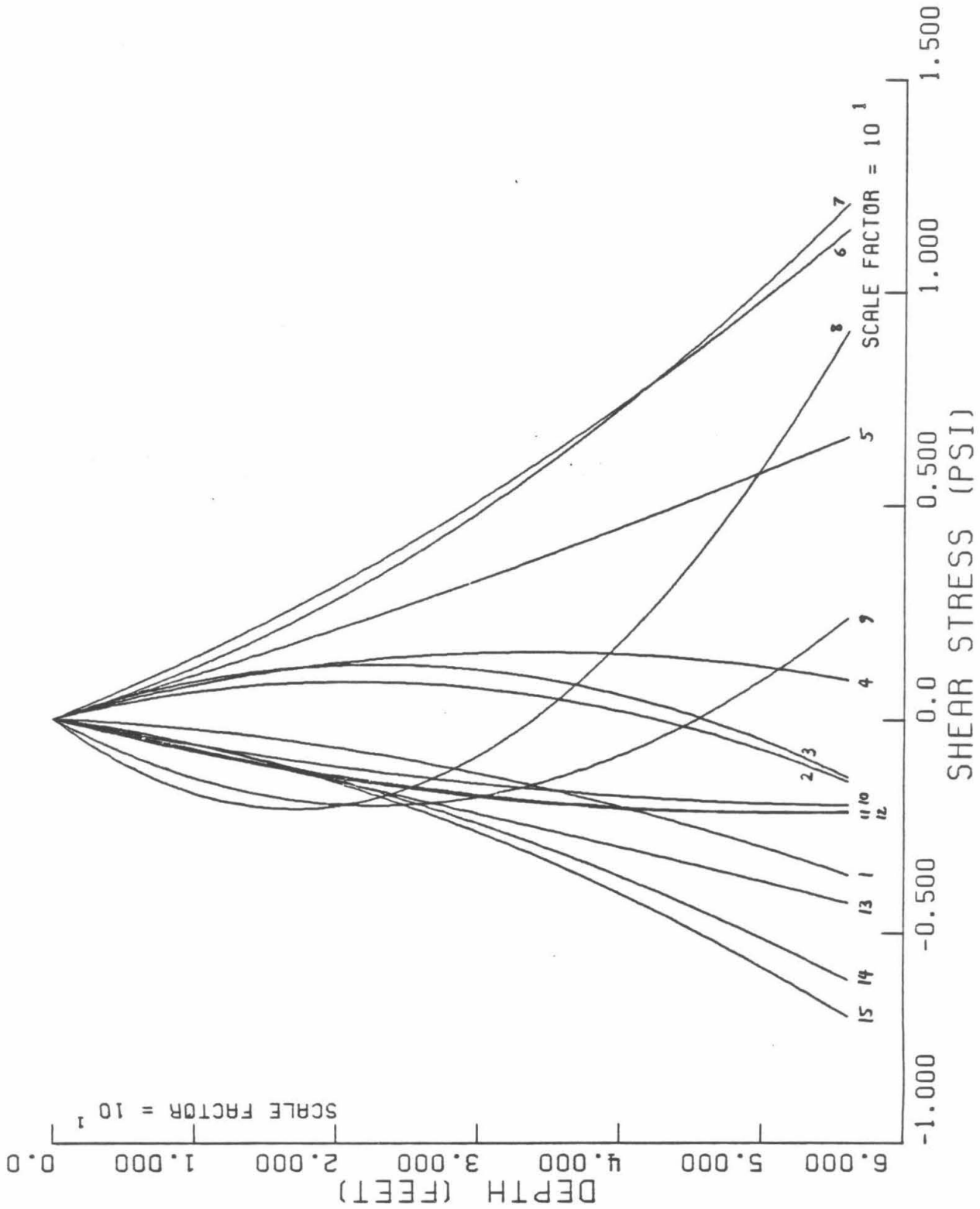

Figure 4.3c. Soil-pile shear stress, t(z)--Interval 1, Test 4

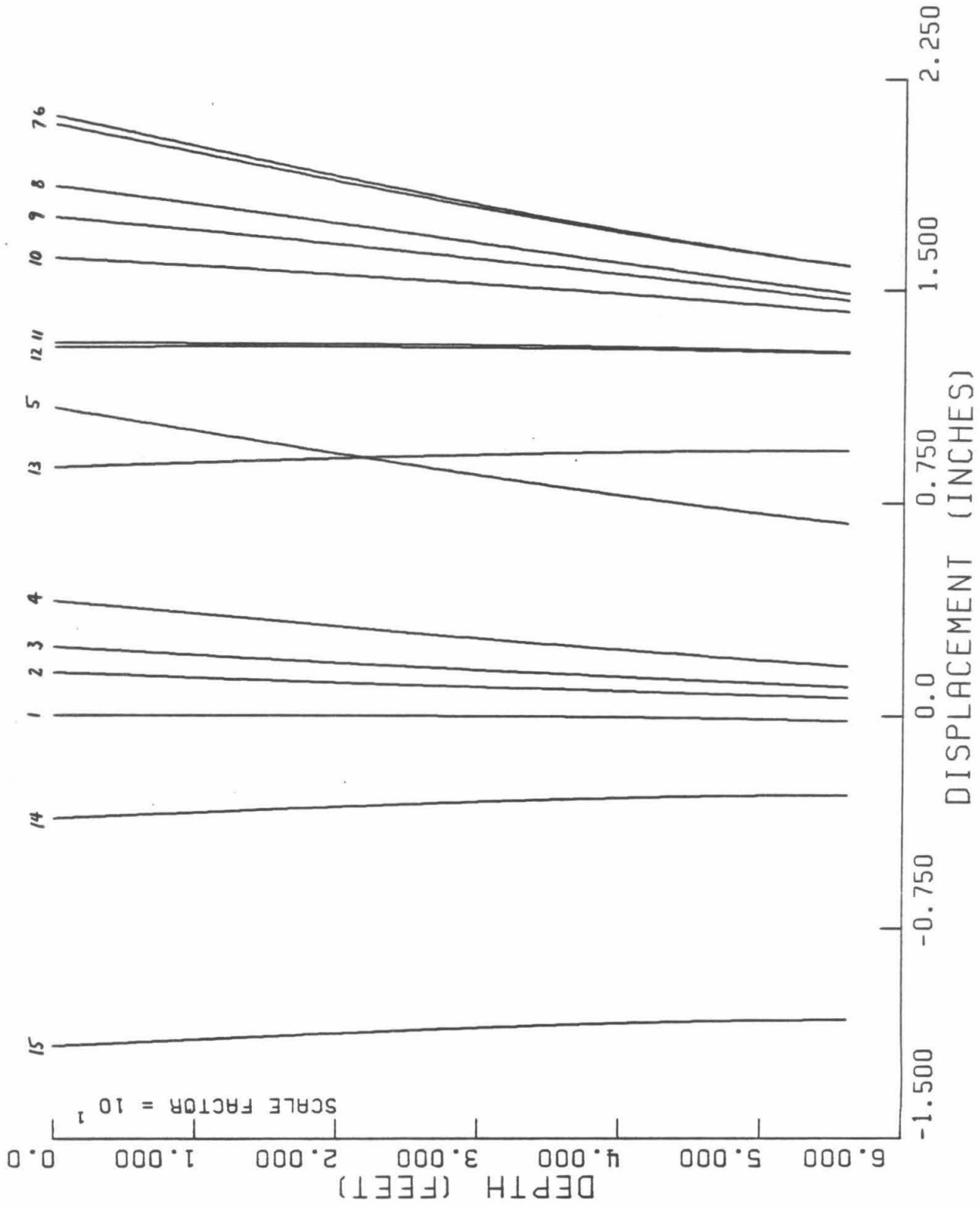

Figure 4.3d. Pile displacement, w(z)—Interval 1, Test 4

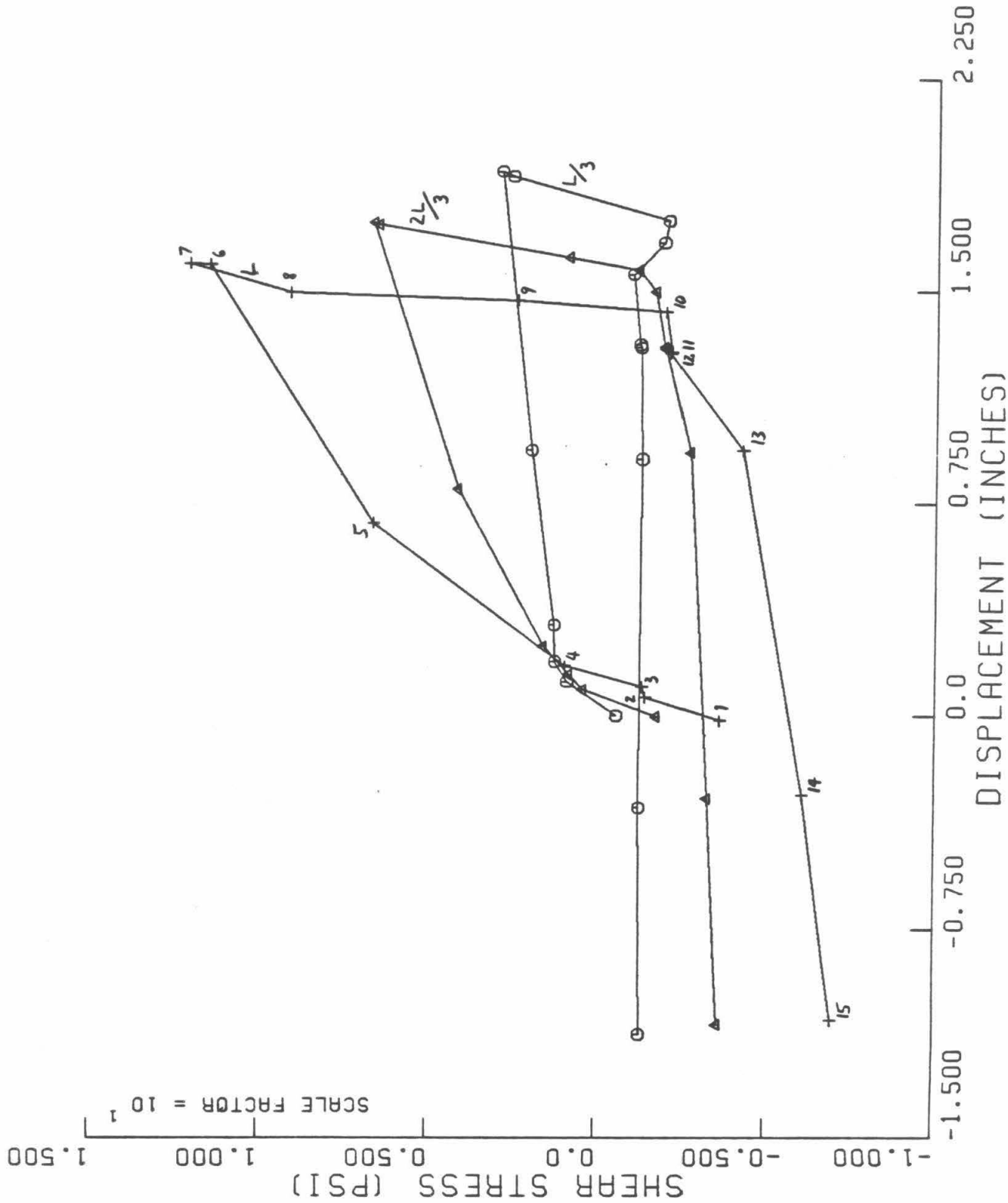

Figure 4.3e. t-z diagrams--Interval 1, Test 4

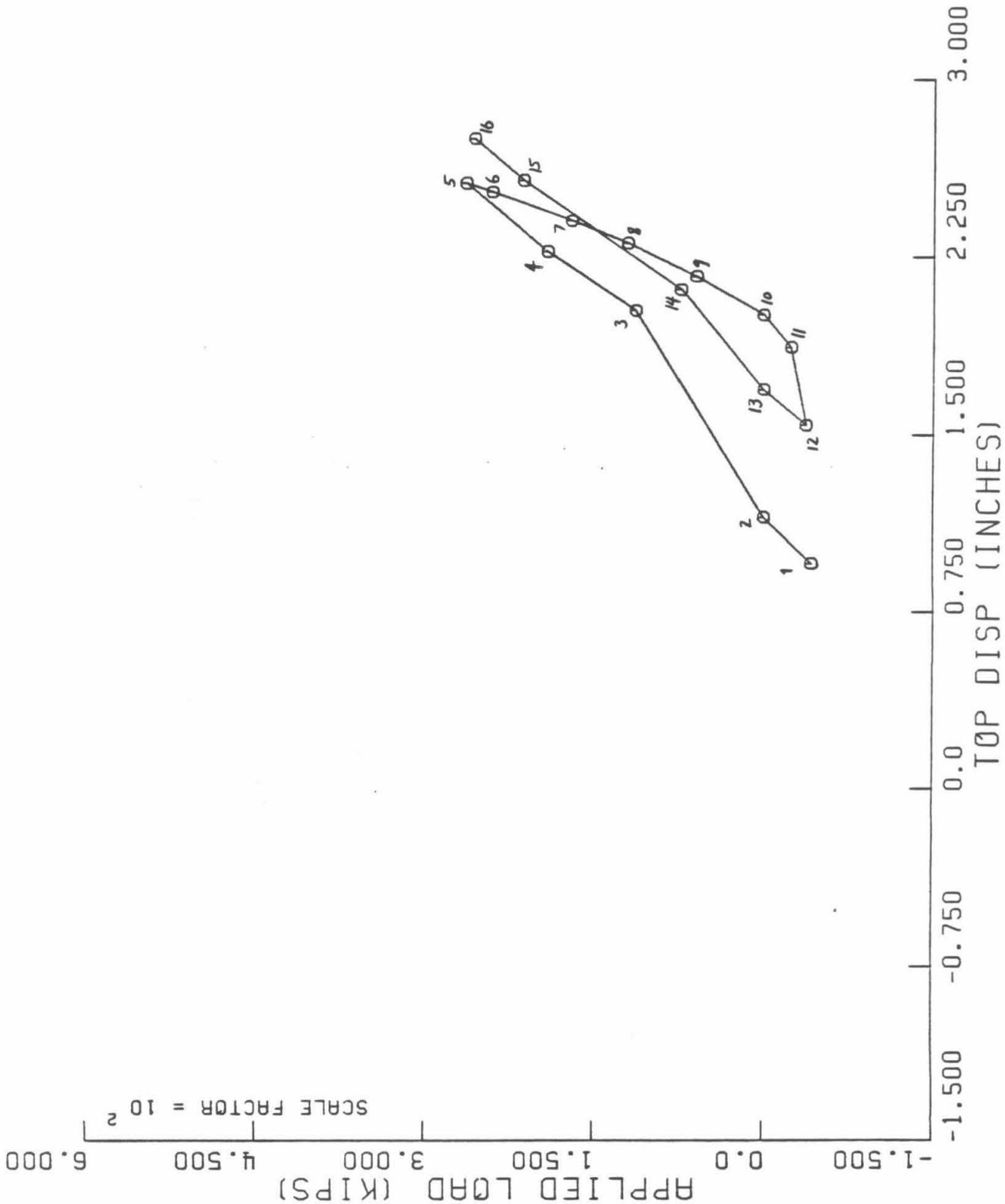

Figure 4.3f. Applied load vs. pile top displacement--Interval 2, Test 4

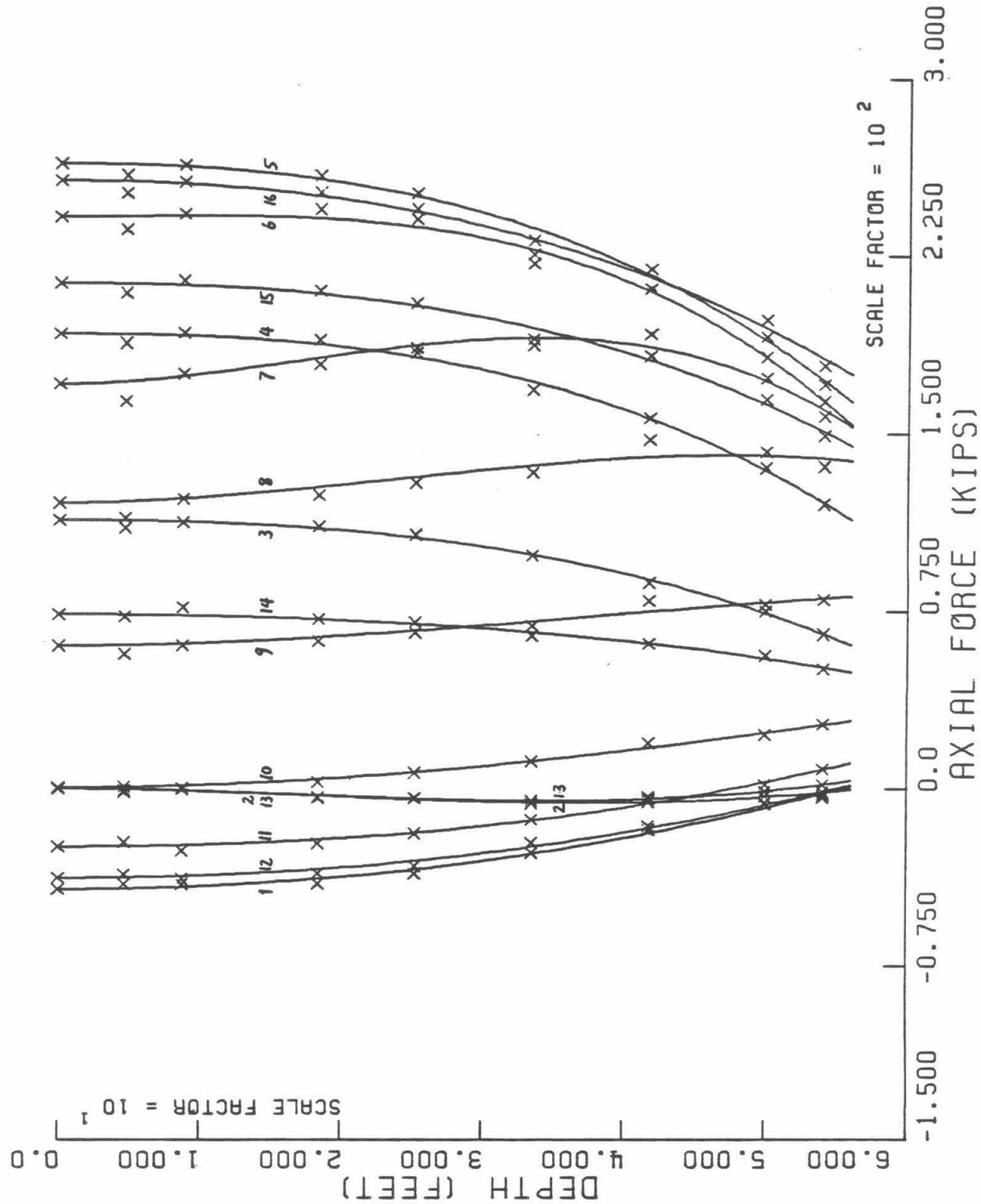

Figure 4.3g. Pile axial force, f(z)--Interval 2, Test 4

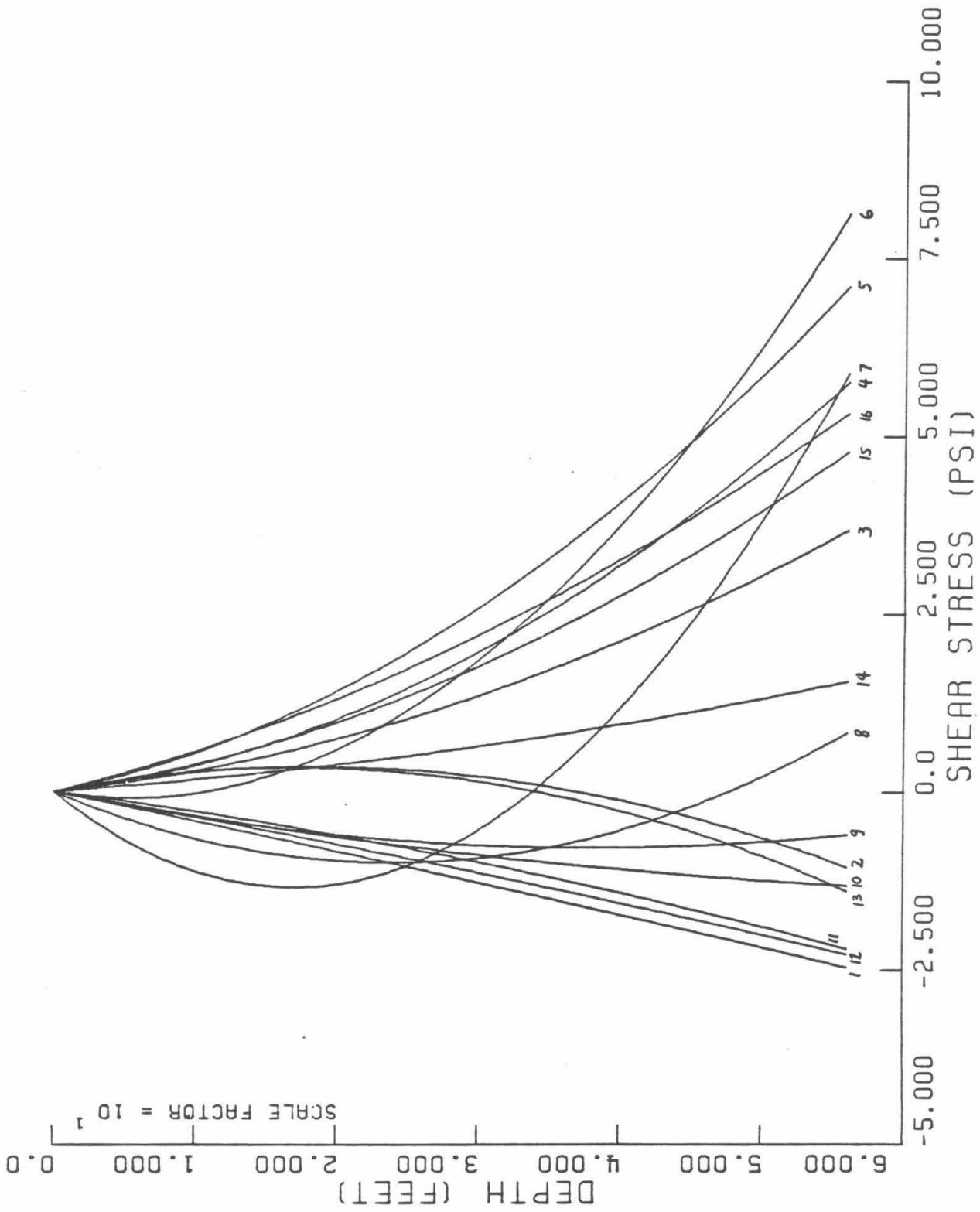

Figure 4.3h. Soil-pile shear stress, t(z)--Interval 2, Test 4

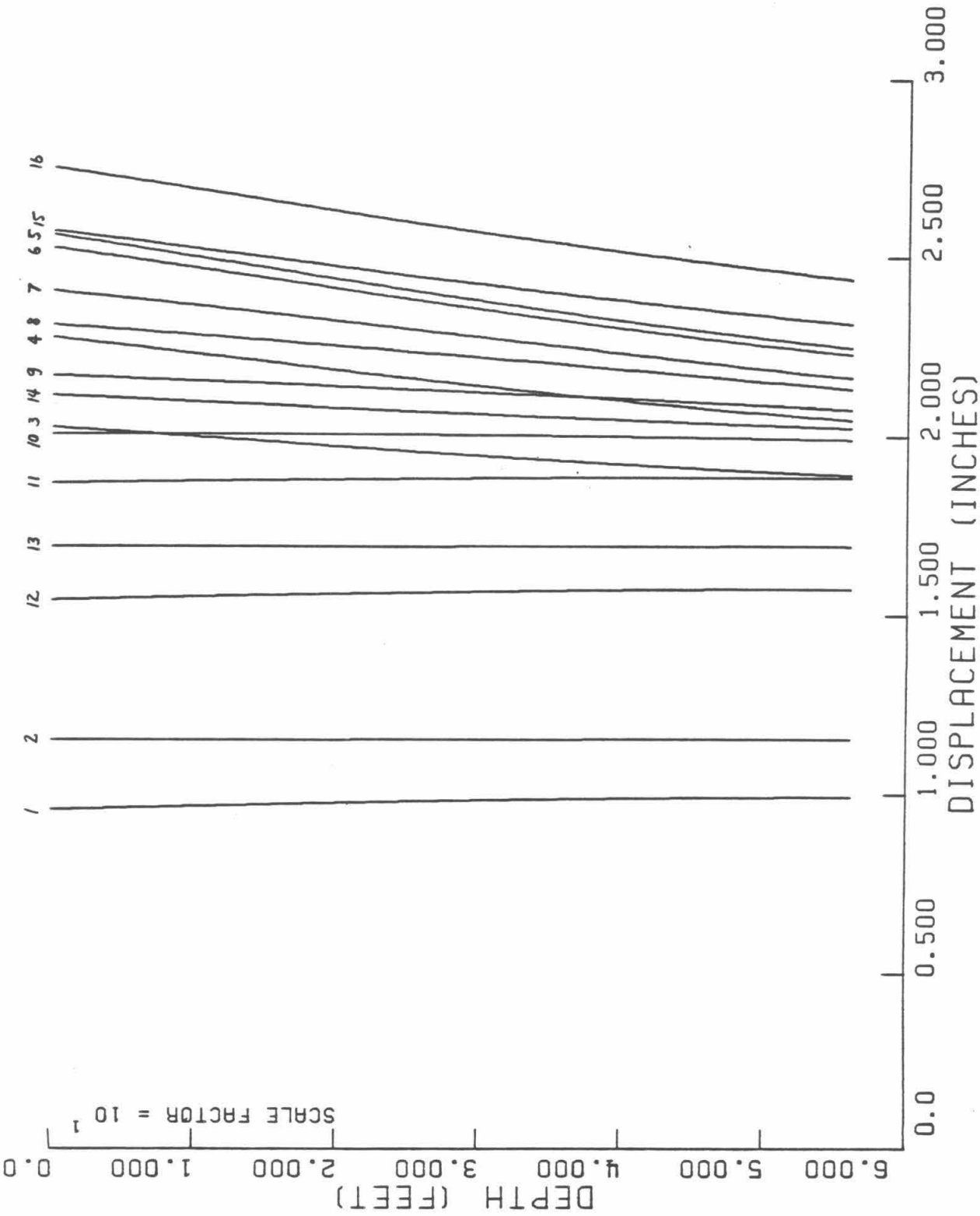

Figure 4.3i. Pile displacement, w(z)--Interval 2, Test 4

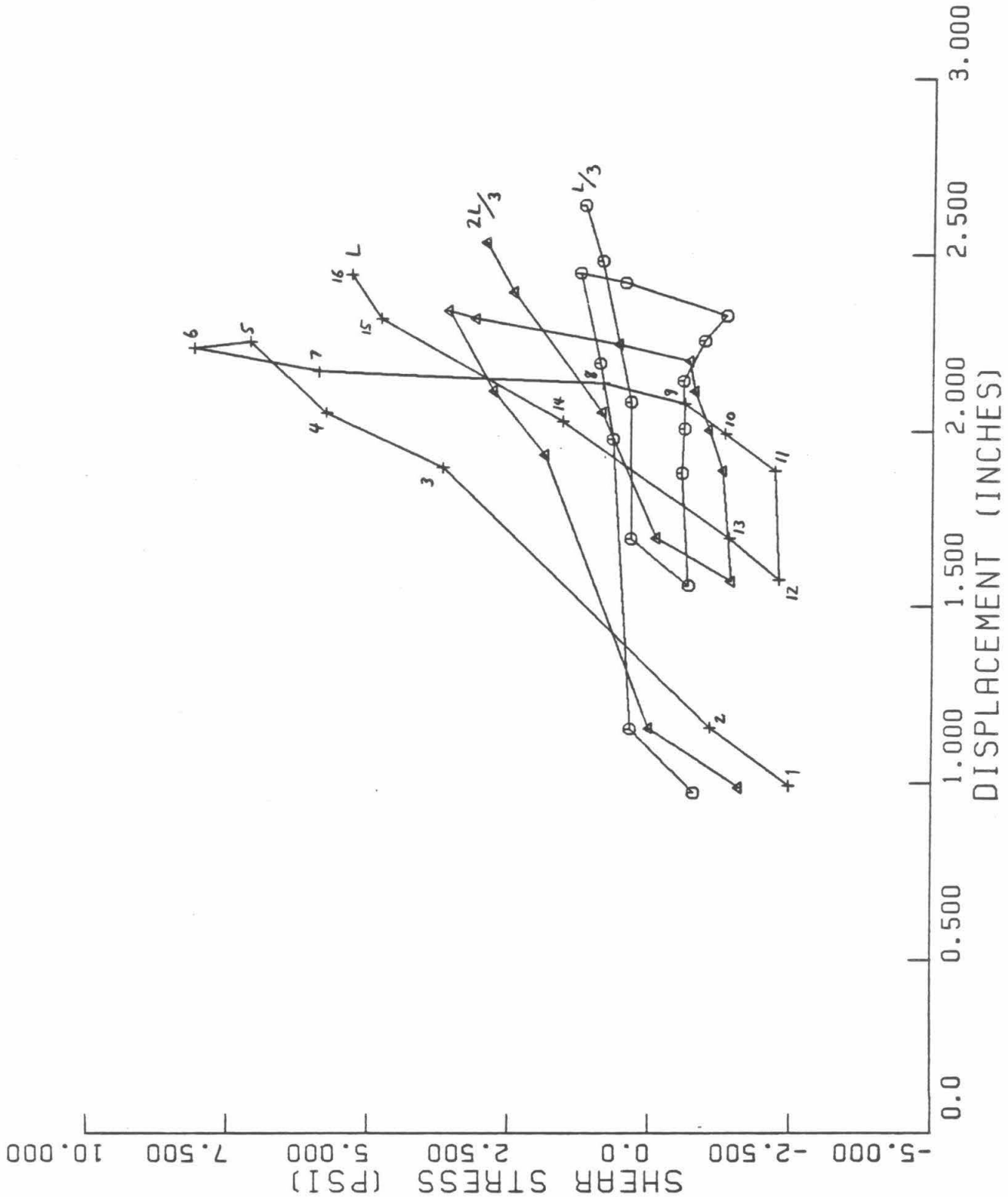

Figure 4.3j. t-z diagrams—Interval 2, Test 4

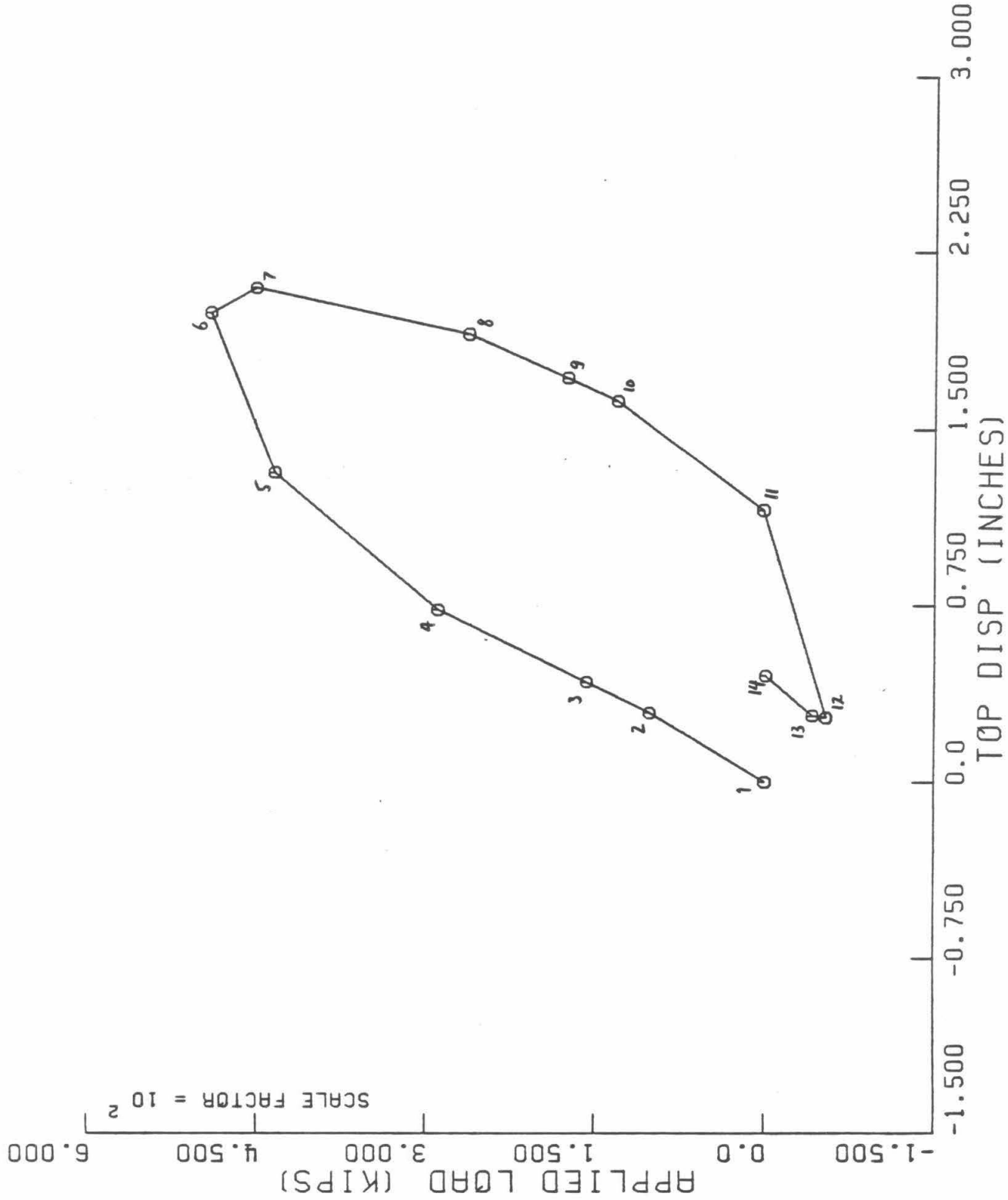

Figure 4.4a. Applied load vs. pile top displacement--Interval 1, Test 5

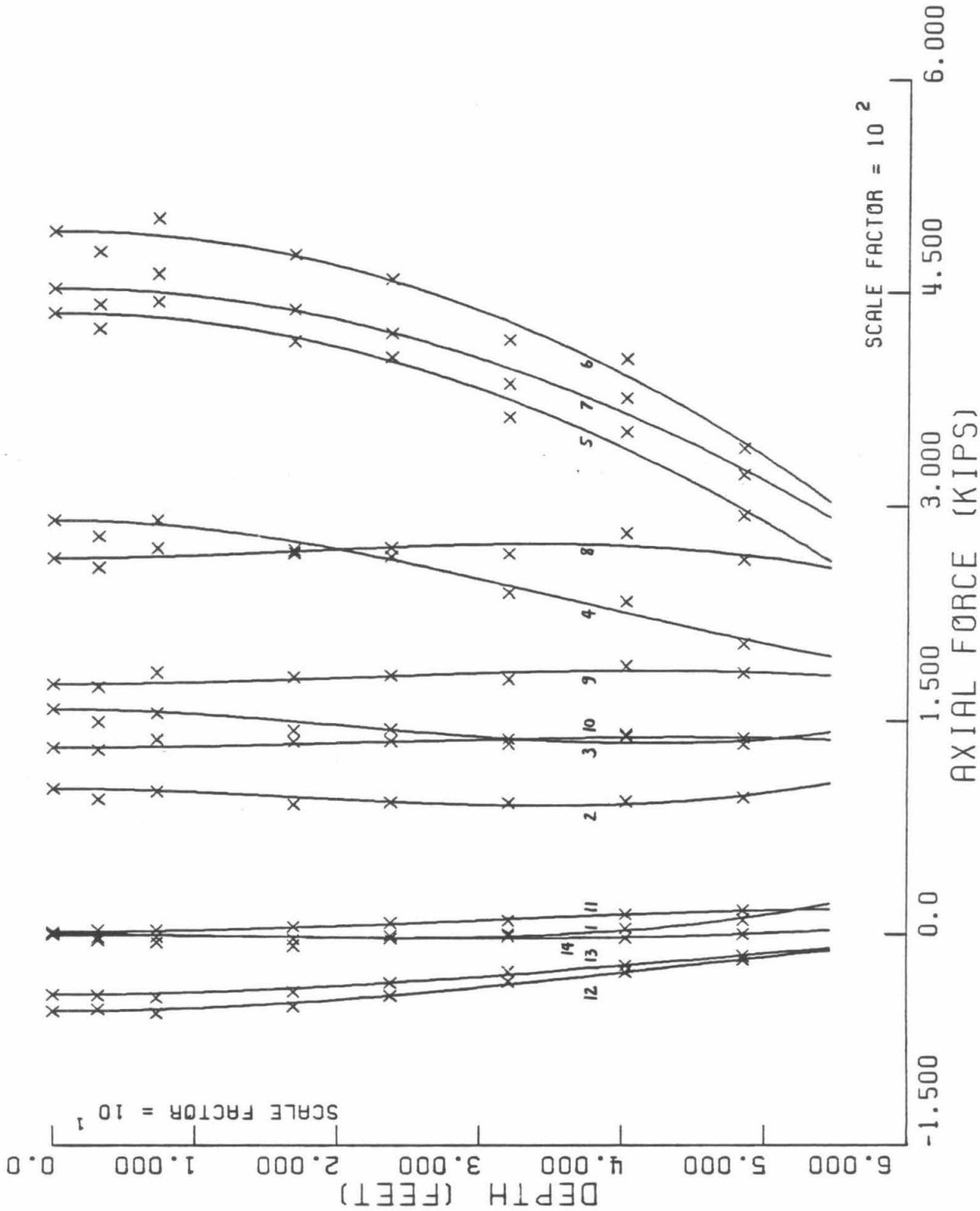

Figure 4.4b. Pile axial force, f(z)—Interval 1, Test 5

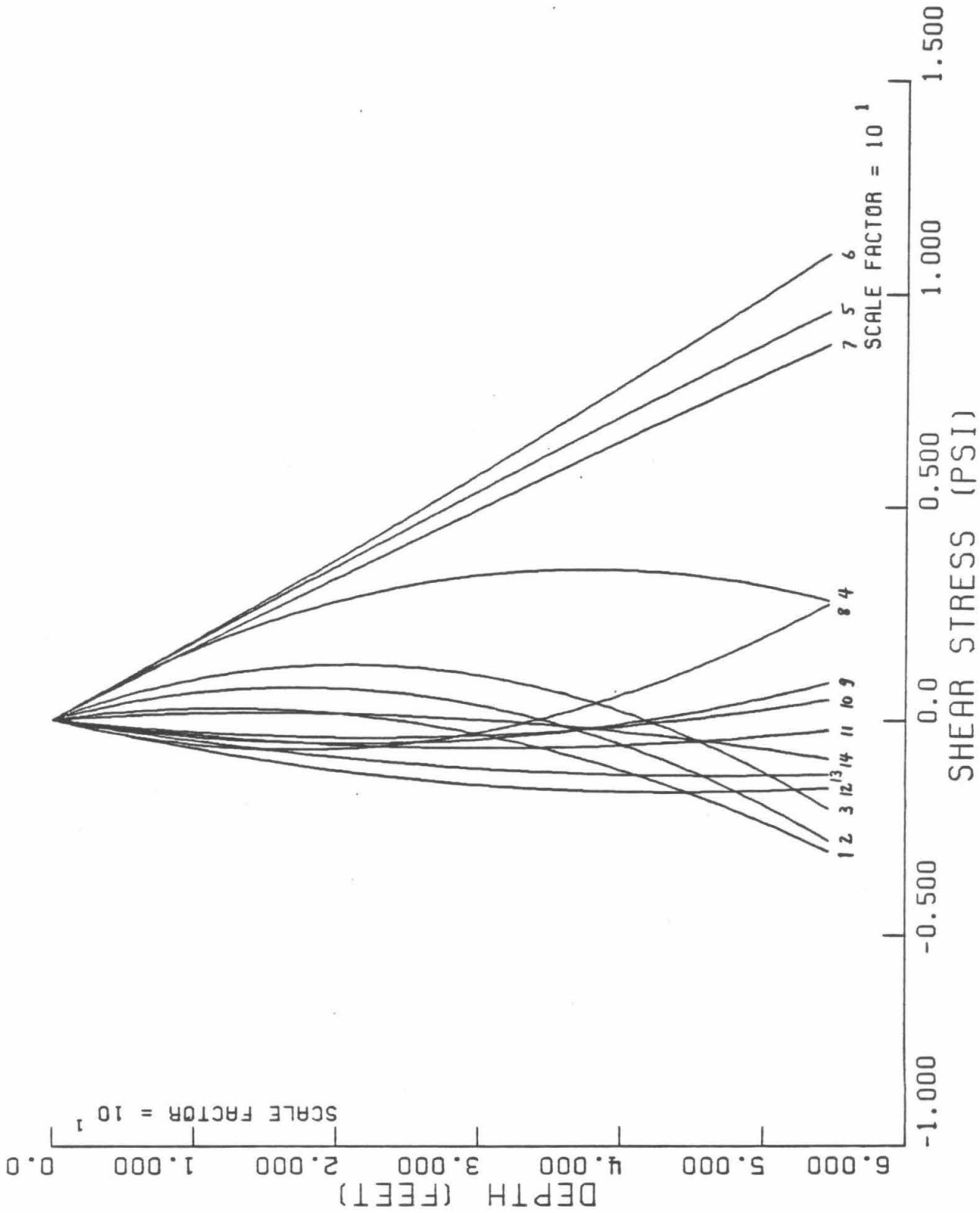

Figure 4.4c. Soil-pile shear stress, t(z)--Interval 1, Test 5

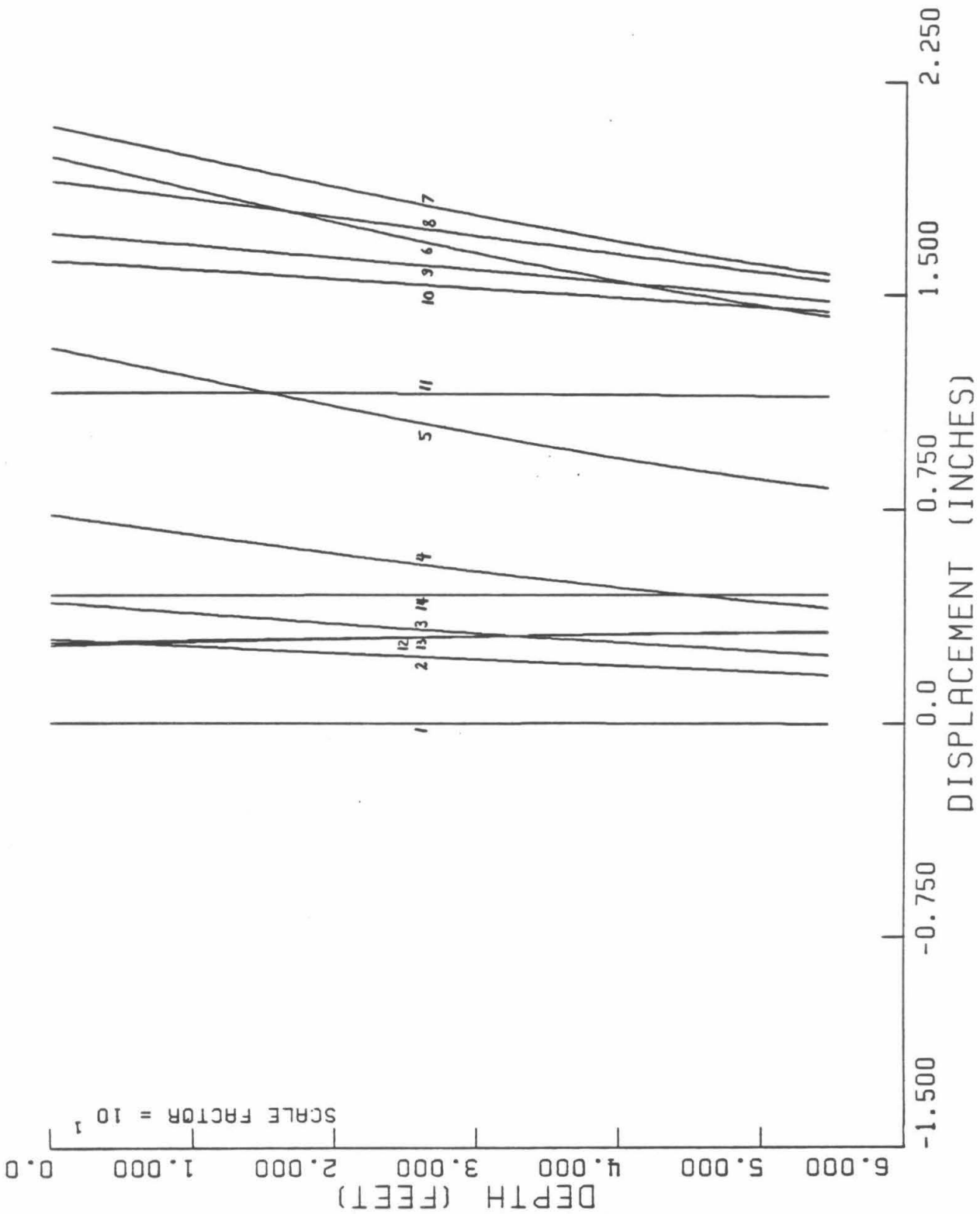

Figure 4.4d. Pile displacement, w(z)—Interval 1, Test 5

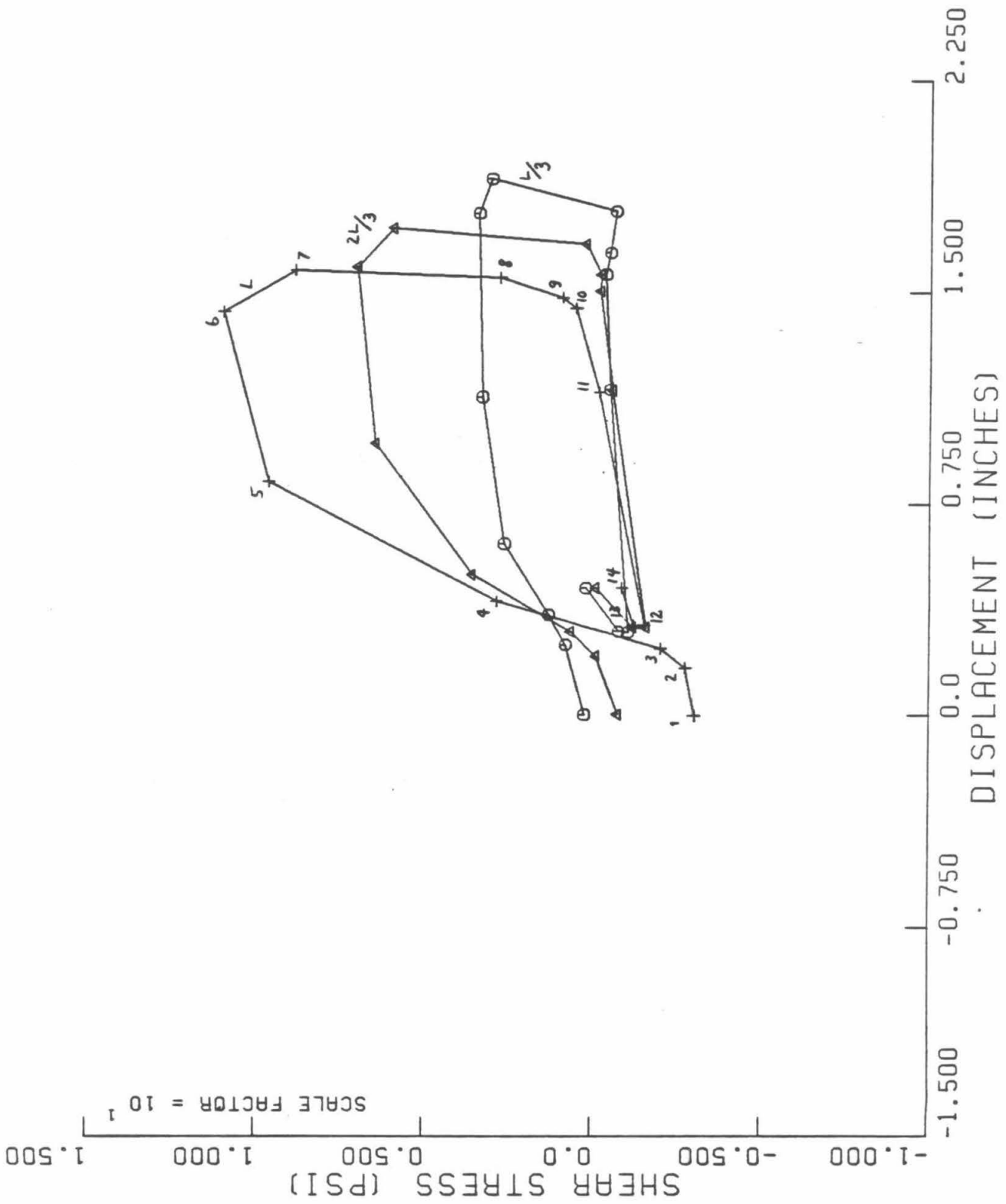

Figure 4.4e. t-z diagrams--Interval 1, Test 5

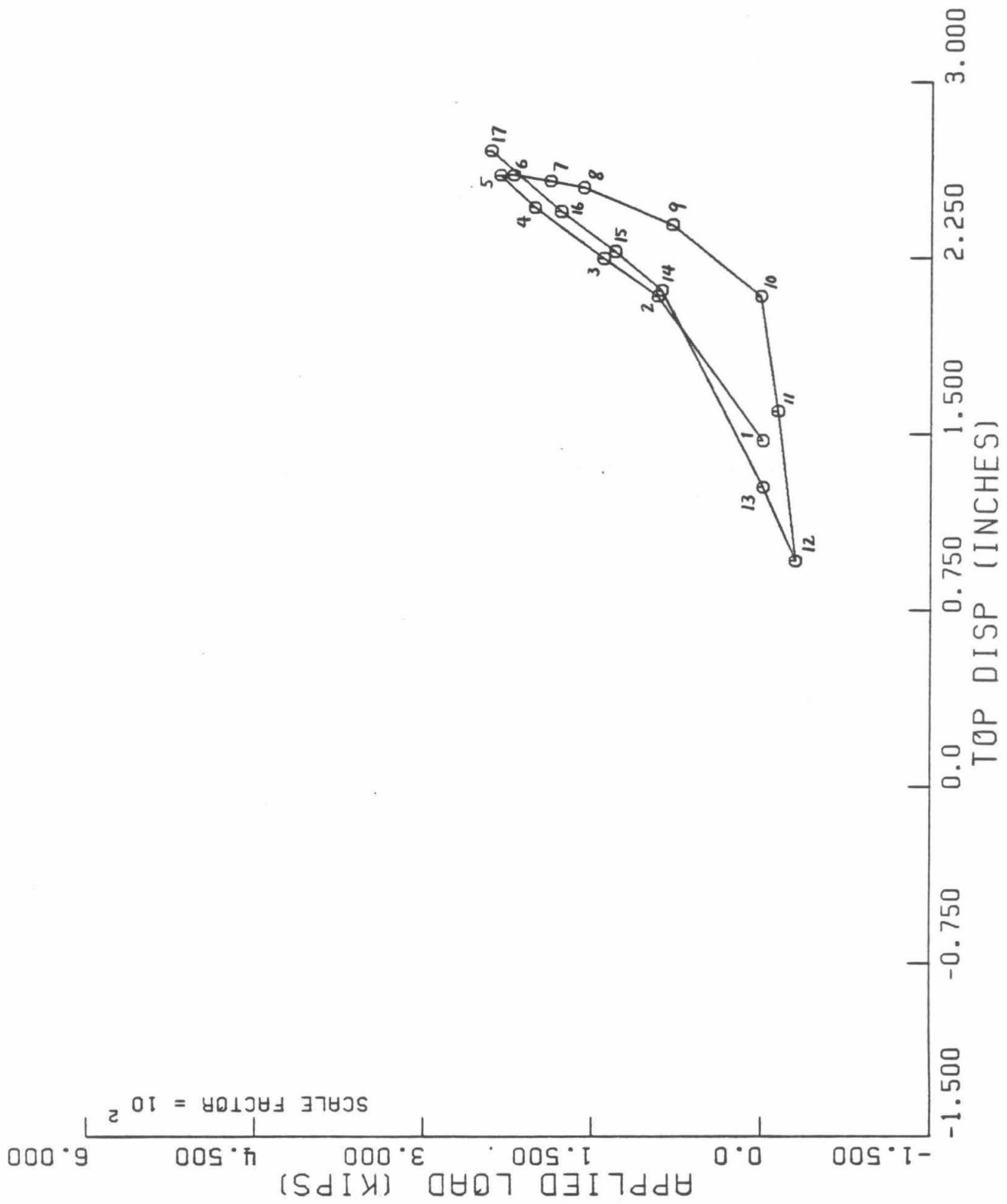

Figure 4.4f. Applied load vs. pile top displacement--Interval 2, Test 5

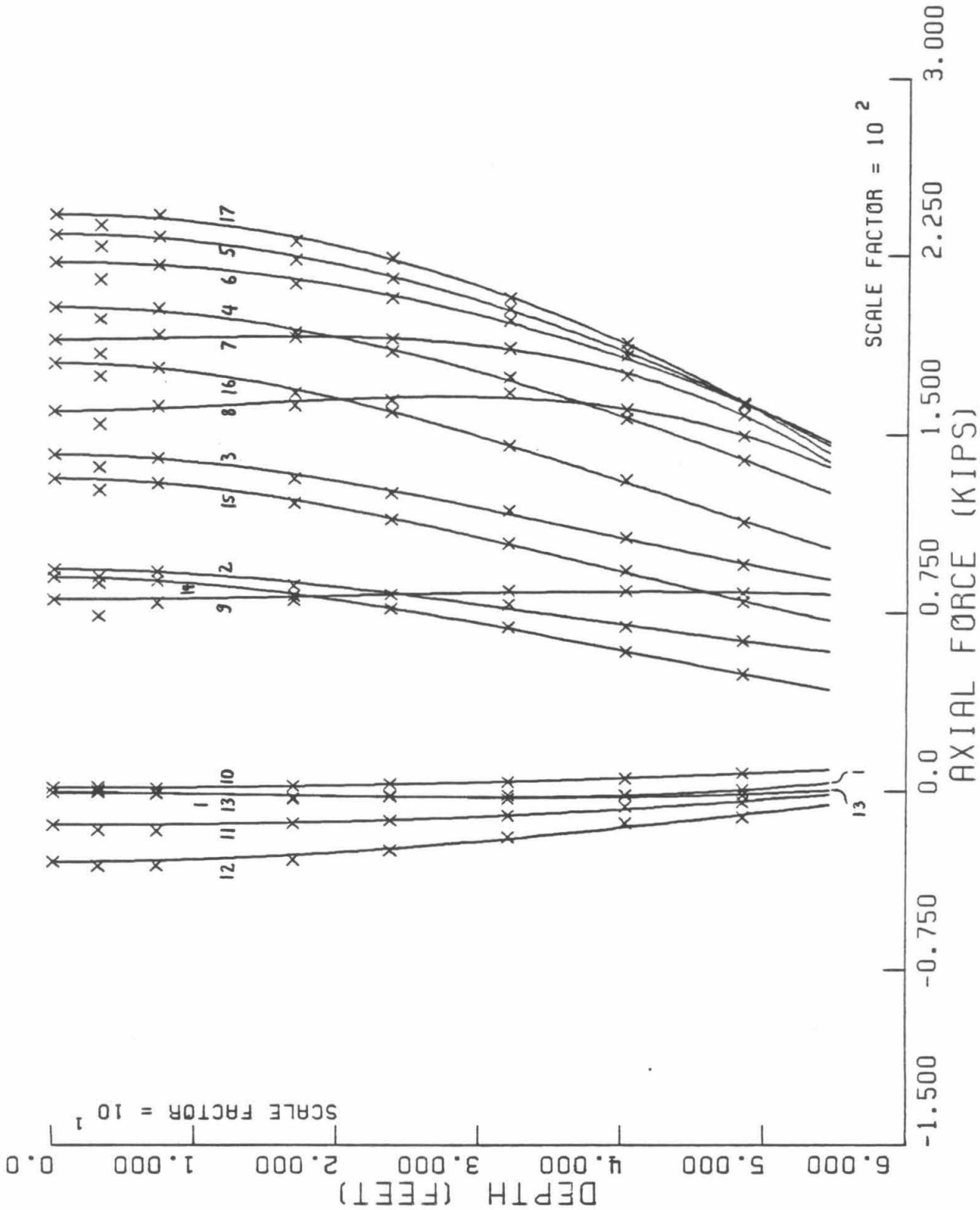

Figure 4.4g. Pile axial force, f(z)--Interval 2, Test 5

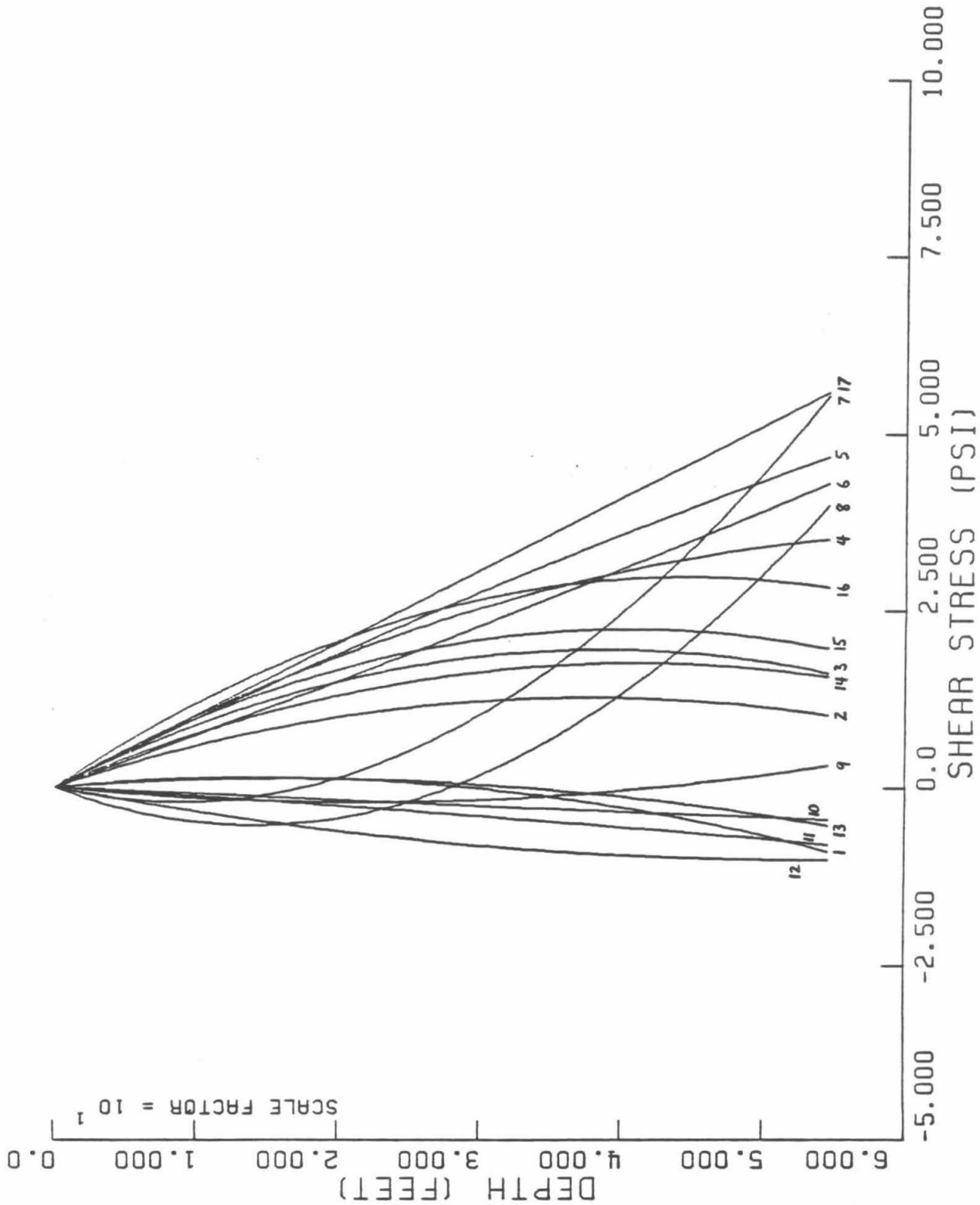

Figure 4.4h. Soil-pile shear stress, t(z)--Interval 2, Test 5

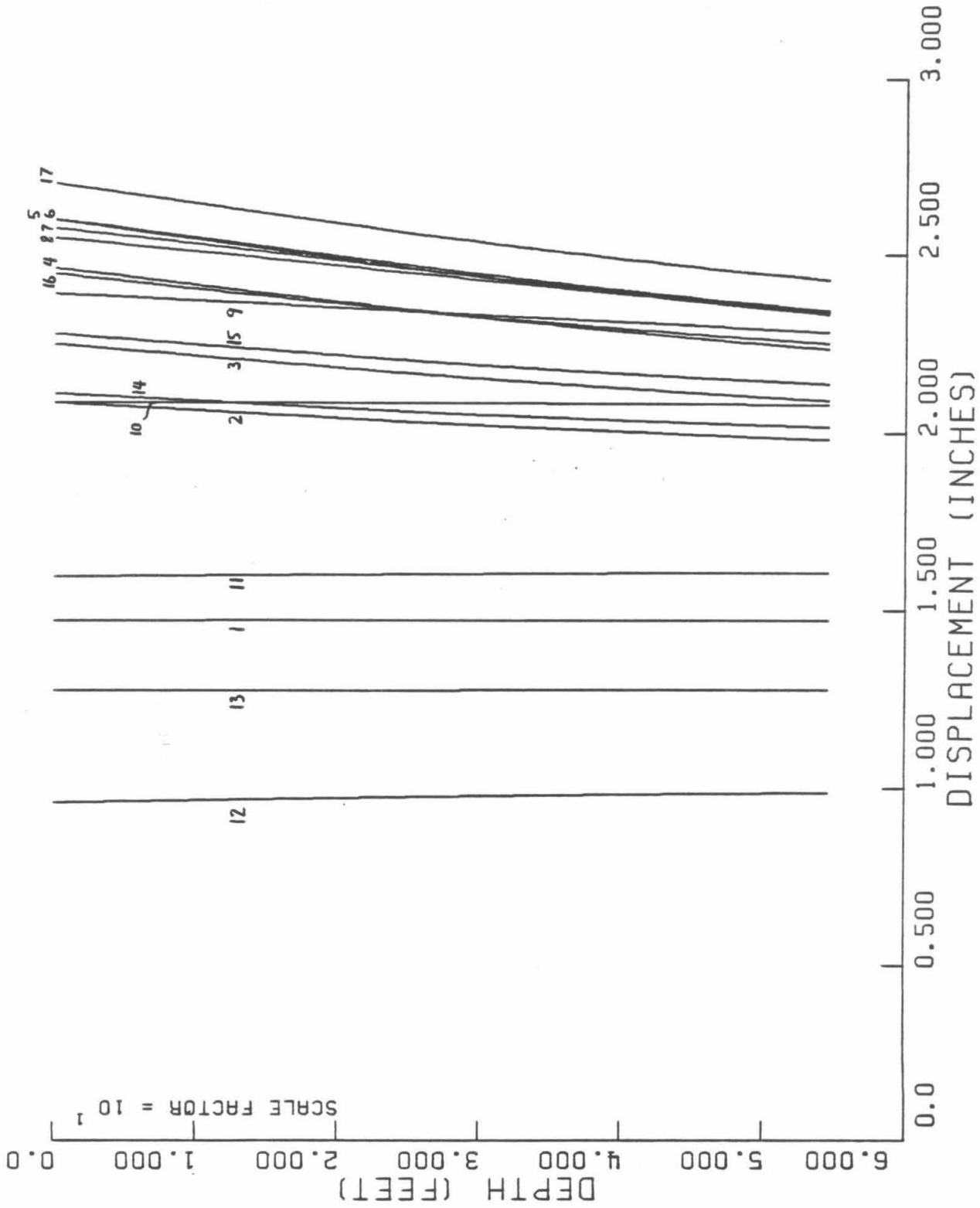

Figure 4.4i. Pile displacement, w(z)--Interval 2, Test 5

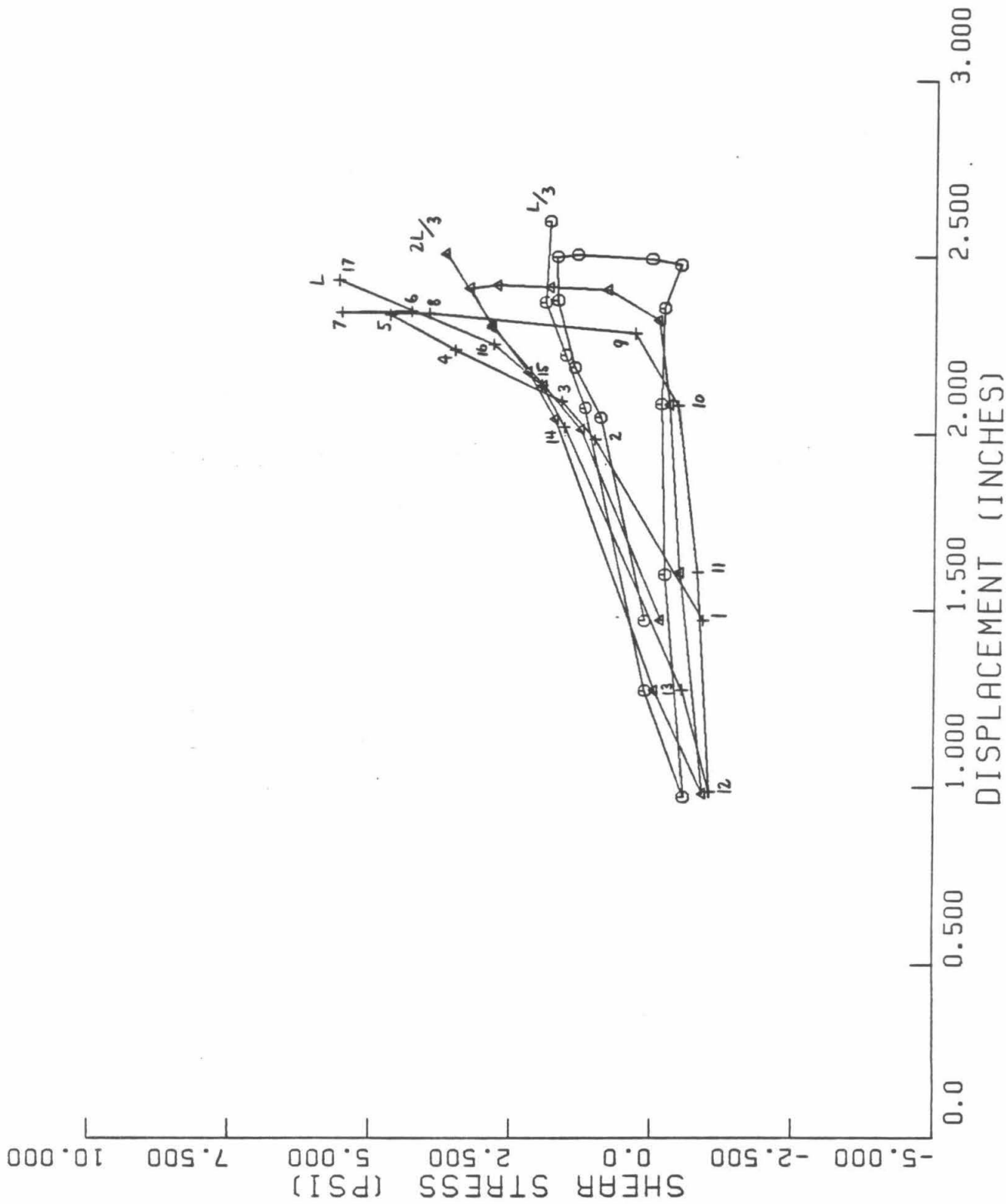

Figure 4.4j. t-z diagrams—Interval 2, Test 5

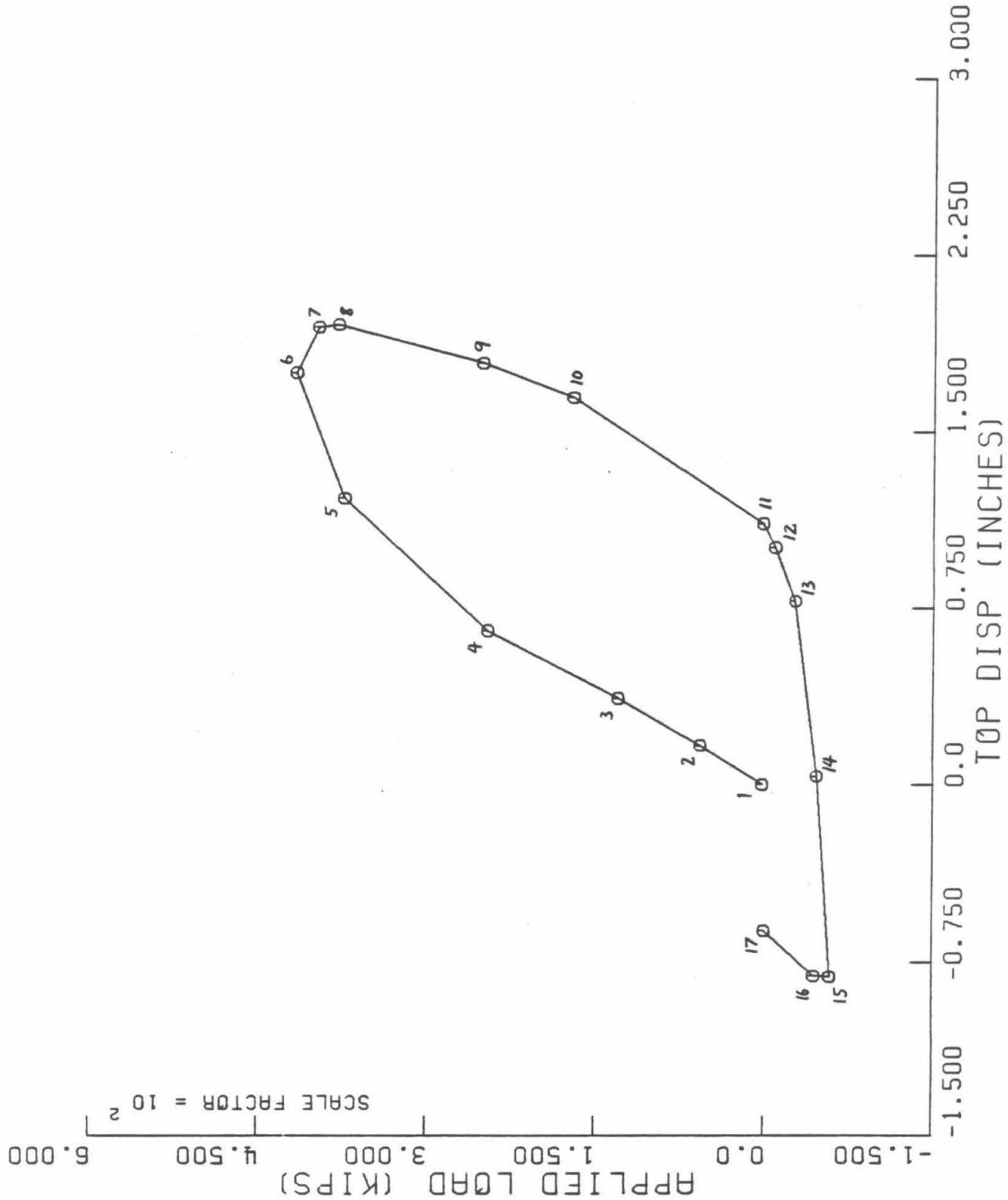

Figure 4.5a. Applied load vs. pile top displacement--Interval 1, Test 6

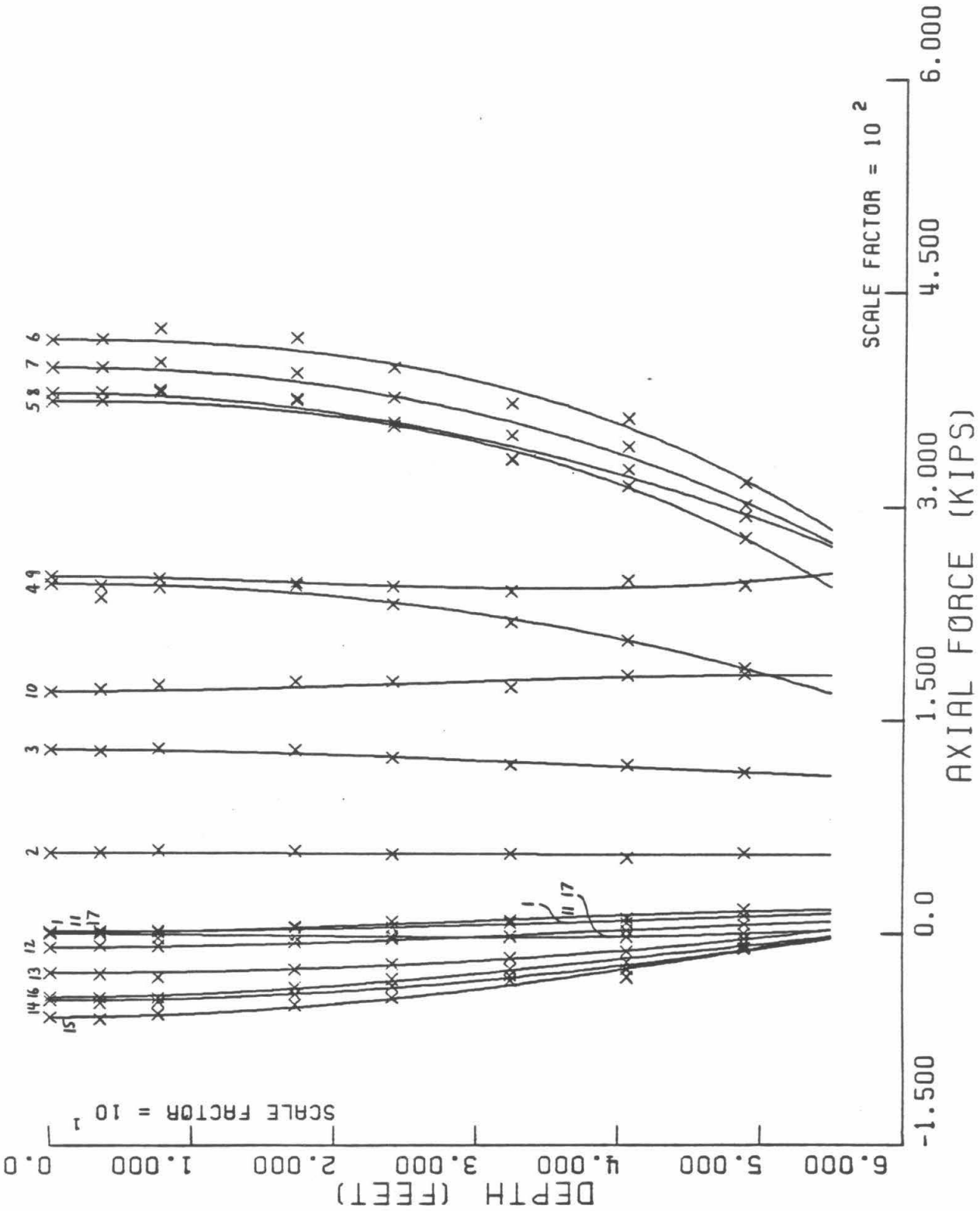

Figure 4.5b. Pile axial force, f(z)—Interval 1, Test 6

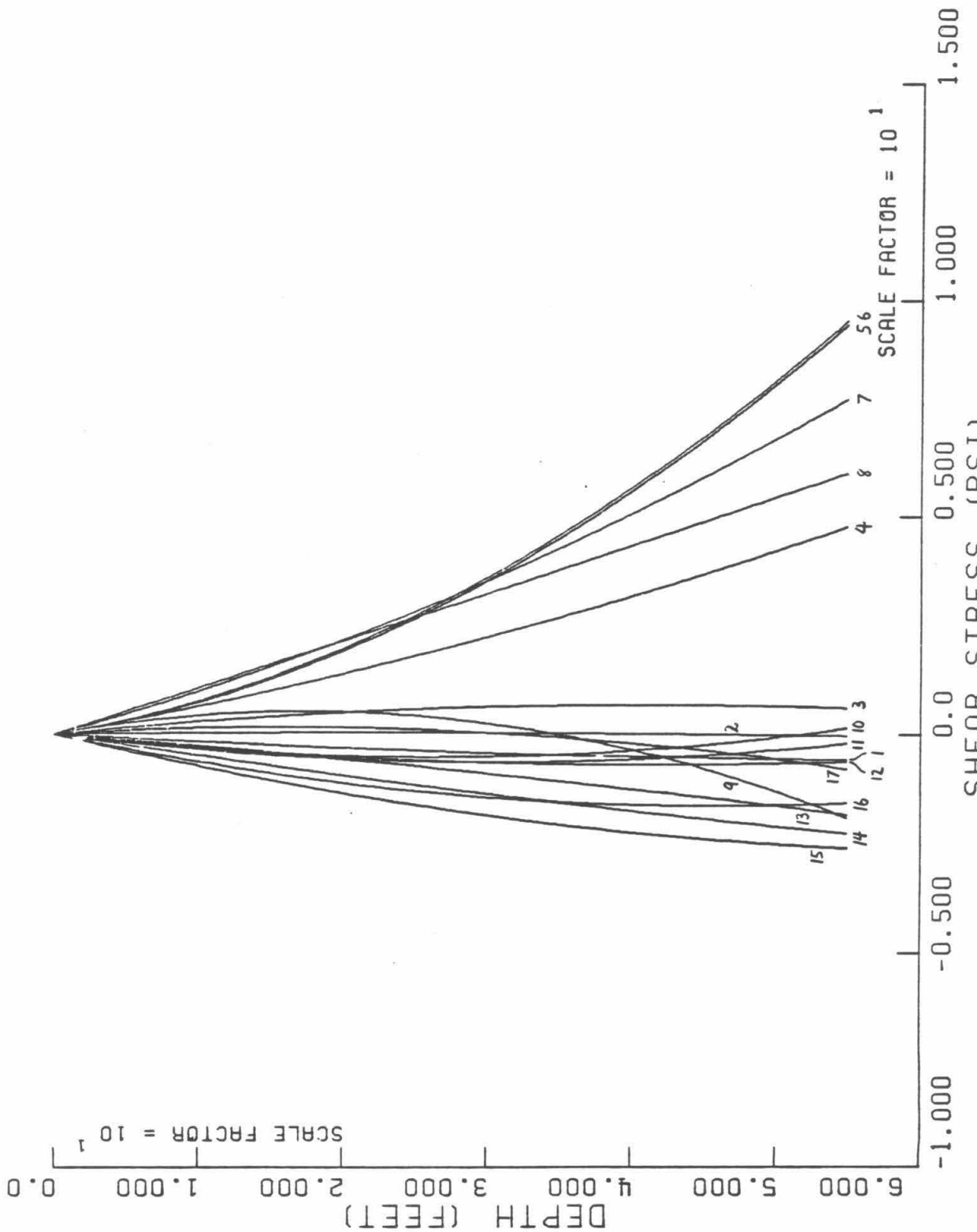

Figure 4.5c. Soil-pile shear stress, t(z)--Interval 1, Test 6

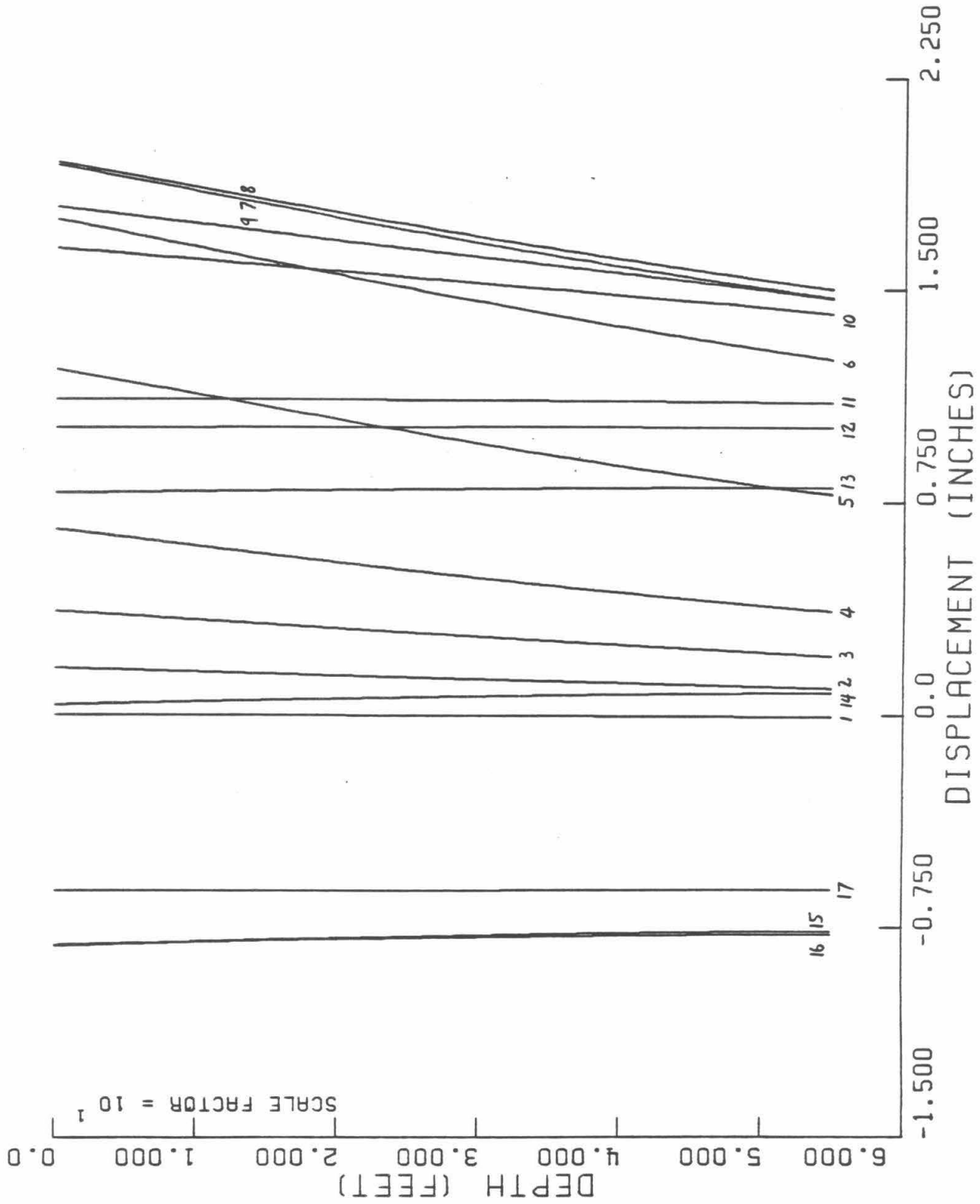

Figure 4.5d. Pile displacement, w(z)—Interval 1, Test 6

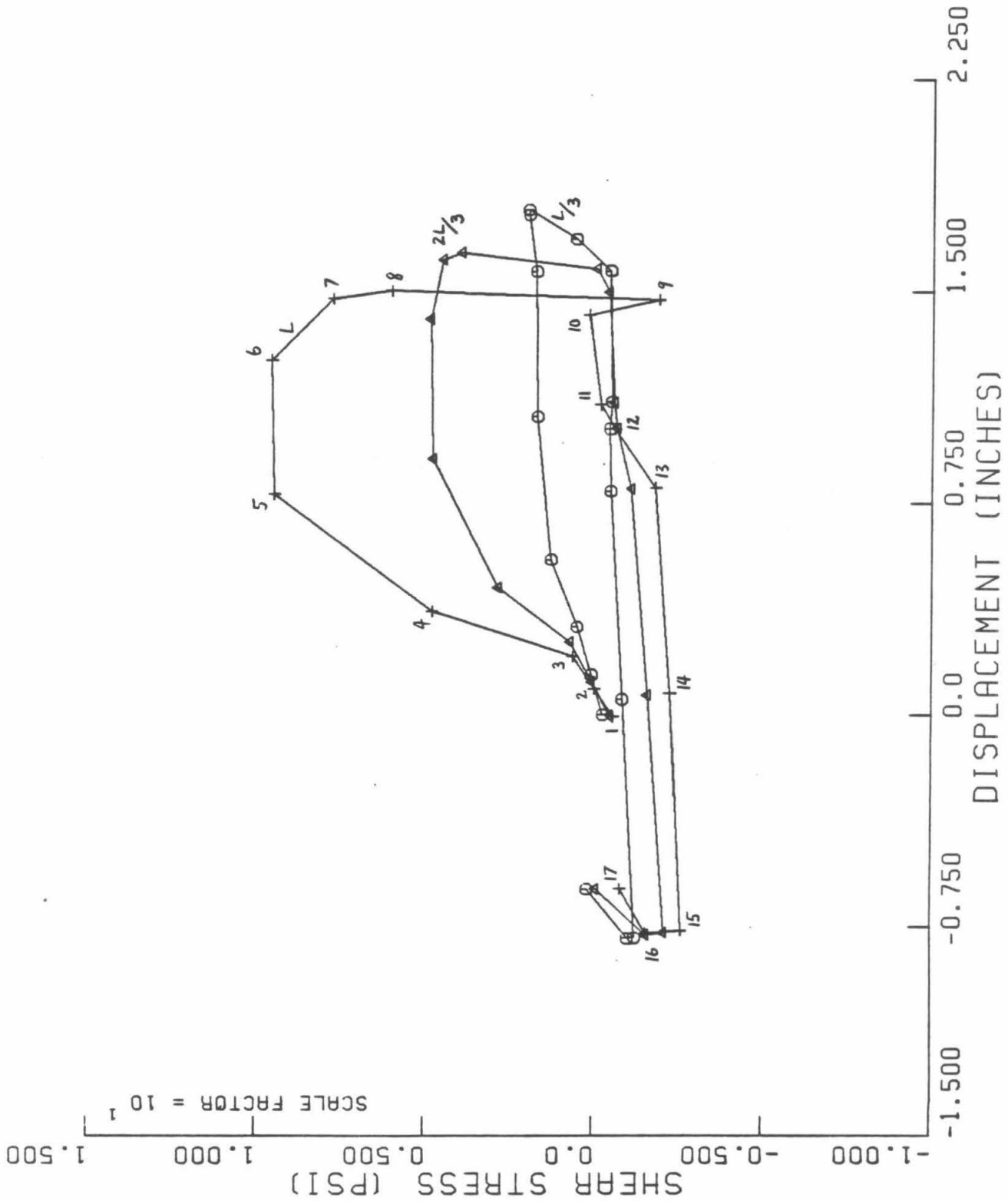

Figure 4.5e. t-z diagrams--Interval 1, Test 6

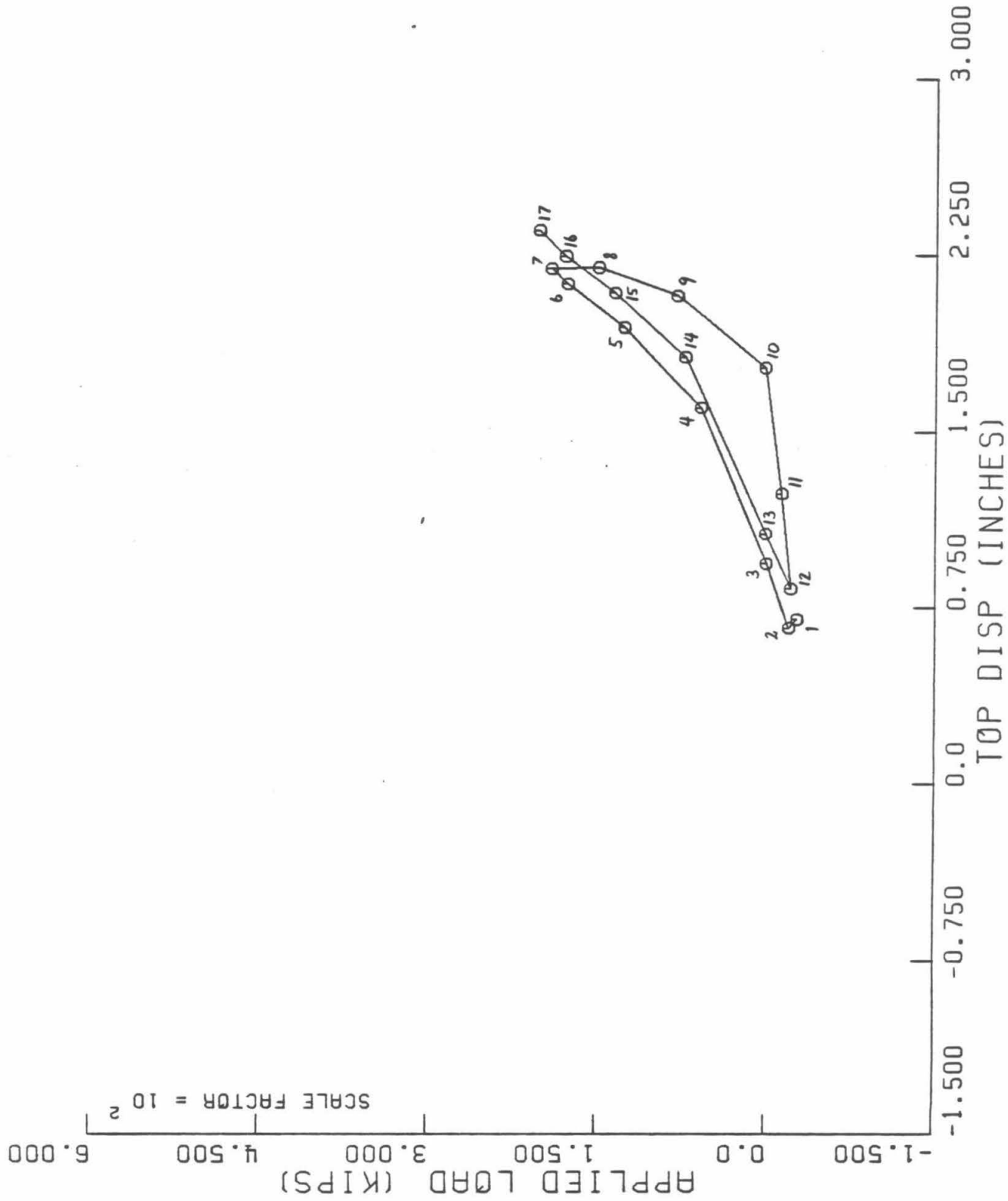

Figure 4.5f. Applied load vs. pile top displacement--Interval 2, Test 6

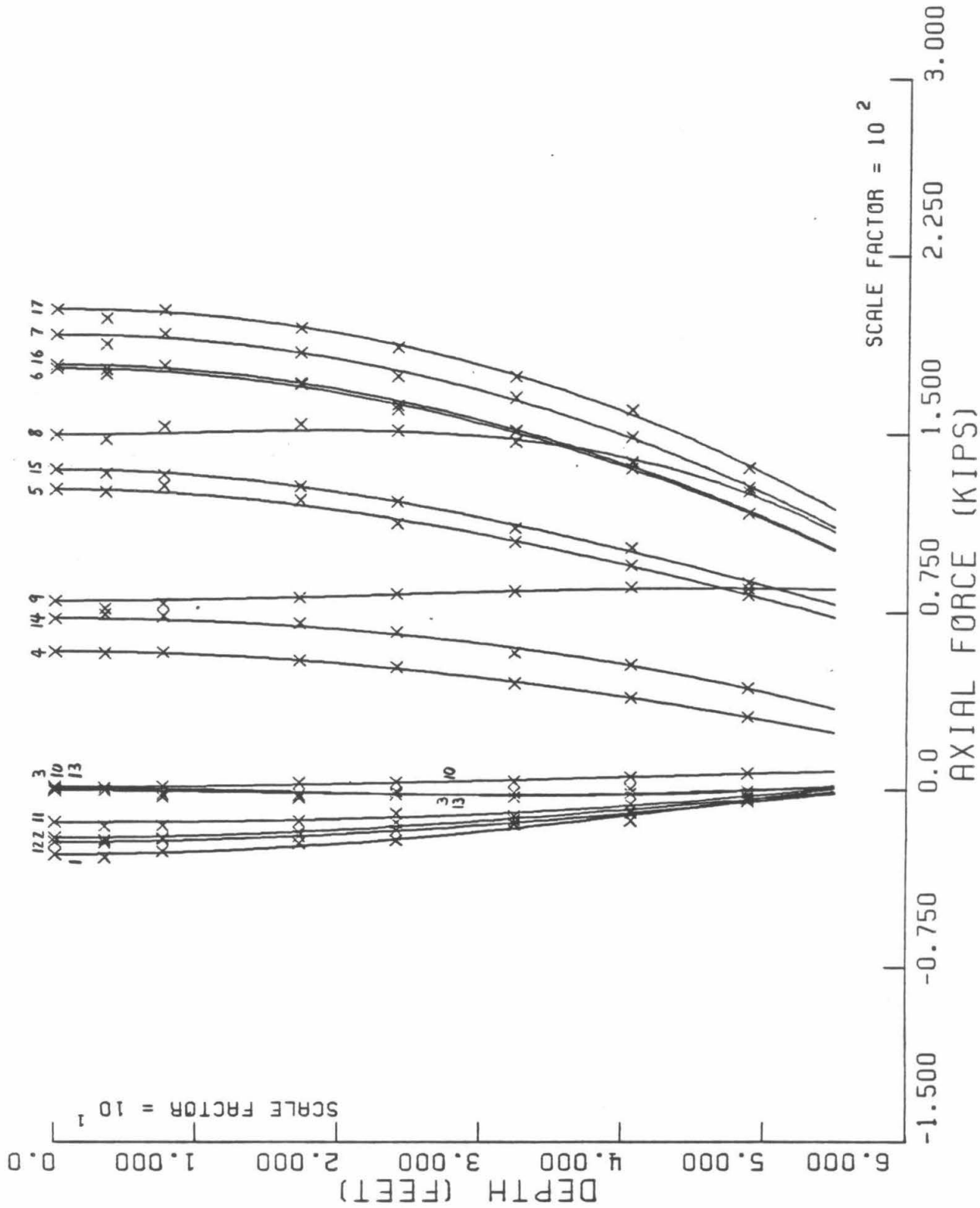

Figure 4.5g. Pile axial force, f(z)--Interval 2, Test 6

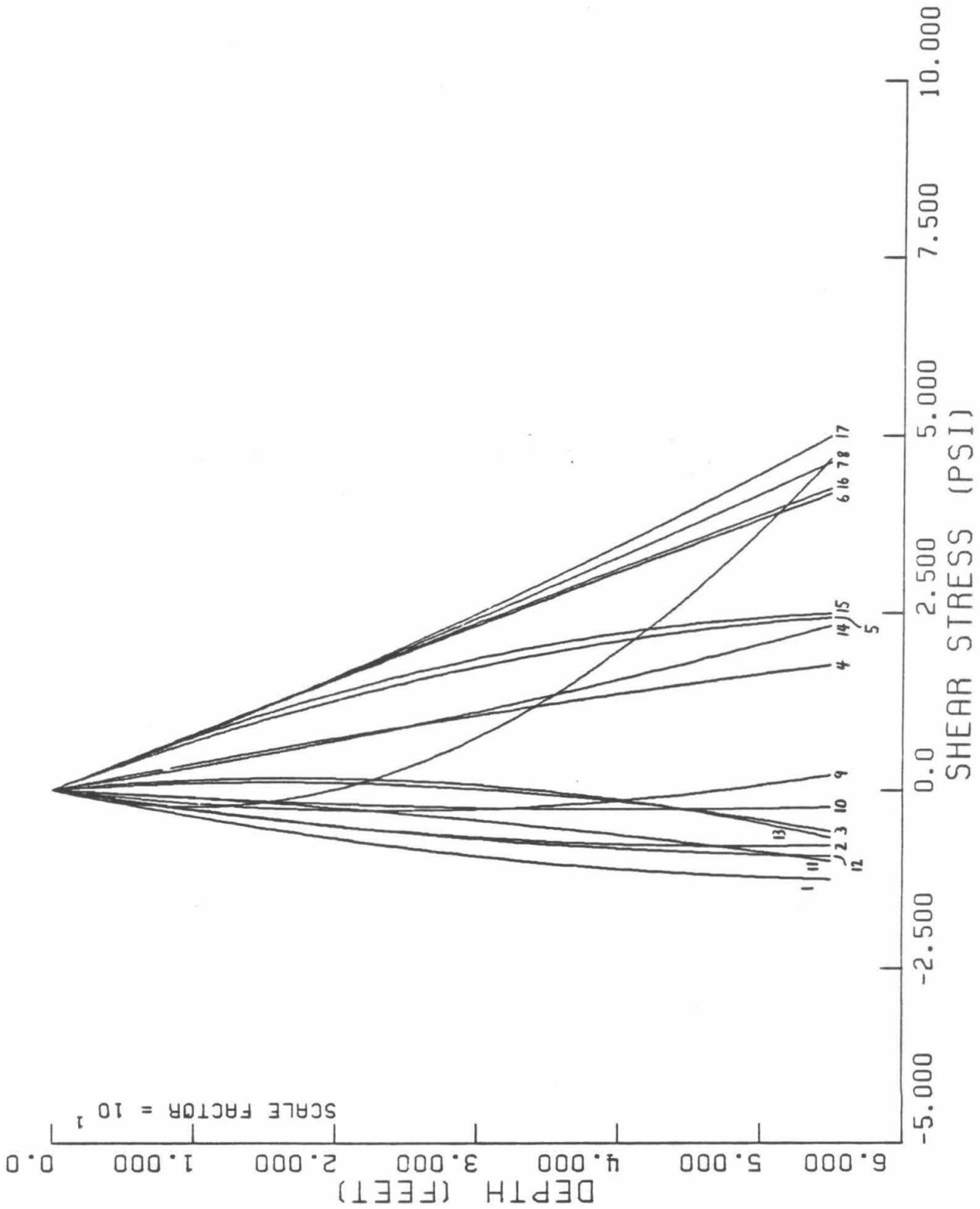

Figure 4.5h. Soil-pile shear stress, t(z)--Interval 2, Test 6

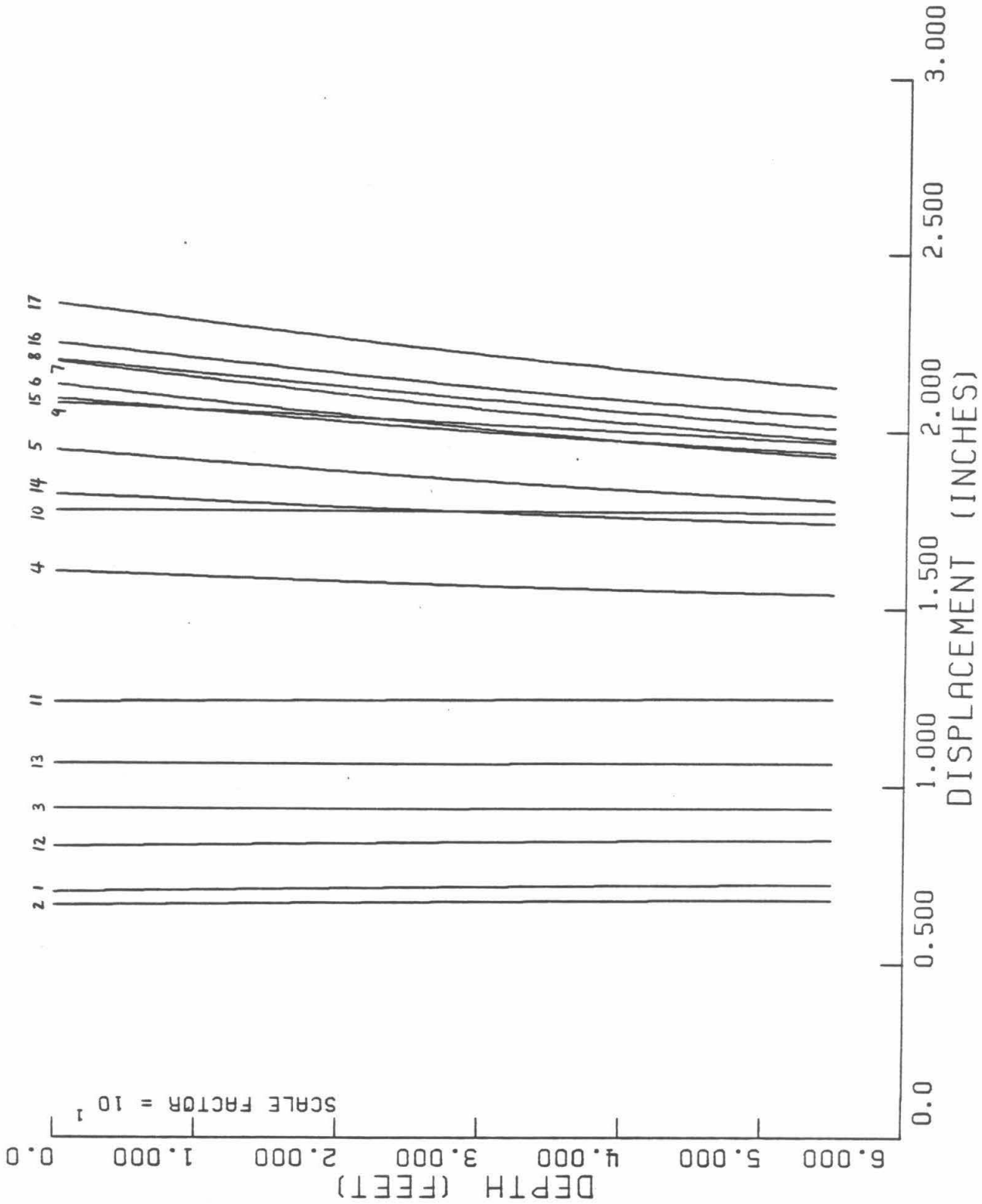

Figure 4.5i. Pile displacement, w(z)--Interval 2, Test 6

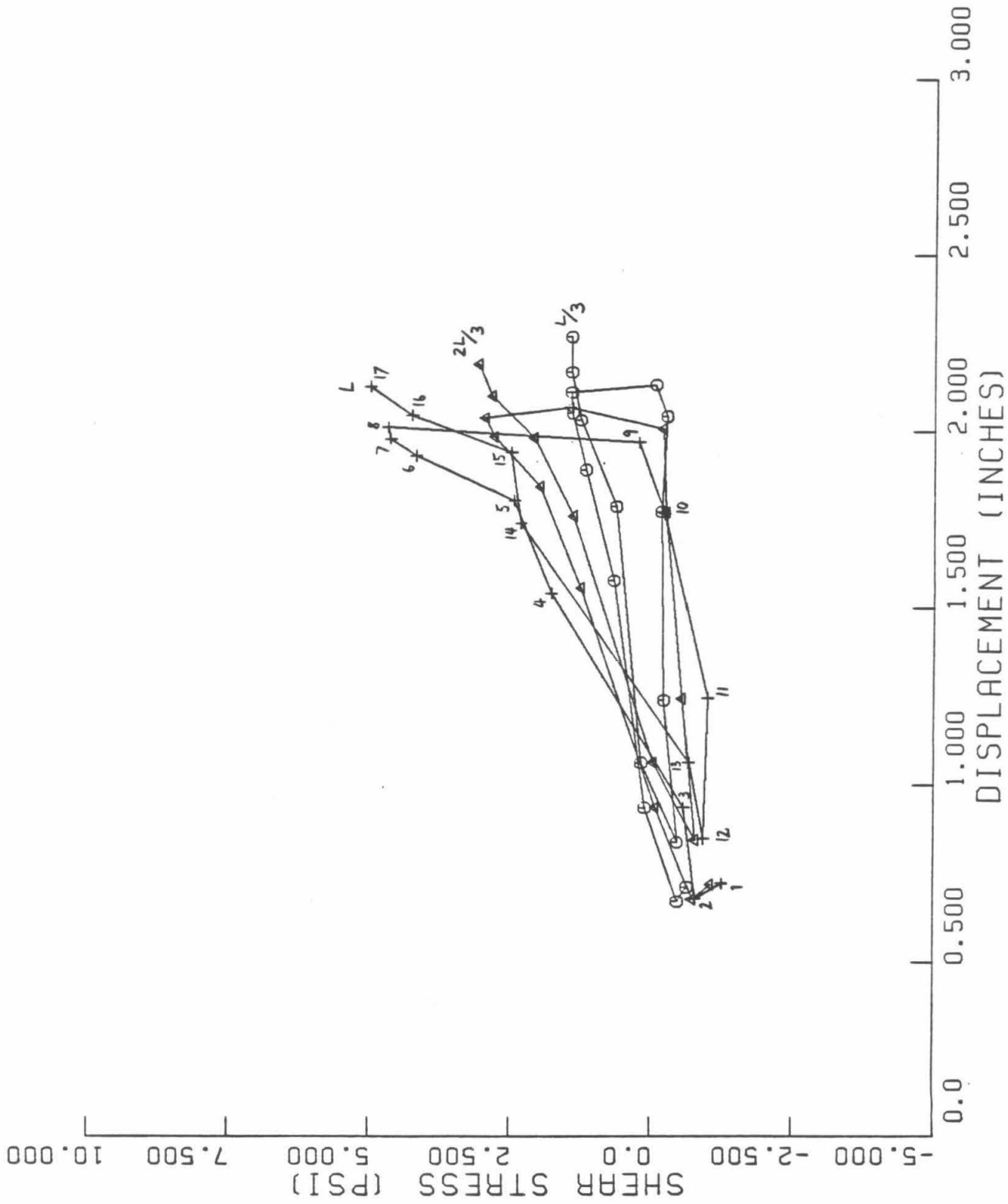

Figure 4.5j. t-z diagrams--Interval 2, Test 6

CHAPTER 5

COMPARISON OF MATCHING CENTRIFUGE MODEL AND FIELD PILE TESTS

The behavior of the prototype soil-pile systems associated with centrifuge model tests 5 and 6 will be compared with that of some particular, similar full-scale systems. The loading tests in the field on which this comparison is based were carried out in 1963 as part of an extensive program of pile driving and loading tests related to the design and construction of locks and dams for the Arkansas River Navigation Project of the U.S. Army Corps of Engineers. Reports on the tests are due to C. I. Mansur, A. H. Hunter, and M. T. Davisson [25,35]. Subsequently in the present thesis, these tests will be referred to as the "Arkansas River pile tests" (ARPT's).

5.1. Characteristics of the Centrifuge Model and Full-Scale Systems

Centrifuge model tests 5 and 6 were planned so that their associated prototype soil-pile systems resembled certain of the systems tested in the ARPT's as closely as possible. A variety of piles had been tested in the ARPT program, including timber piles, steel H-piles, 12-, 16-, and 20-inch-diameter steel pipe piles, and 16- and 20-inch-square prestressed concrete piles. They ranged in depth of embedment from 40 to 55 feet. The specific ARPT's to be simulated were chosen by comparing the sets of parameters (a) cross-sectional shape and dimensions, (b) axial stiffness, and (c) depth of embedment of the various ARPT piles with the combinations of these parameters which could conveniently be generated as centrifuge test prototypes. A good match in the parameters (a), (b), and (c) was found to exist for full-scale tests on 16-inch-diameter steel pipe piles and centrifuge model tests in which the prototype-model scaling factor is 33.0 (see Table 5.1, below), and these tests were chosen as the basis for the present comparison. Other reasons for this choice were that tests within the ARPT program involving 16-inch-diameter steel pipe piles were relatively numerous, and these piles were well instrumented.

The central elements in the comparison of the ARPT and centrifuge model test results are Figures 5.1 and 5.2. These are the primary plotted results of load tests on a 16-inch-diameter steel pipe pile driven using a vibratory hammer, on which corresponding results of Test 6 have been superimposed. The full-scale pile was referred to as "Test Pile 10" in the ARPT report [35]. Two load tests, separated by a period of several days, were performed on this pile. The associated loading sequences were the following:

1. pushing to failure and unloading,

and

2. pulling to failure and unloading.

The centrifuge model system was subjected to both of the loading sequences 1 and 2 in interval 1 of Test 6. The behavior of the full-scale and model soil-pile systems under pushing loading is compared in Figure 5.1 and their behavior under pulling loading in Figure 5.2.

In the course of the complete ARPT program, some 16-inch-diameter pipe piles were driven with a double-acting steam hammer and others emplaced using a vibratory hammer. The hammer used for installation was found to have no appreciable effect on subsequent pile behavior under load, so that the behavior of Test Pile 10 is representative of that of all the 16-inch-diameter pipe piles tested. Similarly, the results of centrifuge model test 6 differ little from those for Test 5, though the pulling-to-failure phase in interval 1 of Test 6 is more fully developed than this phase of Test 5. However, the results of the specific 16-inch-diameter pipe ARPT and centrifuge model tests which are compared directly in Figures 5.1 and 5.2 resemble one another at least as closely as those of any other pair of these matched full-scale and model soil-pile systems.

The matching of the characteristics of the prototype piles associated with Tests 5 and 6 to those of the 16-inch-diameter steel pipe ARPT piles has been described. Pile characteristics for the specific soil-pile systems compared in Figures 5.1 and 5.2 are tabulated below.

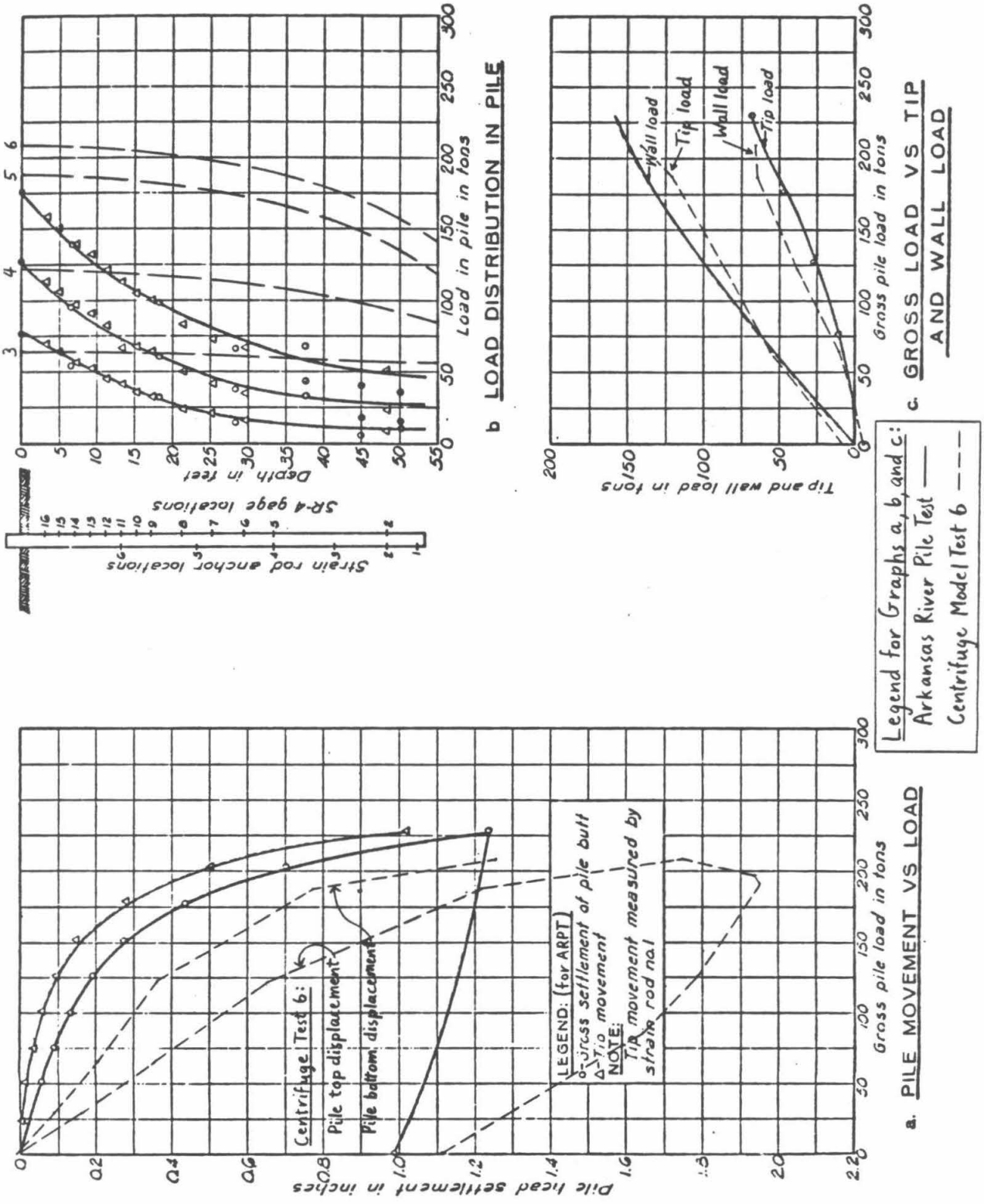

Figure 5.1 Measured behavior of ARPT Test Pile 10 and centrifuge test 6 prototype, under pushing loading

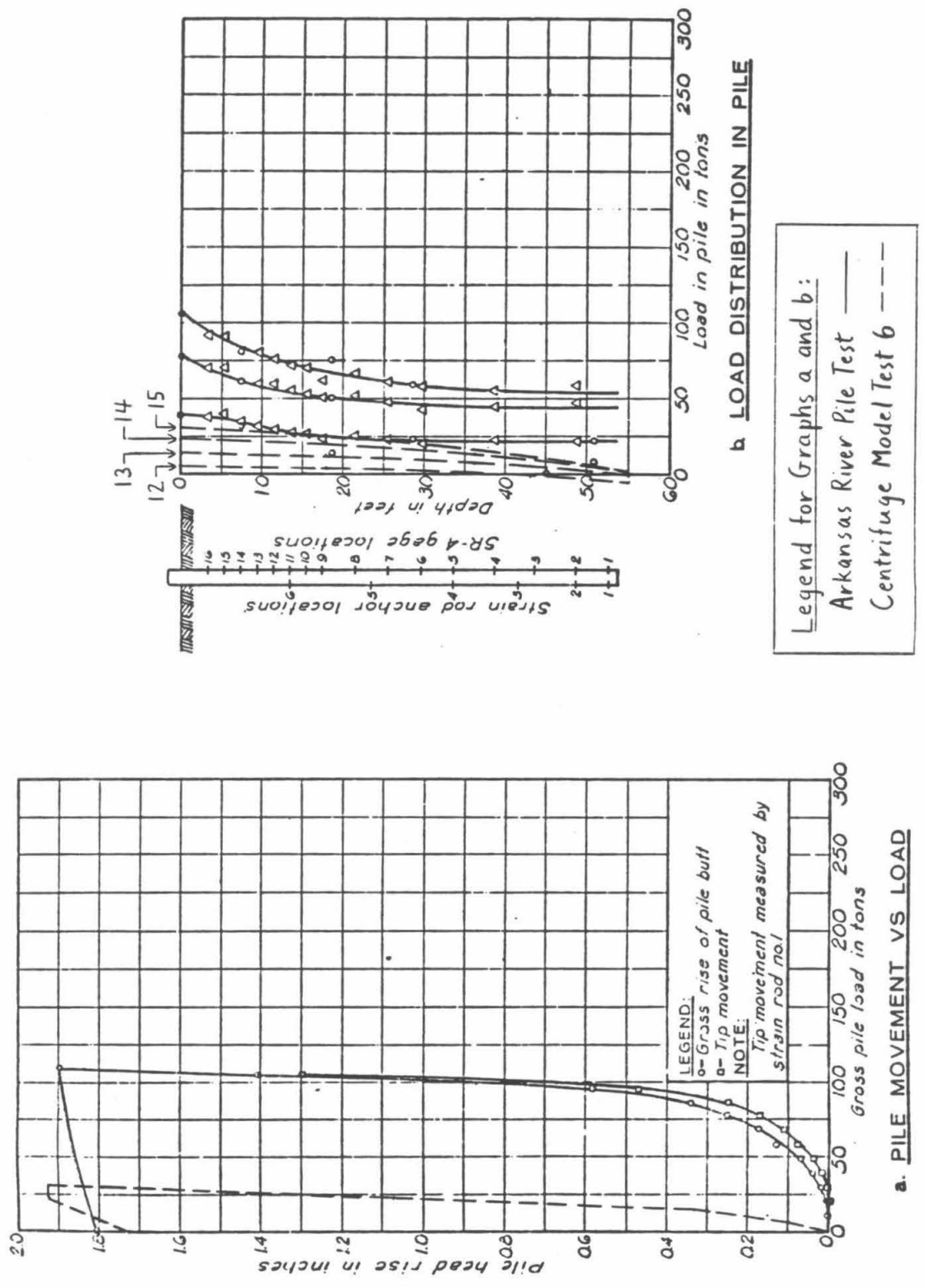

Figure 5.2 Measured behavior of ARPT Test Pile 10 and centrifuge test 6 prototype, under pulling loading

TABLE 5.1. Properties of ARPT Test Pile 10 and the Centrifuge Test 6 Pile, Scaled to Prototype Dimensions

Pile Property	Test Pile 10	Centrifuge Test 6 Prototype
Diameter, D (inches)	17.3, 20.0*	17.3
Axial stiffness, EA (kips)	692,000	506,000
Depth of embedment, L (feet)	53.1	54.9

*These two values represent the effective diameters of Test Pile 10 for purposes of computing pile cross-sectional area and circumference, respectively. The cross-section of Test Pile 10 was not circular because steel channel was welded along the length of the original 16-inch o.d. pipe to house instrumentation.

The soil mass at the site of the Arkansas River Pile Tests was composed of medium to fine sand. Nevada Fine Sand was used in the centrifuge tests. The grain-size distributions of the ARPT soil and NFS are shown together in Figure 5.3. In the ARPT's, the groundwater table lay 2 or 3 feet below ground surface. The water level in the model soil masses of centrifuge tests 5 and 6, which was approximately at the soil surface, corresponds closely to this. Other significant attributes of the full-scale and model soil masses are tabulated below.

TABLE 5.2. Properties of Full-Scale and Centrifuge Model Soils

Soil Property	ARPT	Model Tests 5 and 6
Submerged unit weight (pcf)	63	64
Angle of internal friction, φ (°)	32	33

Both the ARPT soil and NFS are essentially cohesionless.

The coefficient of friction between the pile material (steel) and the site soil for the ARPT's was 0.466. The corresponding friction coefficient for Tests 5 and 6 was 0.555 (GLPT on NFS).

5.2. Comparison of Plotted Results

5.2.1. Pushing Tests (Figure 5.1)

5.2.1.1. 'Pile Movement vs. Load' Graphs (Figure 5.1a)

(Note: Graph captions from the ARPT report [35], as well as coordinate axis labels, have been retained.)

Curves showing (a) pile top displacement, $\delta_a[=w(0)]$, versus applied load, $F_a[=f(0)]$, and (b) pile bottom displacement, $w(L)$, versus applied load are given. The values of $w(0)$, $w(L)$, and $f(0)$ for the centrifuge model system are those of stations 1 through 11 in interval 1 of Test 6 (see Figures 4.5a and 4.5d). The pushing failure load levels for the full-scale and model systems are similar. However, the compliance of the model system is considerably (three to five times) greater than that of full-scale system in the early stages of both loading and unloading.

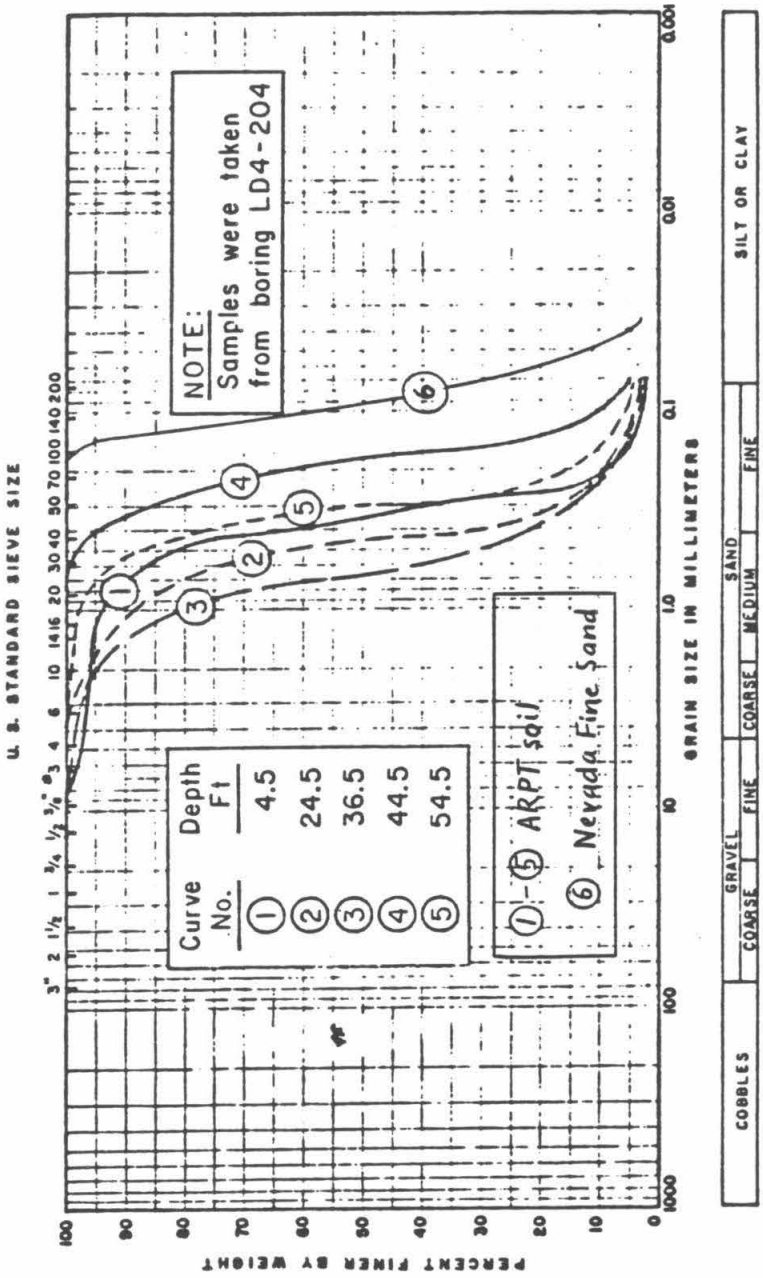

Figure 5.3 Grain size distributions for ARPT soil and NFS

5.2.1.2. 'Load Distribution in Pile' Graphs (Figure 5.1b)

Pile axial force, $f(z)$, in ARPT Test Pile 10 was plotted at three stages in the course of load increase. [The $f(z)$ curves are based on axial strain measurements using both strain rods and electrical resistance strain gauges. The locations of gauge points along the pile are indicated in the drawing to the left of Figure 5.1b.] Curves of $f(z)$ from the corresponding phase of centrifuge test 6 are superimposed, those associated with loading path stations 3, 4, 5, and 6 (see Figure 4.5b). Curves $f(z,\tau_4)$ and $f(z,\tau_6)$ exhibit higher values of $f(0)$ than any of the full-scale curves only because $f(z)$ curves for the highest values of load applied to Test Pile 10 were not presented in the ARPT report.

Note that $f(z)$ curves associated with the centrifuge model tests have consistently different shapes from the ARPT curves. The slopes of the centrifuge test curves, $df(z)/dz$, which are proportional to the soil-pile shear stress, $t(z)$ (see equation 2.8), are zero at the soil surface and increase in magnitude with depth. The $t(z)$ magnitudes associated with the ARPT curves, on the other hand, are maximum at the soil surface and decrease in magnitude with depth. This disparity in the shapes of the $f(z)$ curves apparently represents a fault in the ARPT results. First, in the phase of loading to which these curves correspond, particularly the curves associated with the highest values of applied load, $f(0)$, increasing strength and stiffness of the soil with depth should be reflected in increasing soil-pile shear stress magnitudes. Second, because the soils of the ARPT and centrifuge model tests are cohesionless, $t(z)$ must be essentially zero at the soil surface. The probable source of these errors in the ARPT's is discussed below, in section 5.2.3.

5.2.1.3. 'Gross Load vs. Tip and Wall Load' Graphs (Figure 5.1c)

Over the course of loading to failure, the proportions of the total applied load resisted by (a) soil-pile shear stresses acting along the sides of the pile and (b) normal stresses acting on the pile base are indicated, for both the full- scale and centrifuge model systems. The tip load values for the centrifuge test are those of $f(L)$ at stations 1 through 6 in Test 6, interval 1 (see Figure 4.5b). the measured tip:wall load ratios were significantly higher in the centrifuge test than in the full-scale test. The tip loads were greater and the wall loads smaller in the centrifuge test.

5.2.2. Pulling Tests (Figure 5.2)

5.2.2.1. 'Pile Movement vs. Load' Graphs (Figure 5.2a)

Just as for the pushing tests, both the displacements at the top and bottom of ARPT Test Pile 10 are plotted *vs.* applied load. However, only a plot of top displacement versus applied load was made for the centrifuge test prototype system. Because the levels of pile axial force associated with pulling loading of the centrifuge model system were very low, total pile extension was relatively small and plots of pile bottom displacement and pile top displacement *vs.* applied load would have been virtually coincident on Figure 5.2a. The values of δ_a and F_a for the centrifuge model test curve derive from those of Test 6, interval 1, stations 11 through 17 (see Figure 4.5a). However, the displacement at station 11 has been taken as a reference zero, in order that the displacement be zero at the beginning of pulling, as for the full-scale data. Pulling loads and upward pile movements are taken as positive in Figure 5.2a. The level of pulling load at which failure is reached is much lower for the centrifuge model than for the full-scale system. As under pushing loading, the compliance of the model system is significantly greater than that of the full-scale system in the early stages of both loading and unloading.

5.2.2.2. 'Load Distribution in Pile' Graphs (Figure 5.2b)

The graph from the ARPT report[35] gives pile axial force curves corresponding to three stages in the course of increase in pulling load on Test Pile 10. Curves of $f(z)$ at four points of progressive increase in pulling load on the centrifuge model system, loading path stations 12, 13, 14, and 15 (see Figure 4.5b), are superimposed. Compressive forces in the bottom third of the model pile at station 12 are due to residual soil-pile shear stresses. This reflects the fact that the centrifuge model system was subjected to pushing loading immediately prior to the pulling. As in the pushing test results, the slopes of the two $f(z)$ curves corresponding to the largest values of load applied to Test Pile 10 erroneously indicate a decrease in soil-pile shear stress magnitudes with depth, in contrast to the model system curves. Another significant fault of the ARPT results is that large pulling forces are shown as acting on the base of the pile. There is no known physical phenomenon which could account for such forces. This error is discussed in section 5.2.3, below.

TABLE 5.3. Wall Loads at Pushing and Pulling Failure

	ARPT	Centrifuge Model Test 6
Pushing load (tons)	122	65
Pulling load (tons)	70	15

The wall loads measured at failure in both pushing and pulling in the full-scale and centrifuge model tests are tabulated below. Here it is assumed that the tip load is negligible at pulling failure. Wall loads are significantly lower in the centrifuge model system than the full-scale system. In both systems, wall loads at failure in pushing are much greater than at failure in pulling. **5.2.3. Discussion of the Plotted Results**

Some of the dissimilarities in the measured behavior of ARPT Test Pile 10 and the prototype pile associated with the centrifugal model soil-pile system of Test 6 are attributable to obvious errors in the ARPT results. Examples have already been discussed in sections 5.2.1 and 5.2.2, above--the dissimilar shapes of the pile axial force [$f(z)$] curves from the two tests and the significant pulling forces indicated as acting on the base of Test Pile 10 during pulling. These errors in the representations of $f(z)$ in the ARPT report [35] appear to result primarily from the neglect of residual driving stresses present in the soil-pile system at the beginning of load testing. In constructing the $f(z)$ curves for both the pushing and pulling tests of that report, it was assumed that the axial force throughout the pile was initially zero. This course was adopted because it was impossible to determine with certainty the initial distribution of axial forces due to driving and other prior loading. However, a system of adjustments for the residual stresses was proposed in an appendix to the ARPT report. Though these adjustments leave the slopes of the $f(z)$ curves, which mistakenly indicate decreasing soil shearing strength with depth, unchanged, they eliminate tensile forces acting on the base of Test Pile 10 at pulling failure. The adjustments also bring the ratio of tip to wall load under pushing loading into better agreement with the centrifuge model test results. The ratio tip:total load at pushing failure measured in the

model test was 0.65. In the matching ARPT test, this ratio was 0.3 before adjustments for initial driving stresses and 0.5 afterward. (See Appendix D of reference [35].)

Identifiable differences between the ARPT field soil-pile system and the centrifuge model system also contribute to differences in their behavior, as it is reflected in Figures 5.1 and 5.2. A partial explanation for the disparity in tip:total load ratio at pushing failure which remains after adjustment for residual driving stresses is that the accelerations applied to the centrifuge model soil mass increase with depth. They are not constant over the model system, as was assumed in calculating prototype behavior from the measured behavior of the model. The effect of the increase in centrifugal acceleration with depth is to accentuate the increase in soil strength and stiffness with depth which would otherwise exist, contributing to disproportionately great pile tip resistance. Another difference between the field and model systems which may contribute to excessive model pile tip loads is the limited depth of the centrifuge bucket. The bottom of the bucket represents a rigid boundary of the soil mass approximately 2.4 inches (5 pile diameters) below the base of the model pile (see Figure 2.3).

Only two significant disparities between the measured behavior of the field and model systems remain unexplained, the excessive compliance of the pile top in the model system (see sections 5.2.1.1 and 5.2.2.1, above), and the relatively small loads borne by the pile walls in that system. The first of these disparities can be explained in terms of the second, as follows: Loads acting on the pile tips during pushing loading (see Figure 5.1c) are compared with tip displacements (Figure 5.1a) in Figure 5.4, below. It is seen that, considered as an isolated mechanical system, the base of the centrifuge model pile was stiffer than the field pile base. (Though the displacement of the model pile base corresponding to a given applied load was greater than that of the field pile, so was the tip load.) The excessive compliance of the model pile top was due to two factors: First, a relatively great proportion of the applied load was transmitted to the pile base, resulting in large tip displacements. Second, the relatively high axial forces acting throughout the pile length produced relatively great elastic shortening of the pile. The latter effect was magnified by the circumstance that the stiffness of the prototype pile in the model system (506,000 kips) was somewhat less than that of the full-scale pile (692,000 kips).

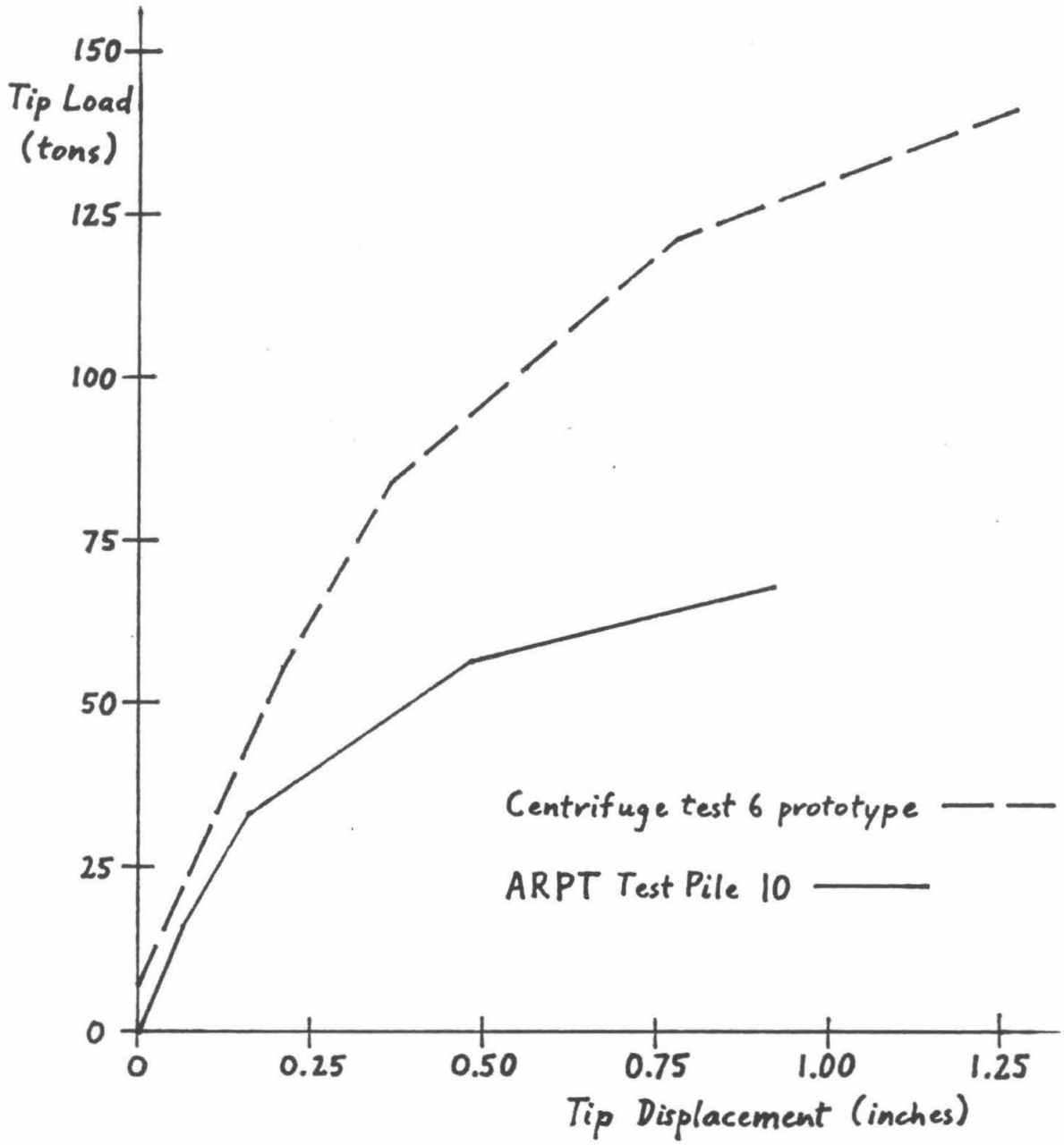

Figure 5.4 Pile base load-displacement behavior--ARPT Test Pile 10 and centrifuge test 6 prototype

The most fundamental disparity between the behavior of the centrifuge model soil-pile system and that of the field system is in the loads sustained by the walls of the two piles. Significant differences in wall loads measured at failure in both pushing and pulling were indicated in Table 5.3, above. Some uncertainty is associated with the value of the wall load on ARPT Test Pile 10 at pushing failure, because of the questionable accuracy of the ARPT load distribution [$f(z)$] curves, but the wall loads in the two systems at pulling failure reflect direct measurements of applied load. The bearing capacity under pulling exhibited by the centrifuge model system is between one-fifth and one- quarter that of the field system. One possible explanation for this disparity is significant edge effects in the centrifuge model due to the proximity to the pile of the centrifuge bucket walls. In a half-space composed of sand of unit weight γ, the normal stress on horizontal planes, σ_z increases with depth, z, according to $\sigma_z = \gamma z$. However, σ_z will increase less rapidly with depth in a column of sand contained in a long vertical pipe, because of the vertical forces given to the sand by the walls of the pipe. Similarly, support provided to the soil by the bucket walls may prevent development of the full lateral soil pressures on the walls of the pile which are present in the field system. (The dimensions of model pile B relative to those of the centrifuge bucket are shown in Figure 2.3.) Another factor which may contribute to the wall loads disparity is the difference in the methods of installing the centrifuge model and field piles. The driving of Test Pile 10 in the field involved the displacement of soil material by the pile, accompanied by compaction of the soil adjacent to the pile and the development of increased lateral stresses at the soil-pile interface. The latter effects increased the capacity of the soil mass to exert shearing resistance against the walls of the pile. No corresponding, strengthening processes occurred in the centrifuge model, where the pile was emplaced by packing soil around it at 1-g conditions.

CHAPTER 6

CONCLUSIONS AND RECOMMENDATIONS

The comparison of plotted results in section 5.2 indicates significant quantitative discrepancies between the behavior of the prototype systems associated with centrifuge tests 5 and 6, and very similar, full-scale systems in the field. More generally, it indicates that the behavior of the prototype systems associated with all of the centrifuge tests, 1-6, may differ significantly from the performance of identical field systems. The principal discrepancies between the centrifuge model and field systems are the following:

1. The model system shows greater pile top compliance than the field system in the early stages of loading and unloading.

2. At bearing capacity failure under pushing loading, the base of the pile sustains significantly greater force in the model system than in the field system.

3. At bearing capacity failure under both pushing and pulling, the pile walls sustain significantly less force in the model system than in the field system. These discrepancies must be taken into account in using the centrifuge test results presented here for predicting field soil-pile system behavior.

In view of the modeling inaccuracies discovered in the Chapter 5 comparison, it cannot be assumed that in the tests using Nevada Fine Sand, full-scale pile behavior in ideal, homogeneous sand deposits is shown directly. However, since the same modeling procedure was applied in Tests 3 and 4 involving dry NFS and in Tests 5 and 6 using saturated NFS, similar, parallel deviations from full- scale soil-pile system behavior may be expected in both of these pairs of tests. Thus, the relationship between the system behavior observed in these pairs of model tests indicates the effect of groundwater on the behavior of the corresponding full-scale piles embedded in deposits of ideal, homogeneous sand. Primary observations concerning the effects of the presence of water on the behavior of 55-foot piles in sand are the following:

1. The presence of water will cause a significant reduction in total bearing capacity in both pushing and pulling. Under pushing loading, this reduction will be given, approximately, by the ratio of the buoyant and dry unit weights of the sand. The reduction in capacity under pulling loading appears to be somewhat greater.

2. Initial system stiffness appears to be unaffected by the presence of water. Dry and saturated systems show similar stiffness until applied load approaches bearing capacity of the latter system. Loaded beyond this point, the pile in saturated sand fails abruptly, while the pile in dry sand shows further bearing strength, but with decreased stiffness. (Note: The last statement is based primarily on observations of t-z stiffness at the pile walls. It is not necessarily valid for systems deriving a large proportion of their bearing strength from tip bearing.)

The following modifications in the procedures and apparatus used in Tests 1-6 are indicated, for increasing the modeling accuracy of future centrifugal modeling studies on piles in axial loading:

1. Reduce the length of the model pile in relation to its distance from the centrifuge center-of-rotation. This will reduce the variation with depth in the centrifugal accelerations applied to the soil mass, and the disproportion in the loads carried by the pile tip and walls.

2. Reduce the diameter of the model pile in relation to the diameter of the centrifuge bucket. In this way, vertical support given to the soil by the bucket walls, an edge effect which is thought to limit the lateral soil pressures against the walls of the model pile (see section 5.2.3), will be reduced, and wall loads increased.

3. Devise techniques for driving the model pile into the soil while the centrifuge is in motion. The strengthening of the soil due to driving which occurs during field installation will then be simulated, and the wall loads increased.

In view of the difficulty of implementing the third of these measures, it is advisable to begin by determining the effects of measures 1 and 2.

REFERENCES

1. American Petroleum Institute Recommended Practice for Planning, Designing, and Constructing Fixed Offshore Platforms, RP2A 11th Ed., Dallas, January, 1980.

2. Baguelin, F., Bustamante, M., Frank, R., and Jezequel, J. F., **Annals de l'Institut Technique du Batiment et des Travaux Publics,** Suppl 330, Serie SF/116, 1975.

3. Balaam, N. P., Poulos, H. G., and Booker, J. R., *Finite Element Analysis of the Effects of Installation on Pile Load-Settlement Behaviour*, **Geotechnical Engineering,** Vol. 6, No. 1, 1975, pp. 33-48.

4. Banerjee, P. K., *Integral Equation Methods for Analysis of Piece-wise Non- homogeneous Three-dimensional Elastic Solids of Arbitrary Shape*, **International Journal of Mechanical Science,** Vol. 18, 1976, pp. 293-303.

5. Banerjee, P. K., and Davies, T. G., *Analysis of Pile Groups Embedded in Gibson Soil*, **Proceedings, 9th International Conference on Soil Mechanics and Foundation Engineering,** Tokyo, Japan, Vol. I, 1977, pp. 381-386.

6. Butterfield, R., and Banerjee, P. K., *A Note on the Problem of a Pile Reinforced Half Space*, **Geotechnique,** Vol. 20, No. 1, 1970, pp. 100-103.

7. Butterfield, R., and Banerjee, P. K., *Elastic Analysis of Compressible Piles and Pile Groups*, **Geotechnique,** Vol. 21, No. 1, 1971, pp. 43-60.

8. Chellis, R. D., **Pile Foundations,** McGraw-Hill Book Company, New York, 1961.

9. Christian, J. T., and Desai, C. S., *Constitutive Laws for Geologic Media*, **Numerical Methods in Geotechnical Engineering,** C. S. Desai and J. T. Christian, Eds., McGraw-Hill Book Co., Inc., New York, N. Y., 1977.

10. Cooke, R. W., and Price, G., *Strains and Displacements around Friction Piles*, **Proceedings**, 8th International Conference on Soil Mechanics and Foundation Engineering, Moscow, 1973.

11. Cooke, R. W., Price, G., and Tarr, K., *Jacked Piles in London Clay: A Study of Load Transfer and Settlement under Working Conditions*, **Geotechnique,** Vol. 29, No. 2, 1979, pp. 113-147.

12. Coyle, H. M., and Reese, L. C., *Load Transfer for Axially Loaded Piles in Clay*, **Journal of the Soil Mechanics and Foundations Division, ASCE,** Vol. 92, No. SM2, Proc. Paper 4702, March, 1966, pp. 1-26.

13. Coyle, H. M., and Sulaiman, I. H., *Skin Friction for Steel Piles in Sand*, **Journal of the Soil Mechanics and Foundations Division, ASCE,** Vol. 93, No. SM6, Proc. Paper 5590, November, 1967, pp. 261-278.

14. Desai, C. S., "Deep Foundations," **Numerical Methods in Geotechnical Engineering,** C. S. Desai and J. T. Christian, Eds., McGraw-Hill Book Co., Inc., New York, N. Y., 1977.

15. Desai, C. S., *Effects of Driving and Subsequent Consolidation on Behavior of Driven Piles*, **International Journal for Numerical and Analytical Methods in Geomechanics,** Vol. 2, 1978, p. 283.

16. Desai, C. S., *Numerical Design-Analysis for Piles in Sands*, **Journal of the Geotechnical Engineering Division, ASCE,** Vol. 100, No. GT6, Proc. Paper 10617, June, 1974, pp. 613-635.

17. Ellison, R. D., D'Appolonia, E., and Thiers, G. R., *Load-Deformation Mechanism for Bored Piles*, **Journal of the Soil Mechanics and Foundations Division, ASCE,** Vol. 97, No. SM4, Proc. Paper 8052, April, 1971, pp. 661-678.

18. **Encyclopedia Britannica**, 15th Ed., 1974.

19. Frank, R., **Etude Theorique du Compartement des Pieux sous Charge Verticale. Introduction de la Dilatance,** Docteur Ingenieur Thesis, University of Paris VI, November, 1974.

20. Gallagher, R. H., **Finite Element Analysis: Fundamentals,** Prentice-Hall, Inc., Englewood Cliffs, N. J., 1975.

21. Gibson, R. E., *The Analytical Method in Soil Mechanics*, **Geotechnique**, Vol. 24, No. 2, 1974, pp. 113-140.

22. Hanna, T. H., *Distribution of Load in Long Piles*, **Ontario Hydro Research Quarterly,** Vol. 18, No. 4, 1966, pp. 1-7.

23. Hunter, A. H., and Davisson, M. T., *Measurement of Pile Load Transfer*, **Performance of Deep Foundations, ASTM 444,** American Society of Testing and Materials, 1969, pp. 106-117.

24. Kezdi, A., *Pile Foundations*, **Foundation Engineering Handbook,** H. F. Winterkorn and H.-Y. Fang, Eds., Van Nostrand Reinhold Company, New York, N.Y., 1975.

25. Mansur, C. I., and Hunter, A. H., *Pile Tests--Arkansas River Project*, **Journal of the Soil Mechanics and Foundations Division, ASCE,** Vol. 96, No. SM5, Proc. Paper 7509, September, 1970, pp. 1545-1582.

26. Matlock, H., and Foo, S. C., *Axial Analysis of Pile Using a Hysteretic and Degrading Soil Model*, **Proceedings**, Conference on Numerical Methods in Offshore Piling, Institution of Civil Engineers, London, England, May, 1979, pp. 99-106.

27. Mattes, N. S., and Poulos, H. G., *Settlement of a Single Compressible Pile*, **Journal of the Soil Mechanics and Foundations Division, ASCE,** Vol. 95, No. SM1, Proc. Paper No. 6356, January, 1969, pp. 189-207.

28. McClelland, B., *Design of Deep Penetration Piles for Ocean Structures*, **Journal of the Geotechnical Engineering Division, ASCE,** Vol. 100, No. GT7, Proc. Paper 10665, July, 1974, pp. 705-747.

29. Meyer, P. T., *Computer Prediction of Axially Loaded Piles with Non-linear Supports*, **Preprints**, Seventh Annual Offshore Technology Conference, Houston, Texas, Paper No. 2186, 1975.

30. Meyerhof, G. G., *Bearing Capacity and Settlement of Pile Foundations*, **Journal of the Geotechnical Engineering Division, ASCE,** Vol. 102, No. GT3, March, 1976, pp. 197-228.

31. Mindlin, R. D., *Force at a Point in the Interior of a Semi-infinite Solid*, **Physics**, Vol. 7, 1936, pp. 195-202.

32. Muki, R., and Sternberg, E., *Elasto-static Load Transfer to a Half-space from a Partially-embedded Axially-loaded Rod*, **International Journal of Solids and Structures,** Vol. 6, 1970, pp. 69-90.

33. Murff, J. D., *Pile Capacity in a Softening Soil*, **International Journal for Numerical and Analytical Methods in Geomechanics,** Vol. 4, 1980, p. 185.

34. Murff, J. D., *Response of Axially Loaded Piles*, **Journal of the Geotechnical Engineering Division, ASCE,** Vol. 101, No. GT3, March, 1975, pp. 356-360.

35. **Pile Driving and Loading Tests: Lock and Dam No. 4, Arkansas River and Tributaries, Arkansas and Oklahoma,** Fruco and Assoc., United States Army Engineer District, CE, Little Rock, Arkansas, September, 1964.

36. Poulos, H. G., *Cyclic Axial Response of Single Pile*, **Journal of the Geotechnical Engineering Division, ASCE,** Vol. 107, No. GT1, Proc. Paper 15979, January, 1981, pp. 41-58.

37. Poulos, H. G., *Load-Settlement Prediction for Piles and Piers*, **Journal of the Soil Mechanics and Foundations Division, ASCE,** Vol. 98, No. SM9, Proc. Paper 9085, August, 1972, pp. 879-897.

38. Poulos, H. G., *Settlement of Pile Foundations*, **Numerical Methods in Geotechnical Engineering,** C. S. Desai and J. T. Christian, Eds., McGraw-Hill Book Co., Inc., New York, N. Y., 1977.

39. Poulos, H. G., *Settlement of Single Piles in Nonhomogeneous Soils*, **Journal of the Geotechnical Engineering Division, ASCE,** Vol. 105, No. GT5, Proc. Paper 14575, May, 1979, pp. 627-641.

40. Poulos, H. G., and Davis, E. H., *The Settlement Behavior of Single Axially Loaded Incompressible Piles and Piers*, **Geotechnique**, London, England, Vol. 18, No. 3, 1968, pp. 351-371.

41. Randolph, M. F., and Wroth, C. P., *Analysis of Deformation of Vertically Loaded Piles*, **Journal of the Geotechnical Engineering Division, ASCE,** Vol. 104, No. GT12, Proc. Paper 14262, December, 1978, pp. 1465-1488.

42. Randolph, M. F., and Wroth, C. P., *An Analytical Solution for the Consolidation around a Driven Pile*, **International Journal for Numerical and Analytical Methods in Geomechanics,** Vol. 3, 1979, pp. 217-229.

43. Randolph, M. F., and Wroth, C. P., *A Simple Approach to Pile Design and the Evaluation of Pile Tests*, **Behavior of Deep Foundations, ASTM STP 670,** Raymond Lundgren, Ed., American Society for Testing and Materials, 1979, pp. 484-499.

44. Reese, L. C., *Design and Evaluation of Load Tests on Deep Foundations*, **Behavior of Deep Foundations, ASTM STP 670,** Raymond Lundgren, Ed., American Society for Testing and Materials, 1979, pp. 4-26.

45. Rocha, M.: *The Possibility of Solving Soil Mechanics Problems by the Use of Models,*" **Proceedings**, 4th International Conference on Soil Mechanics and Foundation Engineering, London, England, Vol. I, 1975.

46. Scott, R. F., **Centrifuge Studies of Lateral Load-Displacement Behavior of Single Piles,** Final Report 1976-77 Research Program for American Petroleum Institute OSAPR Project 8.

47. Scott, R. F., Class notes, California Institute of Technology, 1968.

48. Scott, R. F., **Foundation Analysis,** Prentice-Hall, Inc., Englewood Cliffs, N.J., 1981.

49. Seed, H. B., and Reese, L. C., *The Action of Soft Clay along Friction Piles*, **Transactions, ASCE,** Vol. 122, Paper No. 2882, 1957, pp. 731-754.

50. Smith, I. A., *Numerical and Physical Modeling*, **Numerical Methods in Geotechnical Engineering,** C. S. Desai and J. T. Christian, Eds., McGraw-Hill Book Co., Inc., New York, N. Y., 1977.

51. Terzaghi, K., and Peck, R. B., **Soil Mechanics in Engineering Practice,** John Wiley and Sons, Inc., New York, N.Y., 1967.

52. Terzaghi, K., **Theoretical Soil Mechanics,** John Wiley and Sons, Inc., New York, N.Y., 1967.

53. Touma, F. T., and Reese, L. C., *Behavior of Bored Piles in Sand*, **Journal of the Geotechnical Engineering Division, ASCE,** Vol. 100, No. GT7, Proc. Paper 10651, July, 1974, pp. 749-761.

54. Vesic, A. S., *Tests on Instrumented Piles, Ogeechee River Site*, **Journal of the Soil Mechanics and Foundations Division, ASCE,** Vol. 96, No. SM2, Proc. Paper 7170, March, 1970, pp. 561-584.

55. Vijayvergiya, V. N., and Focht, J. A., Jr., *A New Way to Predict the Capacity of Piles in Clay*, **Preprints**, Fourth Annual Offshore Technology Conference, Houston, Texas, Vol. II, 1972, pp. 865-874.

56. Zienkiewicz, O. C., **The Finite Element Method,** 3rd Ed., McGraw-Hill Book Company (UK) Limited, 1977.

APPENDIX 1

SUMMARY OF A COMPUTER PROGRAM FOR AUTOMATING THE TEST DATA ANALYSIS

The primary product of the analysis discussed in sections 2.6.1-2.6.5, above, is a set of plots which describe the mechanical behavior of a prototype soil-pile system in a given loading path interval. These plots include

1. applied load $F_a = f(0)$ versus pile top displacement $w(0)$,
2. pile axial force $f(z)$,
3. soil-pile shear stress $t(z)$,
4. pile displacement $w(z)$, and
5. t-z diagrams corresponding to three depths along the pile.

The calculations and plotting for the analysis of the six tests were performed using the IBM /370 computer and other facilities of the Booth Computing Center at Caltech. Prominent features of a FORTRAN program written to control these operations are now described:

(Note: The following description is based on a particular form of the program. A listing of this program forms Appendix 2. Line numbers in this description refer to those of this listing.)

1. The following data are input: (ll. 0007-0026)

a. Readings from the seven gauges with which the model pile is instrumented--the load cell, displacements transducer, and five strain gauges of model pile A--at successive stations τ; along the loading path, including the stations which form the basis for t-z interpretation in selected loading path intervals. (For most of the tests, these would be readings digitized from the strip chart recorder record. The digitizing system produced punched cards, and the data in this form could be input directly into the computing system.)

b. The number of separate loading path intervals to be analyzed, and the location of the data for these intervals within the entire body of input data.

c. Gauge zero values for the seven gauges.

d. Gauge calibration factors for the seven gauges.

e. The prototype pile stiffness, EA.

f. The distance from the top of the model pile tube to the soil surface.

g. Prototype-model scaling factors.

h. Locations of strain gauges along the prototype pile.

2. Gauge zeros are subtracted from all gauge readings. (ll. 0027-0034)

3. Multipliers are computed which give prototype pile forces and displacements from the gauge readings. (ll. 0036-0048) These multipliers are composed of transducer calibration factors, digitizer scale factors, and prototype-model scaling factors.

4. The values of depth, z, at which the functions $f(z)$, $t(z)$, and $w(z)$ will be evaluated for plotting are computed. (ll. 0049-0063) One hundred has been found to be a satisfactory number of values.

5. Procedures a-g below are carried out for the first of the selected loading path intervals:

a. The stations in the loading path interval for which $f(z)$, $t(z)$, and $w(z)$ functions are to be generated and on which the t-z diagrams will be based, are identified. (ll. 0069-0074)

b. The loading stations of a, above, at which $f(z)$, $t(z)$, and $w(z)$ are to be plotted are specified. (ll. 0075-0078)

c. The depths, z_i, are specified at which the t-z plots are to be made. (ll. 0079-0082)

d. For each of the selected stations of a:

   i. Apply the multipliers computed in 3, above, to the seven station gauge readings. (ll. 0101-0107)

ii. From the resulting prototype pile force data, generate the coefficients of the polynomial using least squares fitting. (ll. 0111-0113)

iii. Compute $f(z)$ and $t(z)$ from their polynomial formulas, equations (2.11) and (2.10), at the 100 values of z found in item 4, above. (ll. 0114-0119)

iv. Compute $w(z)$ at the same z values by numerical integration (using Simpson's Rule). (ll. 0125-0133) (The 100 values of z at which $f(z)$ has been evaluated for purposes of plotting form a sufficiently fine mesh for the integration also.)

e. Plot $f(z)$, $t(z)$, and $w(z)$ versus depth z for the stations specified in b. (ll. 0155-0179)

f. Plot t-z diagrams. (ll. 0180-0198) For the z specified in a, above, plot and join by line segments points $[w(z_i), t(z_i)]$ at the successive interval loading path stations.

g. Plot applied load versus pile top displacement. (ll. 0199-0211)

Repeat procedures 5.a-5.g, above, for the other test loading path intervals.

APPENDIX 2. DATA ANALYSIS PROGRAM LISTING

```
FORTRAN IV G LEVEL 20.7 VS              MAIN            DATE =     6/27/80      14:37:34

0001                  DIMENSION DOC(3),WD(6,5001),W1(5001),Z(7),SGLOC(6),IDTSET(25)
0002                  DIMENSION WDPLT(102,25),WPLT(102,25),ZSPIN(102),WDSPIN(102)
0003                  DIMENSION WDSK(7),DER(102),WDDPLT(102,25),COEF(11),DATDP(6)
0004                  DIMENSION IWPLOT(15),ITZDEP(10),ZPLOT(25,10),TPLOT(25,10)
0005                  DIMENSION SURFF(700),SURFD(700),STATNS(25),G1F(25)
0006                  DIMENSION NUM1(5),NUM2(5),DPL(5001),WDATPT(6,25)
                C     COMMON /COMSPL/IWANT,DER
0007                  DATA DATDP/334.4,606.3,1018.8,1603.1,2187.5,2300.0/
0008                  DATA EN,ENSQ/100.,10000./
                C READ IN TITLE, 8 CHARACTERS, COL 1-8
                C READ IN LOAD SCALE, COL 21-30
                C READ IN DISPLACEMENT SCALE, COL 31-40
                C READ IN DISTANCE FROM TOP OF PILE TO SOIL SURFACE, COL 41-50
                C READ IN NUMBER OF DATA POINTS, COL 51-55
                C READ IN FLAG FOR PLOTTING, COL 60: 0 FOR PLOT, NONZERO FOR NO PLOT
                C READ IN NUMBER OF POINTS TO BE GENERATED FOR PLOTTING AND
                C  NUMERICAL INTEGRATION, COL 61-65
0009                  READ(5,10)DOC,ALSCAL,DISSCL,PROJ,NP,NPLOT,M
0010               10 FORMAT(3A4,8X,3F10.6,3I5)
0011                  WRITE(6,11)DOC,ALSCAL,DISSCL,PROJ,NP,NPLOT,M
0012               11 FORMAT(1X,3A4,8X,3F10.6,3I5)
                C READ IN SCALES FOR FORCES AT STRAIN GAUGES, COL 1-10,...,41-50
                C READ IN PILE TIP LOAD RATIO, COL 51-60
                C READ IN PILE STIFFNESS, COL 61-71
0013                  READ(5,20)SG1SCL,SG2SCL,SG3SCL,SG4SCL,SG5SCL,ALPHA,EA
0014               20 FORMAT(6F10.3,E11.4)
0015                  WRITE(6,21)SG1SCL,SG2SCL,SG3SCL,SG4SCL,SG5SCL,ALPHA,EA
0016               21 FORMAT(1X,6F10.3,E11.4)
                C READ IN DIGITIZED TEST DATA
                C NEED TO READ ALL DATA HERE?  INTRODUCE IDTSET() HERE?
                C     READ(5,30)ALZERO,ALARB,DISZRO,DISARB,SG1ZRO,SG1ARB,
                C    ,SG2ZRO,SG2ARB,SG3ZRO,SG3ARB,SG4ZRO,SG4ARB,SG5ZRO,SG5ARB,
                C    ,(WD(1,I),W1(I), WD(2,I), WD(3,I),WD(4,I),WD(5,I),WD(6,I),I=1,NP)
                C  30 FORMAT(5(8X,F8.0))
                C     J=0
                C     WRITE(6,40)J,ALZERO,ALARB,DISZRO,DISARB,SG1ZRO,SG1ARB,
                C    ,SG2ZRO,J,SG2ARB,SG3ZRO,SG3ARB,SG4ZRO,SG4ARB,SG5ZRO,SG5ARB,
                C    ,(I,WD(1,I),W1(I), WD(2,I), WD(3,I),WD(4,I),WD(5,I),WD(6,I),I=1,NP)
                CC READ IN GAUGE SIGNAL ZERO VOLTAGES
                C     READ(5,25)SG1ZRO,SG2ZRO,SG3ZRO,SG4ZRO,SG5ZRO,ALZERO,DISZRO
                C  25 FORMAT(7E11.4)
                C     WRITE(6,26)SG1ZRO,SG2ZRO,SG3ZRO,SG4ZRO,SG5ZRO,ALZERO,DISZRO
                C  26 FORMAT(7E11.4)
                CC READ IN A/D CONVERTER GAUGE SIGNAL VOLTAGES
                C     READ(8,30)(WD(2,I),WD(3,I),WD(4,I),WD(5,I),WD(6,I),WD(1,I),
                C    ,W1(I),I=1,NP)
                C  30 FORMAT(8X,7E12.5)
                C     WRITE(6,40)(NP,WD(2,I),WD(3,I),WD(4,I),WD(5,I),WD(6,I),WD(1,I),
                C    ,W1(I),I=1,5)
                C  40 FORMAT((1X,I4,7(2X,F8.0)))
                C READ IN FORCE GAUGE SIGNAL ZERO DIGITIZER VALUES
0017                  READ(5,25)ALZERO,SG1ZRO,SG2ZRO,SG3ZRO,SG4ZRO,SG5ZRO,DISZRO
0018               25 FORMAT(7E11.4)
0019                  WRITE(6,26)ALZERO,SG1ZRO,SG2ZRO,SG3ZRO,SG4ZRO,SG5ZRO,DISZRO
0020               26 FORMAT(7E11.4)
                C READ IN DISPLACEMENTS TAKEN FROM X-Y RECORDER RECORD
```

```
FORTRAN IV G LEVEL 20.7 VS              MAIN                DATE =     6/27/80      14:37:34

0021                  READ(5,35)(W1(I),I=1,NP)
0022                35 FORMAT(5(4X,F6.3))
                    C READ IN DIGITIZED FORCE GAUGE SIGNAL VALUES
0023                  READ(5,30)(WD(1,I),WD(2,I),WD(3,I),WD(4,I),WD(5,I),WD(6,I),
                     ,I=1,NP)
0024                30 FORMAT(6(2X,F8.0))
0025                  WRITE(6,40)(I,WD(1,I),WD(2,I),WD(3,I),WD(4,I),WD(5,I),WD(6,I),
                     ,W1(I),I=1,NP)
0026                40 FORMAT((1X,I4,7(1X,F9.3)))
                    C REDUCE GAUGE SIGNAL VALUES BY GAUGE SIGNAL ZEROS
0027                  DO 50 I=1,NP
0028                  WD(2,I)=WD(2,I)-SG1ZRO
0029                  WD(3,I)=WD(3,I)-SG2ZRO
0030                  WD(4,I)=WD(4,I)-SG3ZRO
0031                  WD(5,I)=WD(5,I)-SG4ZRO
0032                  WD(6,I)=WD(6,I)-SG5ZRO
0033                  WD(1,I)=WD(1,I)-ALZERO
0034                50 W1(I)=W1(I)-DISZRO
                    C      WRITE(6,51)(NP,WD(2,I),WD(3,I),WD(4,I),WD(5,I),WD(6,I),WD(1,I),
                    C     ,W1(I),I=1,5)
                    C   51 FORMAT((1X,I4,7(2X,F8.0)))
0035                  WRITE(6,40)(I,WD(1,I),WD(2,I),WD(3,I),WD(4,I),WD(5,I),WD(6,I),
                     ,W1(I),I=1,NP)
                    C  40 FORMAT((1X,I4,7(1X,F9.3)))
                    C     ALSCAL=ALSCAL*ENSQ/(ALARB-ALZERO)
                    C     DISSCL=DISSCL*EN/(DISARB-DISZRO)
                    C     SG1SCL=SG1SCL*ENSQ/(SG1ARB-SG1ZRO)
                    C     SG2SCL=SG2SCL*ENSQ/(SG2ARB-SG2ZRO)
                    C     SG3SCL=SG3SCL*ENSQ/(SG3ARB-SG3ZRO)
                    C     SG4SCL=SG4SCL*ENSQ/(SG4ARB-SG4ZRO)
                    C     SG5SCL=SG5SCL*ENSQ/(SG5ARB-SG5ZRO)
                    C
                    C FIDDLE FACTORS 1 AND 2 ASSOCIATED WITH NUMERICAL FILTERING (SMOOTHING)
                    C FIDDLE FACTORS 3, 4, AND 5 REPRESENT MV/DU (FORCES) AND V/X-Y-IN (DSP)
0036                  FIDDL1=1.
0037                  FIDDL2=1.
0038                  FIDDL3=0.6410
0039                  FIDDL4=0.1282
0040                  FIDDL5=0.5
0041                  CIRCUM=-1./(.5*3.14159*100.)
                    C
0042                  SG1SCL=SG1SCL*FIDDL2*ENSQ*FIDDL4
0043                  SG2SCL=SG2SCL*FIDDL2*ENSQ*FIDDL4
0044                  SG3SCL=SG3SCL*FIDDL2*ENSQ*FIDDL4
0045                  SG4SCL=SG4SCL*FIDDL2*ENSQ*FIDDL4
0046                  SG5SCL=SG5SCL*FIDDL2*ENSQ*FIDDL4
0047                  ALSCAL=ALSCAL*FIDDL1*ENSQ*FIDDL3
0048                  DISSCL=DISSCL*FIDDL1*EN*FIDDL5
                    C
                    C     NUM1(1)=1237
                    C     NUM2(1)=1827
                    C     NUM1(2)=3133
                    C     NUM2(2)=3360
                    C
0049                  Z(1)=0.0
0050                  DO 60 I=1,6
```

```
FORTRAN IV G LEVEL 20.7 V5                MAIN                DATE =     6/27/80      14:37:34

0051                  J=I+1
0052               60 Z(J)=DATDP(I)-PROJ
0053                  DZSPIN=(Z(7)-Z(1))/(M-2.)
0054                  HOVER3=DZSPIN/3./EA
0055                  HOVER6=DZSPIN/6./EA
0056                  ZSPIN(1)=Z(1)
0057                  IWANT=1
0058                  M1=M-1
0059                  M2=M-2
0060                  DO 80 I=1,M2
0061                  J=I+1
0062               80 ZSPIN(J)=ZSPIN(I)+DZSPIN
0063                  ZSPIN(M)=.5*(ZSPIN(2)+ZSPIN(L))
                   C
                   C ESTABLISH CAPABILITY FOR MULTIPLE SUB-PATHS
0064                  READ(5,110)NPATH
0065                  WRITE(6,111)NPATH
0066               110 FORMAT(I4)
0067               111 FORMAT(1X,I4)
0068                  DO 400 IPATH=1,NPATH
                   C
                   C THE LOADING PATH STATIONS WHICH ARE TO BE SPLINE-FIT AND ON WHICH THE
                   C  T-Z PLOTS ARE TO BE BASED ARE SPECIFIED.  (NOTE: THESE TAKE ON VALUES
                   C  OF THE DIGITIZED DATA SET INDICES.)
0069                  READ(5,110)NDTSET
0070                  WRITE(6,111)NDTSET
0071                  READ(5,120)(IDTSET(I),I=1,NDTSET)
0072                  WRITE(6,121)(IDTSET(I),I=1,NDTSET)
0073               120 FORMAT(20I4)
0074               121 FORMAT(1X,20I4)
                   C OF THESE LOADING STATIONS, THE ONES AT WHICH W, W', AND W'' ARE TO BE
                   C  PLOTTED ARE SPECIFIED.  (NOTE: THESE ARE IDTSET( ) INDICES.)
0075                  READ(5,110)NWPLOT
0076                  READ(5,120)(IWPLOT(I),I=1,NWPLOT)
0077                  WRITE(6,111)NWPLOT
0078                  WRITE(6,121)(IWPLOT(I),I=1,NWPLOT)
                   C THE DEPTHS AT WHICH THE T-Z PLOTS ARE TO BE MADE ARE SPECIFIED.
                   C  (NOTE: ZSPIN INDICES.)
0079                  READ(5,110)NTZDEP
0080                  READ(5,120)(ITZDEP(I),I=1,NTZDEP)
0081                  WRITE(6,111)NTZDEP
0082                  WRITE(6,121)(ITZDEP(I),I=1,NTZDEP)
                   C DETERMINE WHICH BOUNDARY CONDITIONS ARE TO BE USED FOR THE SPLINE
                   C     READ(5,152)IBC,Y1P,YNP
                   C 152 FORMAT(I5,2E11.4)
                   C
                   CC SMOOTHING BEGINS
                   C     N1=NUM1(IPATH)
                   C     N2=NUM2(IPATH)
                   C     J1=N1+4
                   C     J2=N2-4
                   C     N=N2-N1+1
                   C     NN=J2-J1+1
                   C     DO 610 I=2,6
                   C     SUM=0.
                   C     J=N1
```

```
FORTRAN IV G LEVEL 20.7 VS              MAIN                DATE =     6/27/80      14:37:34

                C       DO 600 JJ=1,9
                C       SUM=SUM+WD(I,J)
                C   600 J=J+1
                C       ILEAD=J
                C       ILAG=N1
                C       DO 620 J=J1,J2
                C       DPL(J)=SUM
                C       SUM=SUM+WD(I,ILEAD)-WD(I,ILAG)
                C       ILEAD=ILEAD+1
                C   620 ILAG=ILAG+1
                C       DO 630 J=J1,J2
                C   630 WD(I,J)=DPL(J)
                C   610 CONTINUE
0083                   COMMT1=0.0
                CC       SUM=0.
                CC       J=N1
                CC       DO 640 JJ=1,9
                CC       SUM=SUM+W1(J)
                CC    640 J=J+1
                CC       ILEAD=J
                CC       ILAG=N1
                CC       DO 650 J=J1,J2
                CC       DPL(J)=SUM
                CC       SUM=SUM+W1(ILEAD)-W1(ILAG)
                CC       ILEAD=ILEAD+1
                CC    650 ILAG=ILAG+1
                CC       DO 660 J=J1,J2
                CC    660 W1(J)=DPL(J)
                CC  SMOOTHING ENDS
                C
0084                WDMIN = 1.0E30
0085                WMIN  = 1.0E30
0086                WDDMIN= 1.0E30
0087                ZMIN  = 1.0E30
0088                TMIN  = 1.0E30
0089                SFFMIN= 1.0E30
0090                SFDMIN= 1.0E30
0091                WDMAX =-1.0E30
0092                WMAX  =-1.0E30
0093                WDDMAX=-1.0E30
0094                ZMAX  =-1.0E30
0095                TMAX  =-1.0E30
0096                SFFMAX=-1.0E30
0097                SFDMAX=-1.0E30
0098                DELTOP=PROJ/EA
                C ALL THE VALUES OF APPLIED FORCE AND TOP DISPLACEMENT IN THE
                C  SUB-INTERVAL ARE COMPUTED, FOR MAKING L-D PLOTS
                C       DO 680 I=J1,J2
                C       WD(1,I)=WD(1,I)*ALSCAL
                C   680 W1(I) = W1(I)*DISSCL-WD(1,I)*DELTOP
0099                DO 100 J=1,NDTSET
0100                I=IDTSET(J)
0101                WDSK(1)=WD(1,I)*ALSCAL
0102                W1(I) = W1(I)*DISSCL-WDSK(1)*DELTOP
0103                WDSK(2)=WD(2,I)*SG1SCL
0104                WDSK(3)=WD(3,I)*SG2SCL
```

```
FORTRAN IV G LEVEL 20.7 VS              MAIN                DATE =     6/27/80      14:37:34

0105                  WDSK(4)=WD(4,I)*SG3SCL
0106                  WDSK(5)=WD(5,I)*SG4SCL
0107                  WDSK(6)=WD(6,I)*SG5SCL
0108                  WRITE(6,158)(WDSK(II),II=1,6)
                C NOW LOAD WDATPT(I,J), FROM WHICH THE DATA POINTS WILL BE PLOTTED
0109                  DO 150 K=1,6
0110                150 WDATPT(K,J)=WDSK(K)
0111                  COEF(1)=WDSK(1)
0112                  COEF(2)=0.0
                C NOTE THAT HORNER'S SCHEME COULD BE USED TO ADVANTAGE BELOW
                C FOR 2ND DEGREE POLYNOMIAL FIT
                C     CALL LSQUAR(5,Z(2),WDSK(2),2,COEF,2)
                C     COF32=2.0*COEF(3)
                C     DO 151 K=1,M
                C     X=ZSPIN(K)
                C     WDSPIN(K)=COEF(1)+X*(COEF(2)+X*COEF(3))
                C 151 DER(K)=COEF(2)+X*COF32
                C FOR 3RD DEGREE POLYNOMIAL FIT
0113                  CALL LSQUAR(5,Z(2),WDSK(2),3,COEF,2)
0114                  COF32=2.0*COEF(3)
0115                  COF43=3.0*COEF(4)
0116                  DO 151 K=1,M
0117                  X=ZSPIN(K)
0118                  WDSPIN(K)=COEF(1)+X*(COEF(2)+X*(COEF(3)+X*COEF(4)))
0119                151 DER(K)=COEF(2)+X*(COF32+X*COF43)
                C FOR 4TH DEGREE POLYNOMIAL FIT
                C     CALL LSQUAR(5,Z(2),WDSK(2),4,COEF,2)
                C     COF32=2.0*COEF(3)
                C     COF43=3.0*COEF(4)
                C     COF54=4.0*COEF(5)
                C     DO 151 K=1,M
                C     X=ZSPIN(K)
                C     WDSPIN(K)=COEF(1)+X*(COEF(2)+X*(COEF(3)+X*(COEF(4)+X*COEF(5))))
                C 151 DER(K)=COEF(2)+X*(COF32+X*(COF43+X*COF54))
                C FOR 5TH DEGREE POLYNOMIAL FIT
                C     CALL LSQUAR(5,Z(2),WDSK(2),5,COEF,2)
                C     COF32=2.0*COEF(3)
                C     COF43=3.0*COEF(4)
                C     COF54=4.0*COEF(5)
                C     COF65=5.0*COEF(6)
                C     DO 151 K=1,M
                C     X=ZSPIN(K)
                C     WDSPIN(K)=COEF(1)+X*(COEF(2)+X*(COEF(3)+X*(COEF(4)+X*
                C    1(COEF(5)+X*COEF(6)))))
                C 151 DER(K)=COEF(2)+X*(COF32+X*(COF43+X*(COF54+X*COF65)))
                C       WRITE(6,158)(COEF(II),II=1,6)
0120                158 FORMAT(6E15.6)
                C PILE FORCES PLACED INTO ARRAY FOR PLOTTING
0121                  DO 170 K1=1,M
0122                  IF(WDMIN.GT.WDSPIN(K1))WDMIN=WDSPIN(K1)
0123                  IF(WDMAX.LT.WDSPIN(K1))WDMAX=WDSPIN(K1)
0124                170 WDPLT(K1,J)=WDSPIN(K1)
                C NUMERICAL INTEGRATION USING SIMPSON'S RULE
0125                  WPLT(1,J)=W1(I)
0126                  IF(WMIN.GT.W1(I))WMIN=W1(I)
0127                  IF(WMAX.LT.W1(I))WMAX=W1(I)
```

```
FORTRAN IV G LEVEL 20.7 VS              MAIN                DATE =     6/27/80      14:37:34

0128                WINC=   HOVER6*(WDPLT(1,J)+4.*WDPLT(M,J)+WDPLT(2,J))
0129                DO 160 K=1,M2
0130                WPLT(K+1,J)=WPLT(K,J)-WINC
0131                IF(WMIN.GT.WPLT(K+1,J))WMIN=WPLT(K+1,J)
0132                IF(WMAX.LT.WPLT(K+1,J))WMAX=WPLT(K+1,J)
0133              160 WINC=   HOVER3*(WDPLT(K,J)+4.*WDPLT(K+1,J)+WDPLT(K+2,J))-WINC
                  C SHEAR STRESSES PLACED INTO ARRAY FOR PLOTTING
0134                DO 180 K=1,M1
0135                WDDPLT(K,J)=DER(K)*CIRCUM
0136                IF(WDDMIN.GT.WDDPLT(K,J))WDDMIN=WDDPLT(K,J)
0137                IF(WDDMAX.LT.WDDPLT(K,J))WDDMAX=WDDPLT(K,J)
0138              180 CONTINUE
0139              100 CONTINUE
                  C OUTPUT--NUMBERS AND PLOTS
0140                DO 230 JJ=1,NWPLOT
0141                J=IWPLOT(JJ)
0142                I=1
0143                WRITE(6,201)I,ZSPIN(I),WDPLT(I,J),WPLT(I,J),WDDPLT(I,J)
0144              201 FORMAT(1X,I4,4(5X,E13.6))
0145                DO 240 II=1,NTZDEP
0146                I=ITZDEP(II)
0147                WRITE(6,201)I,ZSPIN(I),WDPLT(I,J),WPLT(I,J),WDDPLT(I,J)
0148              240 CONTINUE
0149                I=M1
0150                WRITE(6,201)I,ZSPIN(I),WDPLT(I,J),WPLT(I,J),WDDPLT(I,J)
0151              230 CONTINUE
0152                IF(NPLOT.NE.0)GO TO 400
0153                ZT=0.0
0154                ZB=2400.
                  C PLOTTING OF AXIAL FORCE AS A FUNCTION OF DEPTH
0155                CALL SCALE(WDMAX,WDMIN,WDR,WDL,15,IE)
0156                CALL LABEL(0.,0.,WDL,WDR,15.,10,'AXIAL FORCE (POUNDS)',20,0)
0157                CALL LABEL(0.,0.,ZB,ZT,10.,5,'DEPTH (INCHES)',14,1)
0158                DO 260 JJ=1,NWPLOT
0159                J=IWPLOT(JJ)
0160                CALL XYPLT(6,WDATPT(1,J),Z,WDL,WDR,ZB,ZT,DOC,0,4)
0161                CALL XYPLOT(101,WDPLT(1,J),ZSPIN,WDL,WDR,ZB,ZT,DOC,0)
0162              260 CONTINUE
0163                CALL SYSEND(-1,0)
                  C PLOTTING OF DISPLACEMENT AS A FUNCTION OF DEPTH
0164                CALL SCALE(WMAX,WMIN,WR,WL,15,IE)
0165                CALL LABEL(0.,0.,WL,WR,15.,10,'DISPLACEMENT (INCHES)',21,0)
0166                CALL LABEL(0.,0.,ZB,ZT,10.,5,'DEPTH (INCHES)',14,1)
0167                DO 270 JJ=1,NWPLOT
0168                J=IWPLOT(JJ)
0169                CALL XYPLOT(101,WPLT(1,J),ZSPIN,WL,WR,ZB,ZT,DOC,0)
0170              270 CONTINUE
0171                CALL SYSEND(-1,0)
                  C PLOTTING OF SHEAR STRESS AS A FUNCTION OF DEPTH
0172                CALL SCALE(WDDMAX,WDDMIN,WDDR,WDDL,15,IE)
0173                CALL LABEL(0.,0.,WDDL,WDDR,15.,10,'SHEAR STRESS (PSI)',18,0)
0174                CALL LABEL(0.,0.,ZB,ZT,10.,5,'DEPTH (INCHES)',14,1)
0175                DO 280 JJ=1,NWPLOT
0176                J=IWPLOT(JJ)
0177                CALL XYPLOT(101,WDDPLT(1,J),ZSPIN,WDDL,WDDR,ZB,ZT,DOC,0)
0178              280 CONTINUE
```

```
FORTRAN IV G LEVEL 20.7 VS              MAIN                    DATE =     6/27/80      14:37:34

0179                  CALL SYSEND(-1,0)
                C PLOTTING OF T-Z DIAGRAMS
0180                  DO 290 JJ=1,NTZDEP
0181                  J=ITZDEP(JJ)
0182                  DO 300 I=1,NDTSET
0183                  IF(ZMIN.GT.WPLT(J,I))ZMIN=WPLT(J,I)
0184                  IF(TMIN.GT.WDDPLT(J,I))TMIN=WDDPLT(J,I)
0185                  IF(ZMAX.LT.WPLT(J,I))ZMAX=WPLT(J,I)
0186                  IF(TMAX.LT.WDDPLT(J,I))TMAX=WDDPLT(J,I)
0187                  ZPLOT(I,JJ)=WPLT(J,I)
0188            300   TPLOT(I,JJ)=WDDPLT(J,I)
0189            290   CONTINUE
                C          C      CALL SCALE(ZMAX,ZMIN,ZR,ZL,15,IE)
                C          C      CALL SCALE(TMAX,TMIN,TT,TB,10,IE)
                C                 ZL=2.
                C                 ZR=17.
                C                 TB=-5.
                C                 TT=5.
0190                  CALL SCALE(ZMAX,ZMIN,ZR,ZL,15,IE)
0191                  CALL SCALE(TMAX,TMIN,TT,TB,10,IE)
0192                  CALL LABEL(0.,0.,ZL,ZR,15.,15,'DISPLACEMENT (INCHES)',21,0)
0193                  CALL LABEL(0.,0.,TB,TT,10.,10,'SHEAR STRESS (PSI)',18,1)
0194                  DO 310 J=1,NTZDEP
0195                  CALL XYPLOT(NDTSET,ZPLOT(1,J),TPLOT(1,J),ZL,ZR,TB,TT,DOC,0)
0196                  CALL XYPLT(NDTSET,ZPLOT(1,J),TPLOT(1,J),ZL,ZR,TB,TT,DOC,0,J)
0197            310   CONTINUE
0198                  CALL SYSEND(-1,0)
                C PLOTTING OF APPLIED LOAD VERSUS TOP DISPLACEMENT
0199                  DO 320 J=1,NDTSET
0200                  IF(WDPLT(1,J).LT.SFFMIN)SFFMIN=WDPLT(1,J)
0201                  IF(WDPLT(1,J).GT.SFFMAX)SFFMAX=WDPLT(1,J)
0202                  SURFF(J)=WDPLT(1,J)
0203                  IF(WPLT(1,J).LT.SFDMIN)SFDMIN=WPLT(1,J)
0204                  IF(WPLT(1,J).GT.SFDMAX)SFDMAX=WPLT(1,J)
0205            320   SURFD(J)=WPLT(1,J)
0206                  CALL SCALE(SFDMAX,SFDMIN,SFR,SFL,15,IE)
0207                  CALL SCALE(SFFMAX,SFFMIN,SFT,SFB,10,IE)
                C       I=J1
                C       DO 320 J=I,NN
                C       SURFF(J)=WD(1,I)
                C       SURFD(J)=W1(I)
                C  320 I=I+1
                C       SFL=-20.
                C       SFR=20.
                C       SFB=-1.E6
                C       SFT=3.E6
0208                  CALL LABEL(0.,0.,SFL,SFR,15.,10,'TOP DISP (INCHES)',17,0)
0209                  CALL LABEL(0.,0.,SFB,SFT,10.,5,'APPLIED LOAD (LBS)',18,1)
0210                  CALL XYPLOT(NDTSET,SURFD,SURFF,SFL,SFR,SFB,SFT,DOC,0)
                C       CALL XYPLOT(NN,SURFD,SURFF,SFL,SFR,SFB,SFT,DOC,0)
0211                  CALL SYSEND(-1,0)
                C
                C TO ESTABLISH MULTIPLE SUB-PATH CAPABILITY
0212            400   CONTINUE
                C
0213            500   STOP
```

```
FORTRAN IV G LEVEL 20.7 VS              LSQUAR              DATE =     6/27/80      14:37:34

0001                  SUBROUTINE LSQUAR(M,X,Y,N,C,K)
                C     M IS THE NUMBER OF DATA POINTS--500 IS THE MAXIMUM ALLOWED
                C     N IS THE ORDER OF THE POLYNOMIAL--10 IS THE MAXIMUM ALLOWED
                C     K IS THE NUMBER OF COEFFICIENTS THAT ARE KNOWN CONSECUTIVELY FROM CO
0002                  DIMENSION X(1),Y(1),C(1)
0003                  DIMENSION SXP(20),SYXP(20),XP(500,20),YXP(500,20)
0004                  DIMENSION A(50,11),B(11)
0005                  IF(K.GT.N)STOP
0006                  KM1=K-1
0007                  K2=K*2
                C     NN IS THE NUMBER OF UNKNOWN COEFFICIENTS TO BE DETERMINED
0008                  NN=N-KM1
0009                  N2=2*N
0010                  SXP(1)=0.0
0011                  SYXP(1)=0.0
0012                  SUMY=0.0
0013                  DO 5 J=1,M
0014                  SUMY=SUMY+Y(J)
0015                  XP(J,1)=X(J)
0016                  SXP(1)=SXP(1)+XP(J,1)
0017                  YXP(J,1)=X(J)*Y(J)
0018                  SYXP(1)=SYXP(1)+YXP(J,1)
0019                5 CONTINUE
0020                  DO 15 I=2,N2
0021                  SXP(I)=0.0
0022                  SYXP(I)=0.0
0023                  DO 15 J=1,M
0024                  XP(J,I)=XP(J,I-1)*X(J)
0025                  SXP(I)=SXP(I)+XP(J,I)
0026                  YXP(J,I)=YXP(J,I-1)*X(J)
0027                  SYXP(I)=SYXP(I)+YXP(J,I)
0028               15 CONTINUE
0029                  IK=KM1
0030                  DO 25 I=1,NN
0031                  IK=IK+1
0032                  IF(IK.EQ.0)GO TO 24
0033                  B(I)=SYXP(IK)
0034                  GO TO 25
0035               24 B(I)=SUMY
0036               25 CONTINUE
0037                  IF(K.EQ.0)GO TO 30
0038                  KP=KM1-1
0039                  DO 55 I=1,K
0040                  KP=KP+1
0041                  DO 55 J=1,NN
0042                  B(J)=B(J)-C(I)*SXP(KP+J)
0043               55 CONTINUE
0044               30 DO 35 I=1,NN
0045                  IJ=K2+I-2
0046                  DO 35 J=1,NN
0047                  IJ=IJ+1
0048                  IF(IJ.EQ.0)GO TO 34
0049                  A(I,J)=SXP(IJ)
0050                  GO TO 35
0051               34 A(I,J)=M
0052               35 CONTINUE
```

```
:ORTRAN IV G LEVEL 20.7 VS              LSQUAR              DATE =     6/27/80      14:37:34

0053                  CALL MATINV(A,NN,B,1,DET)
0054                  DO 45 I=1,NN
0055               45 C(K+I)=B(I)
0056                  RETURN
0057                  END
```